INHIBITION OF ESSENTIAL PROTEIN-PROTEIN INTERACTIONS IN *PLASMODIUM* AND SARS-COV-2

by
Zachary Hunter Berliner

A thesis submitted to Johns Hopkins University in conformity with the requirements for the degree of Master of Science

Baltimore, Maryland
May 2021

Abstract

Plasmodium

Malaria is caused by *Plasmodium* parasites. A critical step during merozoite entry into red blood cells (RBCs) is the formation of a tight junction between the parasite and RBC, as it commits the parasite for invasion. Interaction between two parasite proteins, AMA1 on the parasite surface and RON2 on the RBC, is critical for junction formation. A 47-amino acid peptide in RON2 (RON2L) mediates this interaction. Our lab has shown that the RON2L peptide can act as a self-targeting inhibitor by competing to bind AMA1 and preventing parasites from entering RBCs.

The goals of this study are to 1) evaluate half-life extension approaches by fusing RON2L with human IgG Fc and albumin binding domain (ABD035) and 2) optimize expression of an *in silico* designed AMA1-RON2 inhibitor (Pep12) and assess its biochemical and biological activity. We designed Fc and ABD035 fusion constructs of RON2L and Pep12, optimized protein expression and purification, and evaluated their activity. We describe methods for purifying the Pep12-Fc dimer and RON2L-ABD035. We show that RON2L-ABD035 binds albumin, and both constructs have high affinity for AMA1. Finally, we demonstrate that the Pep12-Fc fusion protein potently blocks parasite invasion of RBCs. Our results demonstrate the promise of AMA1-RON2 inhibitors in preventing symptomatic malaria. We also show the potential viability of using conjugates to extend the half-lives of malaria therapeutics.

SARS-CoV-2

The COVID-19 pandemic, caused by the virus SARS-CoV-2, is the most notable major public health event since the 1918 influenza pandemic. The virus uses the receptor binding domain (RBD) of its Spike protein to bind to human ACE2 to enter host cells. Here, we have expressed and purified both the RBD and full-length Spike proteins in HEK293T cells. We have developed an assay to specifically measure anti-RBD antibodies that block its binding to ACE2. We demonstrate a strong correlation between levels of such blocking antibodies and virus neutralization assay (NT). Evaluation of NT in convalescent plasma or after vaccination can be challenging, particularly in places not prepared to do such complex assays. We therefore present a relatively easy biochemical assay could function as a surrogate under challenging conditions.

Primary Reader and Advisor: Prakash Srinivasan

Secondary Reader: Andrew Pekosz

Acknowledgements

There are so many people who I would like to thank for their help and support on the way to the completion of this thesis.

First, I would like to profusely thank my thesis advisor, Dr. Prakash Srinivasan, for everything you have done for me. Thank you for giving me the opportunity to work with you and on my various projects. I have learned so much about biology and biochemistry from you. You have taught me how to design experiments, to critically evaluate my work and the work of others, and how to be a true scientist. Most of all, you encouraged me to have faith in myself, to be confident in my thoughts, actions, and impulses. I have grown a considerable amount under your mentorship, and I will be forever grateful.

I also want to extend my thanks to the members of the Srinivasan Lab. Dr. Deepti Sarkar, thank you for being my lab partner from the beginning. I would not be here, and I would not know how to do many experimental techniques, if not for your tutelage. You have happily answered *all* of my questions about how to do every experiment, regardless of how detailed my questions were or how busy you were. You were also there for a good laugh, to hear me vent about my ELISAs not working, or to offer sage life advice. Dr. Maryam Saffarian Abbas Zadeh, Vani Daggupati, Sam Adewale-Fasoro, Sean Yanik, and Luciana Dinis, you all have meant so much to me. Each one of you has been there to advise me with my experiments and laugh about things. We have all been stuck together, bubbled up in the lab throughout this chaotic time, but there are no other individuals I would rather be stuck with than you guys. I also want to thank Shuhao Xiao for the work that he did that allowed my project to exist. I would not have

this project without you. Additionally, thank you to Drs. Gabriel Rocklin of Northwestern University and David Baker of the University of Washington for their assistance with the design and development of Pep12.

I also want to thank Dr. Andy Pekosz for being my secondary reader. I really appreciate the advice and feedback that you have given me on this thesis. Additionally, I want to thank you and Dr. Sabra Klein for giving me the opportunity to collaborate with you on SARS-CoV-2. It has been incredible to work on something that is at the forefront of everyone's minds and in the news every single day, and it has also given me the rare opportunity to see my work become impactful in such a short amount of time. Thank you to the members of the Pekosz and Klein Labs for your help with this project, providing me with plasma samples and data. I also want to thank the Casadevall Lab, particularly Dr. Radames Cordero, for providing me with more plasma samples. This project would also not be possible without the numerous collaborators at the Johns Hopkins University School of Medicine, particularly Dr. Yuka Manabe.

Thank you to Dr. Arturo Casadevall for your advice and support, especially in helping me choose a lab; you helped me make a great choice. Thank you, Dr. Gary Ketner, for allowing me to use your centrifuge and incubator and for being a friendly face that I could talk to. I want to thank Dr. Marcelo Jacobs-Lorena and his lab members, Drs. Sung-Jae Cha and Wei Huang, for their kindness and willingness to help me. I want to thank Karen Griffin for her emotional support and for all the work she does; it would have been tough to complete my projects without her assistance. Thank you to Gail O'Connor for literally everything you do. You are absolutely amazing and have been an

indispensable resource throughout my time here at Hopkins. Thank you to the admissions committee of MMI for giving me this wonderful opportunity to learn and grow. I also want to thank all the members of my ScM cohort. You all have been such great friends and comrades through this process, especially given the challenges by the pandemic. This has been one of the most unique two-year periods in school history, I would not have gotten through it without you all.

There are some former teachers I would also like to thank for getting me to where I am. Mr. Patenaude, I fell in love with biology because of you and your A.P. Bio class back at Westlake High School. I want to thank Drs. David Kehoe, Rich Hardy, and Roger Innes for their mentorship in college. You all cultivated my passion for infectious diseases and encouraged me to pursue my goals.

Finally, I would like to give enthusiastic thanks to my family. Thank you to my in-laws, Matt and Fernanda Cesnik, for everything you have done for me throughout my time in this program and beyond. You have pushed me to show everyone what I can do, while providing me with food, housing, and love. Thank you to Matthew Cesnik and Kaitlyn Blansett for being there for me, as well. I want to thank Grandma, Nana, and Papa for your love for me and extreme support of everything I do. Nana, though you were not able to see me start school at Hopkins, I have done my best to follow your guidance. I sincerely want to thank my parents and my sister, Morgan, for absolutely everything. You have picked me up when I struggled, encouraged me to do my best, and reinforced the concept of having fun while you work hard. Everything I have achieved in life has been thanks to you guys.

Most of all, I would like to thank my wife, Abby Cesnik. You have been by my side through all these wild times, from late nights at the lab to the panics about my classwork. You have given me emotional support when I needed it, a person to laugh with and talk to, and a reason to step away from my work. Additionally, thank you to my dog, Henry, and your cousin Jack. It is such a delight spending each day with the two of you.

There is a way out of every box, a solution to every puzzle; it's just a matter of finding it.

Capt. Jean-Luc Picard

Table of Contents

List of Figures

Part I: Engineering an Inhibitor of an Essential *Plasmodium* Protein-Protein Interaction

Introduction

A. Global Burden of Disease

Malaria has afflicted humanity since antiquity. "Father of Medicine" Hippocrates (460 BCE – 370 BCE) and Ancient Greek philosopher Celsus (25 BCE – 54 CE) described in detail the periodic fevers associated with the disease.[1] To this day, malaria is a major global public health issue. In 2015, the World Health Organization (WHO) published the *Global Technical Strategy for Malaria 2016-2030* (GTS), with the stated goal to provide "a framework for the development of tailored programmes to accelerate progress towards malaria elimination."[2] This guide established milestones for reduction of global malaria mortality and incidence over 5-year periods until 2030, with an overall goal of reducing both by at least 90% and eliminating malaria in at least 35 countries.[2] An analysis from the WHO in 2016 determined 21 countries that could reach the GTS milestone of malaria elimination in at least 10 countries by the year 2020, known as the E-2020 initiative; this list was based on the number of indigenous cases from 2000 to 2015, the declared objectives from each country, and the judgment from WHO experts.[3] As of 2019, Paraguay and Algeria have been certified malaria free; China and El Salvador have made formal requests for certification; Iran, Malaysia, and Timor-Leste had no indigenous cases in 2018 and 2019 (though an outbreak in Timor-Leste in 2020 is being investigated); and Belize and Cabo Verde reported no indigenous cases for 2019.[4] Overall, there were approximately 229,000,000 cases of malaria globally in 2019, accounting for 409,000 deaths.[4] By comparison, pandemic Coronavirus Disease 2019 (COVID-19) has resulted in a cumulative total of 421,000 deaths in the United States of

America as of January 26, 2021.[5] Unfortunately, both the malaria case incidence and deaths per population both fall short of the GTS milestones, by 37% and 22%, respectively.[4] Clearly, much work needs to be done in order to meet the targeted 90% reductions by 2030.

B. Parasite Life Cycle

Malaria is caused by parasites of the genus *Plasmodium* and transmitted by female *Anopheles* mosquitoes.[6,7] These parasites are members of the phylum Apicomplexa, which also includes *Toxoplasma gondii* (the etiological agent of toxoplasmosis) and *Crytosporidium* (the cause of cryptosporidiosis).[8,9] Malaria affects a wide variety of vertebrates, from birds and scaled reptiles to mice and bats.[10] Five species of *Plasmodium* are responsible for the disease in humans: *Plasmodium falciparum*, *Plasmodium vivax*, *Plasmodium ovale*, *Plasmodium malariae*, and *Plasmodium knowlesi*.[11] Of those species, *P. falciparum* is the deadliest, and, therefore, the most important one from a public health perspective.[6] However, *P. vivax* is also a major concern.[6] The *Plasmodium* life cycle is complex, spanning many different life stages and occurring in both the mosquito vector and the human host. Initially, when a female *Anopheles* mosquito infected with *Plasmodium* takes a bloodmeal, she injects parasites in the sporozoite stage into the human. Those injected sporozoites quickly move from the dermis, through the vasculature, and to the human liver, where they will invade hepatocytes. This entire process takes at least 30 minutes. Over the next 2 to 10 days, the parasite will rapidly replicate inside the liver cell, resulting in the eventual

release of up to 40,000 merozoites upon lysis of the cell. In *P. vivax* and *P. ovale*, a single sporozoite can form a hypnozoite within a hepatocyte.[11] Hypnozoites can remain dormant in the liver for months or years, complicating the treatment process of malaria caused by those two species.[11] The merozoites released from the liver enter the bloodstream, beginning the asexual blood stage of the life cycle. This erythrocytic stage is responsible for symptomatic disease in malaria. In the blood stage, a merozoite will invade a red blood cell (either an erythrocyte or reticulocyte, depending on the species).[6] Once the merozoite has entered the cell, it will transition to the next steps of its development. It will progress to the ring stage, followed by the trophozoite, before it becomes a schizont, containing 16 to 32 merozoites.[7] The schizont will eventually burst, lysing the cell and releasing the merozoites into the bloodstream, where each of these daughters is able to invade another cell. One asexual cycle takes between 36 and 72 hours, depending on the species.[6] At some point, some merozoites will commit toward forming gametocytes inside the red blood cell instead of continuing the asexual cycle, and the gametocytes traffic toward the skin. When an uninfected female *Anopheles* mosquito bites and infected person, she will take up some of the gametocytes. Inside the mosquito's midgut, the male microgamete will fuse with the female macrogamete, forming first a zygote, then an ookinete. The ookinete then migrates through the midgut epithelium and embeds itself on the tissue on the other side, on the edge of the hemocoel (body cavity). The ookinete transforms into an oocyst. Repeated cell divisions occur inside the oocyst, forming numerous sporozoites. The oocyst eventually bursts, releasing sporozoites into the mosquito body cavity. The sporozoites can invade many

mosquito tissues, causing a systemic infection. Some sporozoites cross into the salivary glands, where they can be injected into another human with a subsequent bloodmeal to infect another host. The life cycle is shown in **Figure 1**.[6]

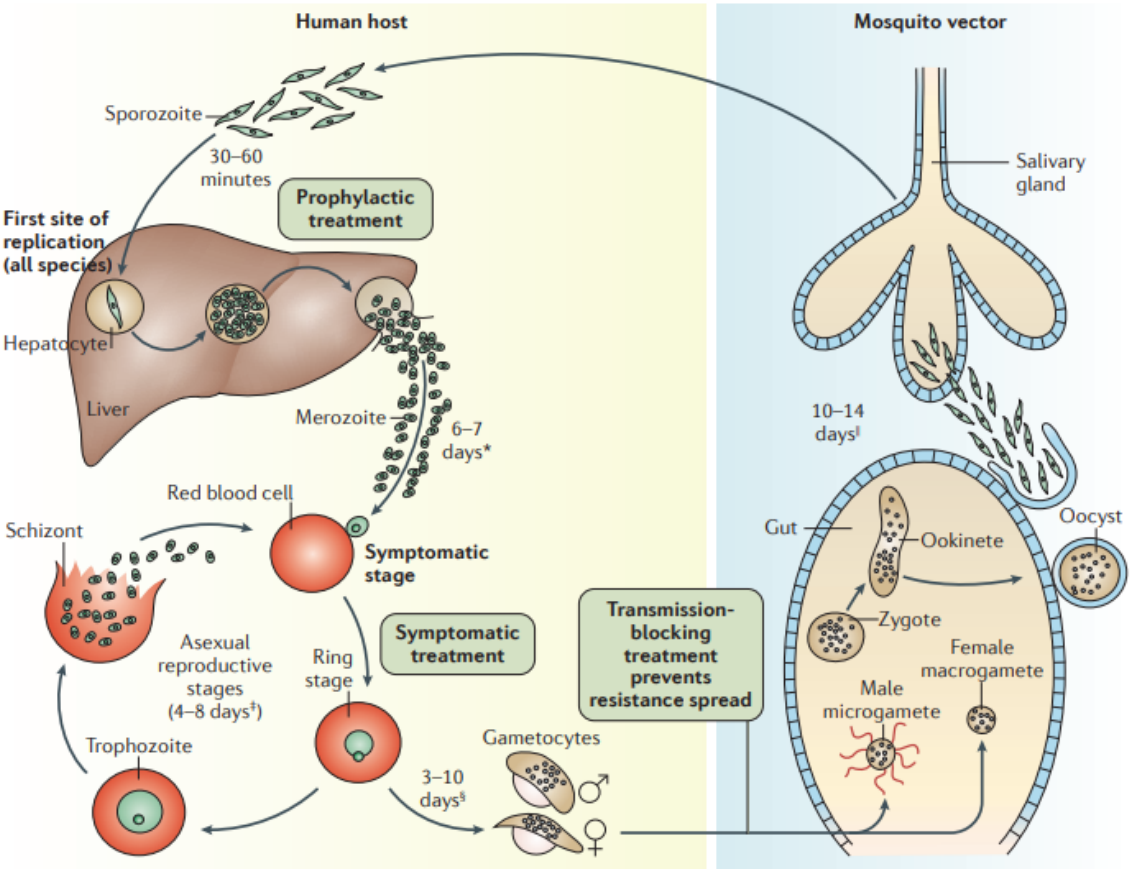

Figure 1. *Plasmodium* Life Cycle.[6]

C. Malaria Drugs and Drug Resistance

Malaria can be prevented, treated, and, in many cases, cured by a variety of pharmaceuticals. Some of those drugs include quinine (QN), chloroquine (CQ), piperaquine (PPQ), pyrimethamine (PYR), and artemisinin (ART).[12] In the mid-1600s, Europeans became aware of the *Cinchona* tree from South America, whose bark could be used to treat fevers.[13] In 1820, scientists derived quinine, the active antimalarial

component, from the bark.[14] Bayer AG synthesized chloroquine from quinine in 1934, and chloroquine soon became the gold standard drug for treating and curing malaria.[15] As is expected when one drug or drug family is disproportionately used to treat a pathogen, resistance to chloroquine was first detected in 1959.[15] By the late 1980s, resistance to chloroquine and other quinoline derivatives in *Plasmodium* falciparum, the parasite species responsible for the deadliest strain of malaria, had become widespread.[15] In 1993, it was discovered that treatment in Malawi with chloroquine resulted in a 58% treatment failure rate, so Malawi stopped the use of the drug that year.[16] The worldwide spread of chloroquine and pyrimethamine resistance is shown in **Figure 2**.[17] CQ and PPQ (another quinoline) resistance is mediated by mutations in the *Plasmodium falciparum* transporter PfCRT, particularly the K76T mutation.[18] These mutations lead to reduced uptake of the drug, allowing the parasites to survive longer.[18] Interestingly, the effectiveness of CQ against *Plasmodium falciparum* malaria was reassessed in Malawi 12 years after the nation stopped using the drug; a randomized study found a cumulative efficacy of 99% for chloroquine, with a worst-case efficacy of 80% when assuming an unknown outcome was a treatment failure.[19] This successful reintroduction is likely a result of the resistant strain containing some sort of fitness cost.[20] The strategy of simply reintroducing chloroquine is not practical, as a resistant strain could arise that does not have the associated reduction in fitness.[20]

Currently, the recommended first-line of treating malaria is with artemisinin-based combination therapy (ACT), which involves the use of ART in combination with other, slower-acting drugs.[4] In 2009, Dondorp et al. reported a dramatic increase in

parasite clearance time in patients from Pailin, Cambodia, compared to patients in Wang Pha, Thailand, after treatment with an artesunate-mefloquine ACT.[21] The WHO recently defined artemisinin resistance as a delay in parasite clearance following treatment with artesunate monotherapy or with an ACT.[22] From that initial detection by Dondorp et al., strains resistant to many other ACTs have also been found.[17] As shown by the map in **Figure 2**, ART resistance has spread to multiple other countries in southeast Asia.[17] Artemisinin resistance has been associated with polymorphisms in the kelch (K13)-propeller domain, though that phenotype appears to still be constrained to southeast Asia.[22,23] As of 2019, southeast Asia has shown treatment failure rates of nearly 20% for artesunate-amodiaquine and artesunate-mefloquine, but the rest of the world does not seem to have significant ACT resistance yet.[4] It is of utmost importance that artemisinin resistance not be allowed to spread to other areas, particularly to Africa. To prevent widespread ACT resistance, more therapies for the disease must be developed.

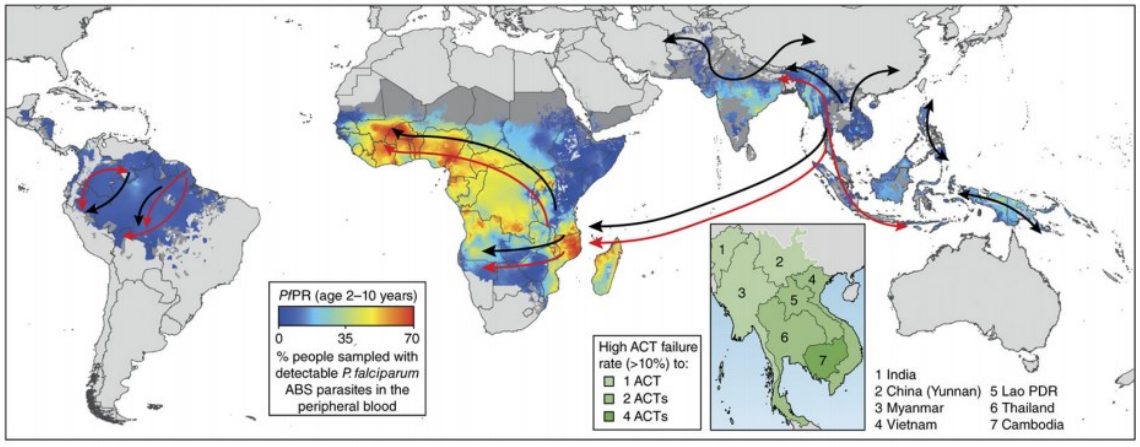

Figure 2. Map of the Spread of Chloroquine, Pyrimethamine, and ACT Resistance.[17] The heatmap indicates the areas with the highest percentage of people with detectable *P. falciparum* ABS (asexual

blood stage) parasites present in the blood. The black arrows depict the movement of chloroquine resistance, and the red arrows show the spread of pyrimethamine resistance.

D. Malaria Vaccines

Vaccines are an important component needed to reduce malaria globally. In August 2006, the WHO published the *Malaria Vaccine Technology Roadmap*, which put forth guidance for the research, development, and implementation of a malaria vaccine.[24] Critically, this document established the goal to develop and license a first-generation malaria vaccine by 2015 that has a protective efficacy of at least 50% against severe disease and death for longer than one year.[24] The vaccine that is furthest along in development is the RTS,S/AS01 vaccine, developed by Glaxo Smith Kline (GSK) in collaboration with the Walter Reed Army Institute of Research.[25] The primary malarial component of the vaccine consists of a repeat region, called NANP, of the *P. falciparum* circumsporozoite protein (CSP).[25,26] The CSP is the protein that surrounds the sporozoite stage of the parasite, and the NANP repeats are highly immunodominant B cell epitopes.[25] The CSP component in the RTS,S also includes three strong T cell epitopes to ensure a strong immune response against the parasite.[25,26] Finally, the CSP is fused to the Hepatitis B Virus surface protein, which will assemble a virus-like particle (VLP) to serve as protein carriers.[25,26] The AS01 is a novel liposome-based adjuvant made by GSK. The Phase III trial for the RTS,S vaccine began in March 2009 and concluded in January 2014, the results of which were published in 2015.[27] In infants 6-12 weeks old, the vaccine with booster reported an efficacy of 25.9% against clinical malaria and 17.3%

against severe malaria (the latter value was not statistically significant).[27] In children 5-17 months old, the vaccine with booster had a 36.3% efficacy against clinical malaria and 32.2% against severe disease.[27] In infants, the half-life of the short-lived antibody response is 45 days and that of the long-lived antibody response is 634 days.[28] Similarly, in children, the half-life of the short-lived response is also 45 days and that of the long-lived response is 591 days.[28] By comparison, the antibody half-lives for Tetanus, Varicella-Zoster Virus (the cause of chicken pox and shingles), and Measles are 11, 50, and 3014 years, respectively.[29] Despite the vaccine falling short of the 50% goal set forth by the *Malaria Vaccine Technology Roadmap*, the European Medicines Agency's Committee for Medicinal Products for Human Use (CHMP) "adopted a positive opinion in accordance with Article 58 of Regulation (EC) No 726/2004."[30] This determination indicated the vaccine for immunization in children from 6 weeks to 17 months.[30] In light of the opinion from CHMP, the WHO issued an opinion on the vaccine.[31] In this opinion, the WHO expressed concerns about the reproducibility of the protection offered to children 5-17 months old and was critical of the 4-dose schedule of the RTS,S vaccine.[31] To address these issues, the organization recommended a pilot implementation in 3-5 countries in sub-Saharan Africa solely in the older age group.[31] The WHO also established the study to address other potential negative health effects, like impact on all-cause mortality and the potential causal relationship of meningitis and cerebral malaria.[31] The pilot study was initiated in 2019 in Malawi, Ghana, and Kenya, and the results are expected to be reviewed in 2021.[4] Though there are many vaccines in development addressing various stages of the parasite life cycle, only three others have

moved to Phase II trials: the ChAd63/MVA ME-TRAP version of the RTS,S/AS01; GMZ2/Alhydrogel; and MSP3-LSP/AlOH.[32] Though the RTS,S vaccine has finished its Phase III clinical trial, the WHO still had enough misgivings about it to trigger further studies; the vaccine's efficacy falls short of the standard set by the WHO in 2006, and it seems that it does not produce long-lasting immunity.[24,27,28,31] These shortcomings with RTS,S, combined with the dearth of viable vaccine alternatives, demonstrate the clear need for the development of more vaccines with higher efficacy.

E. Merozoite Invasion

The asexual blood stage of the parasite life cycle begins with merozoite (the invasive form) entry into red blood cells (RBCs). Several secretory organelles, all located at the apical end of the merozoite, are crucial for invasion: the rhoptries, the micronemes, and the dense granules (**Figure 3**).[33] The rhoptries, which are a pair of tear-shaped organelles, can be further divided into the rhoptry bulbs and the rhoptry necks.[34] The process of invasion is a multi-step process, as shown in **Figure 4**.[35-37] This description will particularly focus on *P. falciparum*. In the first step, the merozoite weakly interacts with the surface of the erythrocyte.[35-37] Though the specific parasite proteins used in this step are not well-defined, it is possible that merozoite surface protein 1 (MSP1) is involved to some degree.[7,35] Next, the parasite reorients so that the apical end is in contact with the red blood cell. This interaction, mediated by the Duffy binding-like proteins and the reticulocyte homology ligands (particularly PfRh5), is much stronger than the initial contact.[35,36] The third step is the critical formation of the

moving junction. The rhoptry neck protein (RON) complex, including RON2, RON4, and RON5, is secreted from the rhoptry neck into the RBC; RON2, a transmembrane protein, inserts into its plasma membrane.[34] Apical membrane antigen 1 (AMA1) is secreted from the micronemes onto the merozoite surface and interacts with RON2 on the RBC surface.[36] AMA1 is also anchored to the actin-myosin motor located beneath the parasite membrane.[38] After the formation of the tight junction by the binding of AMA1 to RON2, the glideosome helps drive the actin-myosin motor to steadily move the parasite into a developing parasitophorous vacuole (PV) inside the RBC.[35,38] The fifth and final stage of invasion is the resealing of the PV and cell membrane.[35,36] At the conclusion of this step, the merozoite is completely encased in the PV within the targeted erythrocyte.[35,36]

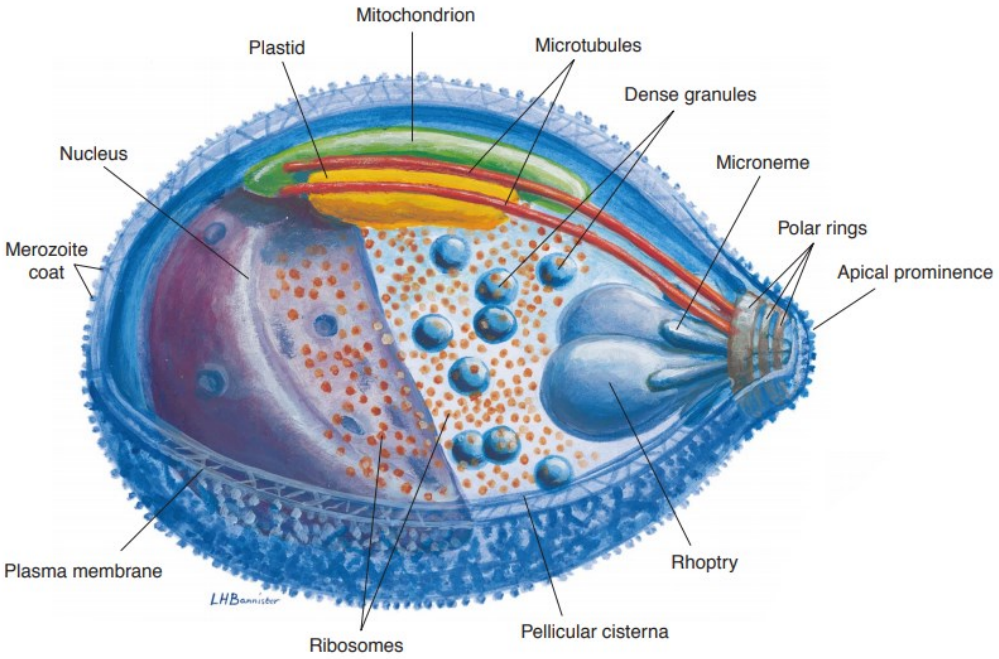

Figure 3. Illustration of a Merozoite and Its Major Organelles.[33] The apical end is on the right side of the figure, and the basal end is on the left.

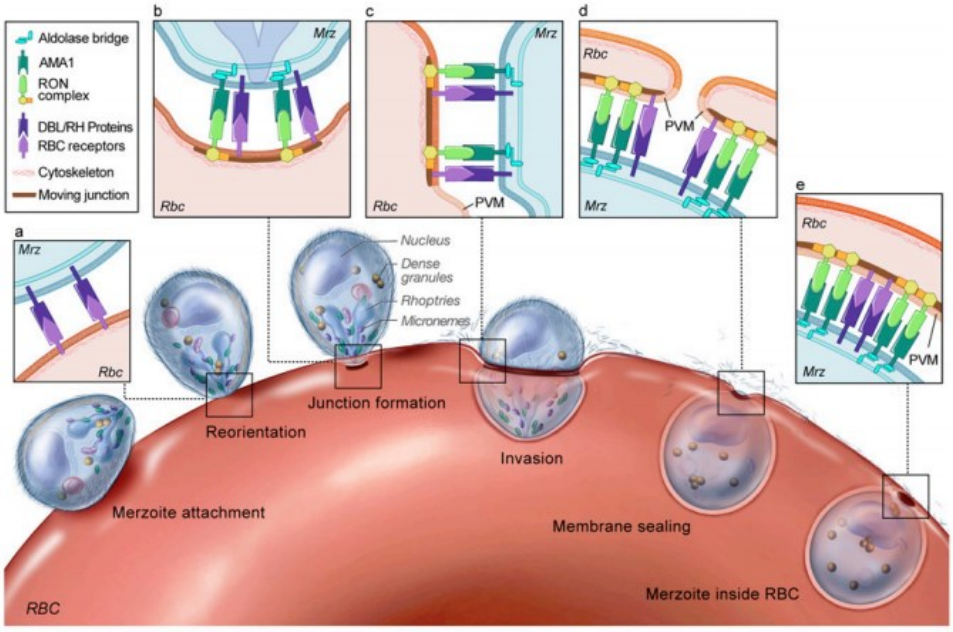

Figure 4. Steps of Merozoite Invasion into a Red Blood Cell.[37] Merozoite (Mrz) in blue; Red Blood Cell (RBC) in red.

F. AMA1-RON2 Interaction

Binding of AMA1 to RON2 is necessary for the formation of the moving junction and subsequent invasion of *Plasmodium* merozoites into erythrocytes.[37,39] As discussed above, AMA1 is secreted onto the merozoite surface, while the RON2 protein is inserted into the plasma membrane of the RBC. This is a unique adaptation whereby the parasite provides both the receptor and ligand required for a critical step in invasion. AMA1 and RON2 are also both expressed in sporozoites.[40,41] Through the use of the AMA1 inhibitor R1, Yang et al. (2016) determined that AMA1 is also highly important for invasion of sporozoites into liver cells.[42] Knockdown of *ron2* in sporozoites was also associated with reduced infection of mosquito salivary glands and invasion of hepatocytes.[43] The AMA1-

RON2 interaction, therefore, is incredibly important for three major invasion processes during the parasite life cycle.

G. AMA1-RON2 as an Anti-Malarial Target

Researchers have investigated multiple ways of inhibiting the interaction between AMA1 and RON2 to prevent parasite invasion into erythrocytes and hepatocytes. Broadly, inhibitors can be characterized as small molecule inhibitors or peptide inhibitors, based off the origins of the inhibitor. For small molecules, a screen of 21,733 of them yielded 3 compounds that inhibited AMA1-RON2 complex formation and blocked merozoite invasion.[44] Upon further optimization, 2 daughter molecules, NCGC00262650 and NCGC00262654, inhibited merozoite invasion across multiple strains of *P. falciparum* with "a 3- to 5-fold lower IC_{50}" as compared to the parent compound.[44]

Several peptide-based inhibitors have also been identified. In 2005, Harris et al. described R1, a peptide discovered by phage display that specifically targets AMA1.[45] R1 demonstrated strong dose-dependent inhibition of *P. falciparum* 3D7 and D10 strains.[45] However, R1 was shown to exclusively bind to AMA1 in only those two strains.[45,46] Though N-methylation of certain residues improves the association between R1 and the AMA1 of other *P. falciparum* strains, the strain-specificity of this peptide is a major barrier to its utility in a medical capacity.[46]

Lamarque et al. (2012) and Tyler and Boothroyd (2011) identified a region conserved in Apicomplexa near the C-terminal end of RON2 that interacted with

AMA1.[39,47] Srinivasan et al. (2011) and Vulliez-Le Normand et al. (2012) further characterized the region to a short, 47-amino acid peptide between two alpha-helices of RON2, a region termed "RON2L."[37,48,49] Critically, RON2L contains two highly-conserved cysteines, which form a disulfide bond essential for RON2L binding to AMA1.[37] This peptide binds inside a hydrophobic groove of AMA1, as does R1.[37,48] Previous studies by the lab have determined that exposure of the malaria parasites to the RON2L peptide or other small-molecule inhibitors of the AMA1-RON2 interaction can potently block merozoite invasion of red blood cells.[37,44] Similarly, antibodies that block this AMA1-RON2 interaction also block merozoite invasion.[49,50] A study in mice showed that vaccination with an AMA1-RON2L complex can confer protection to mice against lethal challenge with the YM strain of *P. yoelii*, a species of mouse malaria.[49] A follow-up vaccination study in *Aotus* monkeys found that the AMA1-RON2L complex protected against *P. falciparum* FVO strain parasite challenge.[50] Recent studies in our lab conjugated RON2L to the heavy and light chain of a human IgG1 (2A10) that retained its ability to bind AMA1 and block merozoite invasion.[51] This inhibitor was able to equally bind multiple strains of *P. falciparum*, as measured by ELISA.[51] By GIA, the inhibitor exhibited dose-dependent inhibition against *P. falciparum* from the 3D7 strain.[51] As shown by these various studies from our lab, RON2L is a potent inhibitor of merozoite invasion that functions by preventing the AMA1-RON2 interaction.

H. Antibody-Mediated Immunity and Fc Fusion

The most conspicuous method by which antibodies can combat infection by intracellular pathogens is through the activity of neutralizing antibodies. In the case of the *Plasmodium* asexual blood stages, this method would feature antibodies binding to the surface of merozoites to prevent them from invading red blood cells.[52] However, there are other mechanisms antibodies can use to protect against malaria. One study found that antibodies can fix complement component C1q to the merozoite, initiating the complement cascade to prevent invasion.[53] This antibody-mediated complement-dependent (Ab-C') inhibition appears to be more commonly used than direct inhibition.[53] A third mechanism features the "cooperation between antibodies and cells."[52] In Ab-dependent cellular inhibition (ADCI), blood monocytes recognize antibodies bound to merozoites using the Fc receptors FcγRIIa and FcγRIIIa and block the division of trophozoites.[52,54,55] ADCI is independent from phagocytosis of opsonized pathogens.[55]

Antibodies, particularly the Fc portions, are very advantageous for conjugation to pharmaceuticals. These conjugates are called Fc fusion proteins. The inclusion of the Fc domain allows the Fc fusion protein to trigger the complement fixation, ADCI, and phagocytosis described above.[56] IgG_1, IgG_2, and IgG_4 all have long half-lives due to recycling by the neonatal Fc receptor (FcRn).[57] This recycling is also initiated by the Fc domain, so Fc fusion proteins can also be long-lived in the serum.[56,57] The first Fc fusion protein, devised by Capon et al. in 1989, was designed to block HIV-1 infection of T cells by fusing the gp120-binding domain of CD4 to the Fc domain of IgG1.[57,58] Enbrel® (etanercept), the first Fc fusion protein on the market, was approved in 1998 for

treatment of rheumatoid arthritis.[57] Since then, many other Fc fusion proteins have been approved for marketing in the US, including Amevive® (alefacept) for psoriasis; Zaltrap® (ziv-aflibercept) for metastatic colorectal cancer; and Trulicity® (dulaglutide) for type 2 diabetes mellitus (T2DM).[57]

I. Albumin and Albumin Fusion Proteins

Albumin is the most abundant plasma protein in humans, with an average concentration of around 632μM.[59] It is a single-chain polypeptide that is 585 amino acids long and 66.439kD in molecular weight.[59,60] Human serum albumin (HSA) is an incredibly stable protein, with 17 disulfide bonds, and it is also a highly soluble protein that is very pH- and temperature-resistant.[59] HSA's unique biology means that it can bind a wide variety of ligands, from ions to carboxylates to fatty acids.[59] The protein can also reach many different tissues, including accumulating in cancerous or inflamed regions, so it can transport molecules all throughout the body.[60] Crucially, albumin is incredibly long lived as a result of FcRn recycling and its size, with an average half-life of 19 days.[57] This long half-life, along with its role as a molecular transporter, makes HSA an intriguing target for fusion to pharmaceuticals.[57] In 1992, Yeh et al. created the first notable HSA conjugate, fusing albumin to CD4 to block HIV.[61] They reported a 140-fold half-life increase as compared to soluble CD4.[61] Since then, many other researchers have used HSA to extend the lives of their proteins, like Smith et al. (2001), who extended the half-life of their Fab by 7-fold.[60,62] The first HSA fusion protein approved

for marketing was the T2DM drug albiglutide, known as Tanzeum® in the US and Eperzan® in the EU, though many others are on the market or in development.[57]

J. Albumin-Binding Peptides

One concern with fusion to the large albumin protein is the possibility of steric hinderance reducing the activity of the fusion protein.[63] For example, in a 2011 study from Miyakawa et al., IFNγ fused to mouse serum albumin resulted in a 200-fold lower potency than un-modified IFNγ, despite the fusion protein lasting much longer in serum.[64] Therefore, efforts have been made to use albumin-binding peptides (ABPs), small molecules or peptides that bind to albumin, instead of the full albumin protein.[60] In 2002, Dennis et al. used phage display to identify a number of ABPs, including SA21.[65] In a 2013 follow-up study, Miyakawa et al. fused an SA21 sequence to IFNγ instead of the HSA fusion. The fusion retained about 50% of the biological activity of IFNγ alone while lasting longer in the serum.[66] Other ABPs have been developed based on bacterial albumin-binding proteins that help camouflage the bacteria from the immune system.[67] For instance, streptococcal protein G (SPG) is a bacterial protein that can bind both albumin and immunoglobulins through a 15 residue ABD.[67] ABD035, an albumin binding peptide derived from SPG, was developed based on its stability and high affinity to HSA.[68] ABD035 exhibited an affinity for HSA with K_D of 500fM, a 2400-fold improvement compared to G148-ABD, the native SPG peptide.[68] A study published in 2014 by Levy et al. that compared the effects of SA21 and ABD035 as fusion partners for the drug exenatide resulted in long circulation times in rats and non-human primates.[69,70] Both

conjugates showed activity in mice 24 hours after glucose challenge, and both significantly reduced HbA1c, body weight, and food intake in diabetic mice over 4 weeks.[69] Based on the results of this study, both SA21 and ABD035 were able to dramatically extend the activity of exenatide, with ABD035 lasting longer than SA21 in circulation of non-human primates.[69] Other studies have also demonstrated that fusion of various therapeutics to ABD035 result in drastically increased half-lives.[71-74]

K. Summary

Here, we designed peptide-based inhibitors of the AMA1-RON2 interaction and evaluated their potential as a novel antimalarial strategy. We also tested these inhibitors using two different approaches, namely as a fusion protein with a human IgG1 Fc or a small albumin-binding peptide (ABD035). These were tested with the eventual goal of improving inhibitor stability and enhancing retention *in* vivo. We also used an *in silico* approach to design a more potent inhibitor (Pep12) based on the structure of RON2L and conducted proof-of-concept studies to test expression, folding, and biochemical and neutralizing activity. The goal of this study is to develop a novel antimalarial approach by self-targeting the parasites, using its own trick against itself. Such AMA1-RON2 inhibitors are expected to be strain-transcendent and, therefore, are likely to confer protection from disease.

Materials and Methods

Plasmid Design and Cloning

Plasmid Design

A total of four different plasmids were designed. The first, Pep12-Fc-pcDNA3.1, includes the Pep12 peptide and the Fc portion of the heavy chain of human IgG1, with the Pep12 upstream of the Fc (**Figure 5A**). Two other plasmids utilize the SA21ABP peptide. SA21ABP-PfRON2L-pcDNA3.1 Nterm (**Figure 5B**) has the SA21ABP located upstream of the PfRON2L peptide, while PfRON2L- SA21ABP-pcDNA3.1 Cterm (**Figure 5C**) has the SA21ABP downstream of PfRON2L. The sequence for SA21ABP was taken directly from Dennis et al. (2002).[65] A fourth construct, PfRON2L-ABD035-pcDNA3.1, includes ABD035 in place of SA21ABP, and the albumin binding domain is downstream of PfRON2L (**Figure 5D**). The sequence used is the one noted in Jonsson et al. (2008).[68] Each of those four plasmids included a signal sequence at the N-terminal end of the protein sequence so that the proteins will be secreted by the cell along the secretory pathway. It has been found that small variations in the signal sequence can significantly alter the degree of protein secretion.[75] Each plasmid also featured a (Gly-Gly-Gly-Gly-Ser)$_3$ motif as a linker between the RON2L or Pep12 and the fusion partner (Fc, SA21ABP, or ABD035). The purpose of the linker is to connect the components of the constructs without compromising the function of the individual proteins.[76,77] Specifically, the $(G_4S)_3$ linker we selected has been used to produce functional proteins.[78] All albumin-binding constructs contained a 6x histidine tag for the purposes of purification using nickel resin. The backbone of each plasmid was the pcDNA™3.1

plasmid from Invitrogen (Cat. #V79020/V79520). This plasmid contains a cytomegalovirus (CMV) enhancer-promoter for high-level expression and a bovine growth hormone (BGH) polyadenylation signal and transcription termination sequence for enhanced mRNA stability.[79]

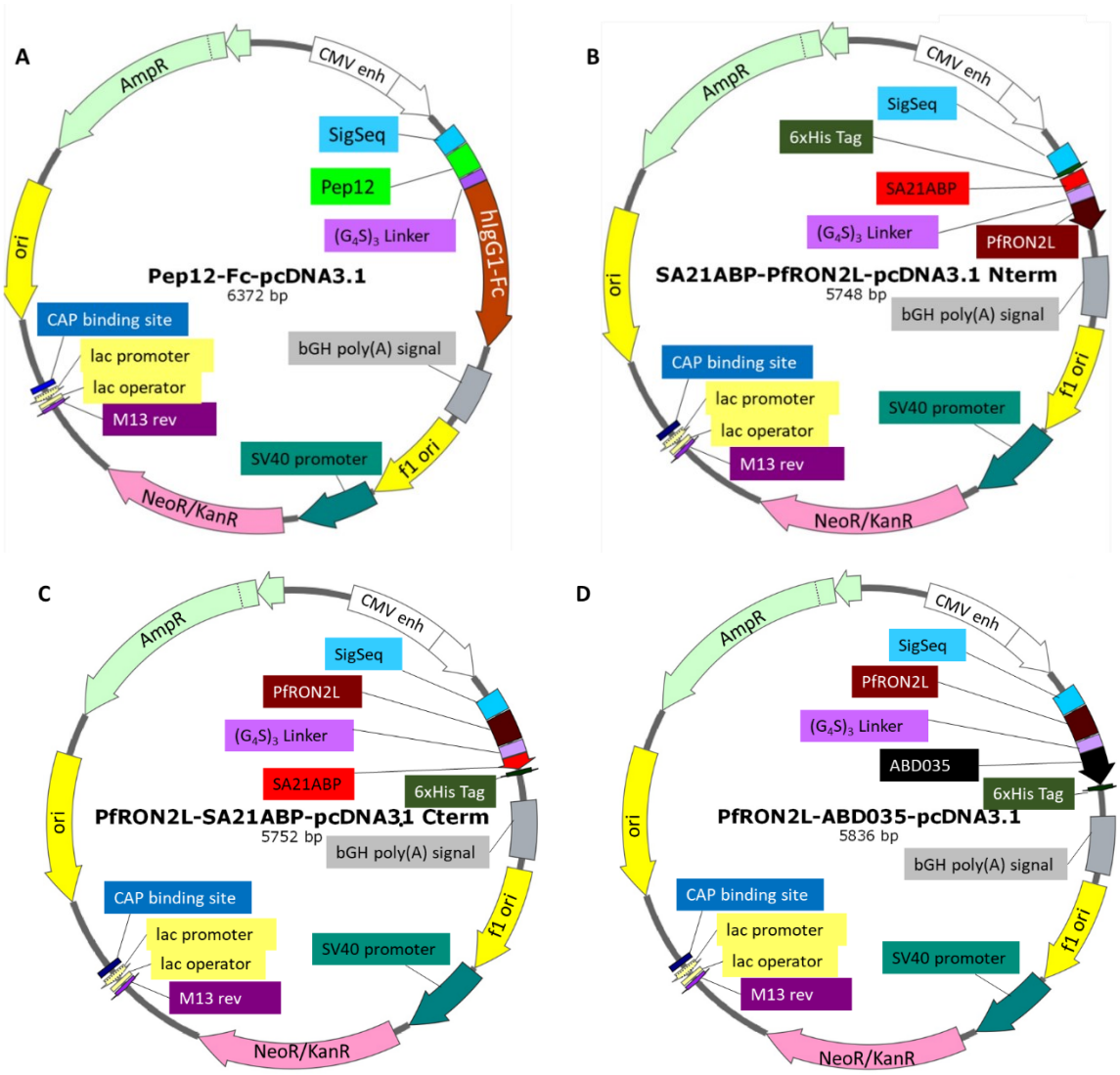

Figure 5. Plasmid Maps. Maps of (**A**) Pep12-Fc-pcDNA3.1 (B) SA21ABP-PfRON2L-pcDNA3.1 Nterm, (**C**) PfRON2L-SA21ABP-pcDNA3.1 Cterm, and (**D**) PfRON2L-ABD035-pcDNA3.1.

Digestion, Gel Extraction, and Gibson Assembly

DNA fragments coding for Pep12 and RON2L were synthesized (IDT Biologika) and cloned by Gibson Assembly into linearized pcDNA3.1, resulting in Pep12-Fc, SA21ABP-PfRON2L (ABP-Nterm), PfRON2L-SA21ABP (ABP-Cterm), and PfRON2L-ABD035 (RON2L-ABD035). All synthetic CAN fragments contained a 20 base pair overhang necessary for the Gibson Assembly procedure.[80,81]

For the Gibson Assembly, the NEBuilder HiFi DNA Assembly Protocol from New England BioLabs was followed.[82,83] Briefly, 50ng of the vector (the double-digested backbone) was mixed with the insert at a 1:2 vector to insert ratio and ligated using NEBuilder HiFi DNA Assembly Master Mix (New England BioLabs, Cat. #E2621) at 50.0˚C for 60 minutes.

Transformation into E. coli*, Verification of Insert by Colony PCR, and Plasmid Preparation*

The plasmids were transformed into XL-10 Gold® Ultracompetent Cells (Agilent Technologies, Cat. #200314) or DH5α cells and selected on Amp^+ LB agar plates. Multiple colonies were picked off of the transformation plate and used for colony PCR. Briefly, a mixture for each colony in a PCR reaction contained 2µL of OneTaq Polymerase Buffer 5x (NEB, Cat. #B9022S), 0.2µL of 10mM dNTP, 0.05µL of OneTaq Polymerase (NEB, Cat. #M0480L), 0.2µL each of the pcDNA3.1 Seq. Fwd. and PcDNA3.1 Seq. Rvs. primers (see **Appendix A** for primer sequences), and 7.35µL of MiliQ water. PCR products were verified by agarose gel electrophoresis. Each colony that was determined to contain the plasmid of choice was cultured in LB Broth containing 100µg/mL ampicillin overnight in an incubator-shaker set to 37˚C and 225rpm. Plasmids were

purified on a ZymoPURE™ Plasmid Miniprep or Midiprep Kit (Zymo Research, Cat. #D4209 or Cat. #D4201).[84,85] The concentrations of the purified plasmids were measured on a NanoDrop® 1000 Spectrophotometer. The final amino acid sequences of Pep12-Fc and RON2L-ABD035 are shown in **Appendix B**.

Protein Production

HEK293T Cell Transfection

Human Embryonic Kidney 293T cells (HEK293T) cells were cultured using DMEM/High Glucose (HyClone, Cat. #SH30243.01) containing 10% Fetal Bovine Serum (FBS) (Gibco, Cat. #26140-079) and 1% Penicillin Streptomycin (Gibco, Cat. #15140). The cells were maintained in vented tissue culture flasks at 5% CO_2 at 37˚C. Cells were passaged to new flasks when they reached 70-80% confluency. Once the cells were passaged approximately 20 times, frozen cells stored in 90% DMEM and 10% DMSO were thawed and subsequently maintained.

For transfections, the jetPRIME transfection procedure was followed.[86] Transfections were performed in flasks at 70-80% confluency. About 2 hours prior to transfection, the media of the flask was replaced with new media. For Pep12-Fc transfections, the media was replaced with 10% Ultra Low IgG Fetal Bovine Serum (VWR, Cat. #10018-826). For a 5mL transfection, 10µg of plasmid was diluted in 332µL of jetPRIME Buffer (Polyplus, Cat. #712-60). 10µL of jetPRIME Reagent (Polyplus, Cat. #114-15) was added to the diluted mixture, tapped and vortexed to mix, and spun down. The mixture was allowed to sit at room temperature for 10 minutes before

adding to culture flasks. The supernatant was collected 2-3 days later and centrifuged at 4,000rpm for 3 minutes to remove debris. Eventually, the procedure was optimized to use 1mg/mL polyethylenimine (PEI) instead of the jetPRIME Reagent. The PEI was made following a protocol from Cold Spring Harbor.[87] In a 5mL transfection (with 10µg of DNA), 40µL of PEI was used. Any larger transfections were scaled up proportionately.

Expi293F Cell Transfection

Since one of the components of the DMEM media used for maintenance and transfection of HEK293T cells is FBS, albumin will be present in the cell supernatant. Considering that the ABP-Cterm, ABP-Nterm, and RON2L-ABD035 constructs are designed to bind albumin, the presence of albumin in the supernatant could render purification and analysis of those constructs difficult. We selected the Expi293™ Expression System from Gibco, which uses Expi293F™ cells (Gibco, Cat. #A14527), a high-yield transient expression system based on suspension-adapted HEK293 cells.[88] Therefore, the Expi293™ Expression System from Gibco, using Expi293F™ cells (Gibco, Cat. #A14527) and serum-free, protein-free Expi293™ Expression Medium (Gibco, Cat. #A14351-01), was used for protein expression. The Expi293™ Expression Medium (Gibco, Cat. #A14351-01) is serum-free and does not contain albumin.[88] Additionally, this expression system yields 2-10 times more protein than other expression systems.[88] The cells were maintained in PETG vented shaker flasks in the Expi293™ Expression Medium at 8% CO_2 and 37˚C with a relative humidity of 90% on a shaker set to 100rpm. When the cells reached a density of around 3-5 x 10^6 live cells/mL, they were passaged

to a density of 0.4 x 10^6 live cells/mL. The cells were counted using a hemocytometer or a Countess™ II FL Automated Cell Counter from Life Technologies after the cells were stained with Trypan Blue Stain (Lonza, Cat. #17-942E).

On the day of transfection, the cells were diluted to a density of 3 x 10^6 viable cells/mL. For a 10mL transfection, 10µg of plasmid was diluted in 600µL of Opti-Plex™ Complexation Buffer (Gibco, A40968-01). 32µL of ExpiFectamine™ 293 Reagent (Gibco, Cat. #A14524) was diluted in 520µL of Opti-Plex™ Complexation Buffer and allowed to sit for 5 minutes. The diluted ExpiFectamine™ 293 Reagent was added to the diluted plasmid, mixed, and incubated at room temperature for 10-20 minutes. This complexation mixture was slowly added to the flask, and the flask was replaced in the incubator-shaker. Between 18- and 22-hours post-transfection, 60µL of ExpiFectamine™ Transfection Enhancer 1 (Gibco, Cat. #A14524) was added to 600µL of ExpiFectamine™ Transfection Enhancer 2 (Gibco, Cat. #A14524). We optimized the collection day, so the supernatant was collected on day 4 post-transfection. The supernatant was then centrifuged at 4,000rpm for 10 minutes, filtered through a 0.22µm filter, and stored at -80˚C.

SDS-PAGE to Confirm Protein Expression

Proteins secreted in the supernatants were initially evaluated by SDS-polyacrylamide gel electrophoresis (SDS-PAGE) under reducing conditions and confirmed by western blot, as described below.

ELISA to Confirm Expression of Pep12-Fc

To determine if the Pep12-Fc protein was expressed in both the HEK293T and Expi293™ cells, enzyme-linked immunosorbent assays (ELISAs) were performed. For each ELISA, a 96-well plate was coated with 1µg/mL Goat x-Human IgG-Fc Fragment Affinity Purified (Bethyl, Cat. #A80-104A) diluted in 1x PBS and allowed to sit overnight at 4˚C. The following day, ELISA Blocking Buffer (1x PBS, 0.1% Tween 20, and 1% BSA) was added to each well and incubated for 1 hour at room temperature. For the standard, Human Reference Serum (Bethyl, Cat. #R510-110) was added to ELISA Blocking Buffer to reach a concentration of 1.98µg/mL. The standard and protein samples were diluted four-fold down the plate, and each sample was run in duplicate. After 1 hour incubation at room temperature, the plate was washed 3 times with Wash Buffer (1x PBS and 0.1% Tween 20), followed by incubation for 1 hour with Goat Anti-Human IgG (H+L), Mse/Bvn/Hrs SP ads-HRP (Southern Biotech, Cat. #2016-05) diluted at 1:10000. Following a wash step, each well was incubated with BioFX TMB Super Sensitive One Component HRP Microwell Substrate (Surmodics, Cat. #TMBS-0100-01) for 2 minutes. The reaction was quenched with an equal volume of either TMB Stop Reagent, 450nm (Bioworld, Cat. #21530071-1) or BioFX 450nm Liquid Stop Solution for TMB Microwell Substrates (Surmodics, Cat. #LSTP-1000-01). The plate was read at 450nm-650nm using a microplate reader, and concentrations were calculated based off the interpolated standard curve in GraphPad Prism.

His-Tag Pulldown to Check Expression of ABP-Cterm, ABP-Nterm, and RON2L-ABD035

Because ABP-Cterm, ABP-Nterm, and RON2L-ABD035 all had 6x histidine tags, pull-downs could be performed using HisPur™ Ni-NTA Resin (Thermo, Cat. #88221). ABP-Nterm, ABP-Cterm, or RON2L-ABD035 supernatants were incubated with the beads overnight at 4˚C. The next day, the samples were washed 5 times with 25mM imidazole in 20mM sodium phosphate buffer pH 7.4, 300mM NaCl (25mM IBB). After the final wash, the beads were centrifuged for 5 minutes at 10,000rpm. The bead pellets were resuspended in 10µL of 1x PBS and boiled with LDS Sample Buffer (Novex, Cat. #B0007) and Sample Reducing Agent (Novex, Cat. #B0009). The samples were spun for 5 minutes at 10,000rpm and the supernatants were run on SDS-PAGE.

To confirm the results of the SDS-PAGE gel, a western blot was performed. Following the transfer of the proteins to a 0.2µm PVDF membrane, the membrane was incubated with Western Blocking Buffer (1x TBS, 0.1% Tween 20, 2% skim milk) for one hour on an orbital shaker. 6x-His Tag Monoclonal Antibody (Invitrogen, Cat. #MA1-21315) was diluted 1:500 in Western Blocking Buffer, and the membrane was incubated with the antibody on a rocker overnight at 4˚C. The next day, the membrane was washed 3 times with Wash Buffer (1x TBS, 0.1% Tween 20) for 5 minutes each and incubated with secondary antibody made of HRP-Goat Anti-Mouse IgG (H+L) (Invitrogen, Cat. #62-6520) secondary antibody diluted 1:1000 in blocking buffer for 1 hour. After the membrane was washed another 3 times, it was incubated for 5 minutes with SuperSignal™ West Pico PLUS Chemiluminescent Substrate (Thermo, Cat. #34578) and visualized on a Syngene G:Box imager.

Protein Purification

Ammonium Sulfate Precipitation

Initially, an ammonium sulfate (AS) precipitation method was evaluated to purify the Pep12-Fc fusion protein. A test was set up to determine the ideal percentages of AS to use to purify Pep12-Fc.[89] As shown in **Figure 6**, 10mL of supernatant was mixed with a particular volume of Saturated Ammonium Sulfate Solution (Teknova, Cat. #A2030) to reach the desired percent saturation. The solutions were incubated on ice for 1 hour and centrifuged at 10,000rpm and 4˚C for 30 minutes. The supernatants were mixed with the next volume of AS to increase the percent saturation by 10% and allowed to incubate for another hour on ice. Meanwhile, the pellets were dissolved in 1mM PMSF in 1x PBS. The mixture with a 10% increase in AS was then spun for 30 minutes at 10,000rpm and 4˚C. The resulting pellet was also resuspended in 1mM PMSF in 1x PBS. All of the resuspended pellets, along with the final supernatant, were stored at -80˚C to be tested by ELISA to determine purification efficiency (as described above).

Once the ideal percentages had been selected (25% AS to remove contaminants followed by 55% AS to precipitate Pep12-Fc), the protein precipitate was dissolved in 20mL of 1mM PMSF in 1x PBS and stored (4˚C or -80˚C) until use.

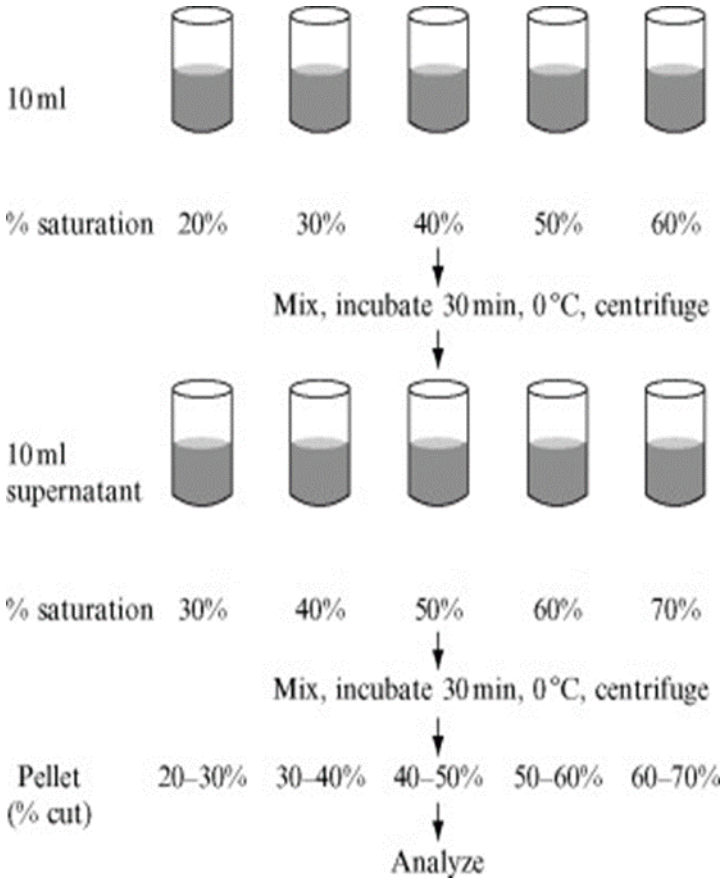

Figure 6. Schematic of AS Purification Test.[89] The initial supernatant was brought to a percent saturation with ammonium sulfate (AS). After the mixture was incubated and spun down, the remaining supernatant had its AS saturation increased by 10%. That mixture was also spun down. The first pellet, second pellet, and remaining supernatant were all tested by ELISA to determine the most effective percentage of AS to use to purify the Pep12-Fc Protein. Image adapted from Burgess (2009).[89]

Protein A Purification of Pep12-Fc

Staphylococcal Protein A, also known as Protein A, is commonly used for purification of antibodies because of the ability of Protein A to bind to IgG.[90] This approach was used to purify the Pep12 protein, as it contains an Fc fusion. The protein was purified on a Bio-Rad NGC Quest 10 Chromatography System using a Bio-Scale™

Mini Affi-Prep® Protein A Cartridge (Bio-Rad, Cat. #732-4600). First, an equal volume of Protein G IgG Binding Buffer (Thermo, Cat. #21011) was added to the Pep12-Fc supernatant. For Equilibration, 10mL of IgG Binding Buffer was pumped through the system. Sample Application was done using a sample pump. The column was then washed with 15mL of IgG Binding Buffer. Protein was eluted in five 2mL volumes of IgG Elution Buffer (Thermo, Cat. #21009) and neutralized immediately with 60µL of TrisCl pH 9.5. The entire method was done with a flow rate of 0.4mL/min. The purification was visualized on a chromatogram detecting absorbance at 280nm.

IMAC Purification of ABD05

Immobilized-metal affinity chromatography (IMAC) is purification based on the idea that metal ions, like Ni^{2+} and Cu^{2+}, can bind histidine and cysteine.[91] Since the RON2L-ABD035 protein contained a His tag, the protein could be purified on an IMAC column on the NGC Quest 10 Chromatography System using the Bio-Scale™ Mini Nuvia™ IMAC Ni-Charged column (Bio-Rad, Cat. #780-0811). Unless otherwise noted, the method was conducted at 7mL/min. The column was equilibrated with 25mM Imidazole in 20mM Sodium Phosphate Buffer pH 7.4, 300mM NaCl (25mM IBB), and the sample was applied through a sample pump at a flow rate of 1mL/min. Equilibration was done with 15mL of 25mM Imidazole Binding Buffer. Sample Application occurred through the sample pump at a flow rate of 1mL/min. A Wash step occurred with 15mL of 25mM Imidazole Binding Buffer. The Elutions were performed at a flow rate of 3mL/min. The column was then washed with 5 column volumes (CV) of 25mM IBB. Since we previously

determined that the ABD elutes around 300mM imidazole, we used the following Elution pattern: two steps of 2mL elutions with 100mM imidazole; two steps of 2mL elutions with 300mM imidazole; and three steps of 2mL elutions with 500mM imidazole. The final Wash used 30mL of 25mM Imidazole Binding Buffer, with the first 6mL of the wash also collected in 2mL fractions. The other wash step, along with the flow-through from sample application, was collected as well.

CHT Purification of Pep12-Fc

To attempt to separate the Pep12-Fc oligomers by size and just isolate the dimeric form, the Pep12-Fc protein was purified using CHT Ceramic Hydroxyapatite. CHT is a mixed-mode medium that can be used to purify a variety of proteins, from antibodies to viruses.[92] The column used was the Bio-Scale Mini Cartridge, CHT Type II, 40µm Media (Bio-Rad, Cat. #7324332), and the purification was done on the NGC Quest 10 Chromatography System. The Protein A-purified Pep12-Fc was first concentrated on an Amicon® Ultra-4 10kD Centrifugal Filter (Milipore, Cat. #UFC801096), and the buffer was exchanged from 1x PBS to 10mM $NaPO_4$, 100mM NaCl, pH 6.5 (the running buffer for the CHT purification method). The method was in accordance with 3.3.11 Scouting Protocol IB: IgG from Bio-Rad, with the exception that there was no Ca^{2+} supplementation.[93] The entire method was run with a flow rate of 6.2mL/min. The column was first Pre-Equilibrated with 3CV of 500mM $NaPO_4$, pH 6.5. Next, the column was Equilibrated in 10mM $NaPO_4$, 100mM NaCl, pH 6.5. About 100µL of the Pep12-Fc protein was injected into the sample loop during the Equilibration step, and 1mL of the

running buffer was run through the sample loop for Sample Application. Next, the column was washed with 5CV of running buffer. Elution was done with 20CV of elution buffer on a linear gradient, starting from 10mM $NaPO_4$, 100mM NaCl, pH 6.5, 15mM MES and ending with 10mM $NaPO_4$, 2mM NaCl, pH 6.5, 15mM MES (the gradient was the molarity of NaCl in the solution). Each fraction collected contained 4.5mL of elute. Finally, the column was Washed with 1CV of 10mM $NaPO_4$, 100mM NaCl, pH 7.5. This method was also performed using two other running buffers, with the 10mM $NaPO_4$ replaced with 40mM $NaPO_4$ and with 80mM $NaPO_4$.

Size Exclusion Chromatography of Pep12-Fc

To attempt to separate the Pep12-Fc oligomers by size and just isolate the dimeric form, the Pep12-Fc protein was purified by Size Exclusion Chromatography (SEC). The Protein A-purified Pep12-Fc was first concentrated on an Amicon® Ultra-4 10kD Centrifugal Filter to a concentration of around 7mg/mL, as measured by a NanoDrop® 1000 Spectrophotometer. The SEC was performed on an ENrich™ SEC 650 10 x 300 Column (Bio-Rad, Cat. #780-1650) on the NGC Quest 10 Chromatography System. The method was performed at a flow rate of 0.75mL/min. The Equilibration had 1.25CV of de-gassed 1x PBS passed through the column. 200-240µL of Pep12-Fc was injected into the sample loop during the Equilibration step. During the Sample Application step, 4mL of 1x PBS was passed through the sample loop. The protein was Eluted with 25mL of 1x PBS. Each collection tube received 0.6mL of elute.

SDS-PAGE and Western Blot to Confirm Protein Purification

For both the Pep12-Fc and RON2L-ABD035 proteins, SDS-PAGE was used to confirm that the protein was purified and to identify which collections contained the proteins. For Pep12-Fc, gels were run under both reducing and non-reducing conditions. The gels for RON2L-ABD035 were solely run under reducing conditions. For non-reducing gels, the volume of reducing agent was replaced with an equal volume of MiliQ water.

The gel was transferred to a 0.2µm PVDF membrane for western blotting. For Pep12-Fc, the Mixed Range MW program (25V, 1.3A) was run for 9 minutes. For ABD, the Low MW program (25V, 1.3A) was run for 5 minutes. The membrane was then incubated for at least 30 minutes on an orbital shaker with Western Blocking Buffer composed of 1x TBS, 0.1% Tween 20, and 2% skim milk. Goat anti-Human IgG (H+L)-HRP diluted to 1:10000 was used to detect Pep12-Fc. The ABD primary antibody was 6x-His Tag Monoclonal Antibody (Invitrogen, Cat. #MA1-21315) diluted to 1:500 and HRP-Goat Anti-Mouse (H+L) (1:1000 dilution) secondary antibody were used to detect RON2L-ABD035. Finally, the blots were incubated for 5 minutes with SuperSignal™ West Pico PLUS Chemiluminescent Substrate (Thermo, Cat. #34578) and imaged on a Syngene G:Box imager.

Protein Activity

ELISA to Determine Pep12-Fc Sample Concentrations

ELISAs were performed for Pep12-Fc samples from various fractions/collections from the many different purifications to determine the concentrations of protein. Either 96-well plates or half-area 96-well plates were used in these experiments. These ELISAs were performed in the same manner as those described in *ELISA to Confirm Expression of Pep12-Fc*, except the protein was first diluted 1:1000 in blocking buffer before the two- or four-fold dilutions down the plate. The concentrations of each sample tested were extrapolated from the generated standard curve.

ELISA to Test Binding of Pep12-Fc to AMA1

ELISAs were conducted to assess the ability of Pep12-Fc collections and oligomers to bind AMA1. This experiment was also done in either a normal 96-well plate or a half-area 96-well plate. The wells were coated with 1µg/mL of AMA1 isolated from the *P. falciparum* strain 3D7. Some wells were coated with 1µg/mL of Goat x-Human IgG-Fc Fragment Affinity Purified for the purpose of a loading control. Pep12-Fc samples being tested were diluted to 1:100 in ELISA Blocking Buffer, then diluted 2-fold going down columns in duplicate. A standard could not be used, as no standard would bind directly to the AMA1. The rest of the procedure was identical to the one described previously. IC_{50} values were calculated using the known concentrations that had been calculated from the Fc-coated ELISAs.

ELISA to Test RON2L-ABD035 Binding to AMA1

ELISAs were performed to ensure that the RON2L-ABD035 construct, which included RON2L, could still bind to AMA1 from the 3D7 strain of *P. falciparum*. These ELISAs were done in half-area 96-well plates. This ELISA underwent numerous optimization steps in the coating solution, blocking buffer, concentration of AMA1, and concentrations of primary and secondary antibodies. In preparation for this ELISA, the concentrations of ABD samples were determined using the Qubit™ Protein Assay Kit (Invitrogen, Cat. #Q33211) on a Qubit™ Fluorometer. The plate was coated with 2µg/mL of RON2L-ABD035 and stored at 4˚C. The next day, ELISA Milk Blocking Buffer (1x PBS, 0.1% Tween 20, 1% skim milk) was added to the plate and incubated for 1 hour. Milk was used as a component of the blocking buffer because of the ABD protein's ability to bind to albumin. The starting dilution of AMA1 was optimized to 0.5µg/mL in ELISA Milk Blocking Buffer. AMA1 was diluted 2-fold down duplicate columns, and the dilutions were added to the plate to incubate for 1 hour. The dilution of the primary antibody, anti-AMA1 previously isolated from mice, was optimized to 1:1000 (3µg/mL). Once the plate was washed 3 times with Wash Buffer, the anti-AMA1 was added to the plate and incubated for an hour. The optimized dilution of 1:2500 secondary antibody was prepared using HRP-Goat Anti-Mouse IgG (H+L) (Invitrogen, Cat. #62-6520) in ELISA Milk Blocking Buffer. After 3 washes with Wash Buffer, the wells received the secondary antibody and were let sit. An hour later, the plate was once again washed 3 times. Room temperature BioFX TMB Super Sensitive One Component HRP Microwell Substrate was added, incubated for 2 minutes, and the reaction was then stopped using an equal

volume of TMB Stop Reagent, 450nm or BioFX 450nm Liquid Stop Solution for TMB Microwell Substrates. The plate was read at 450nm-650nm.

ELISA to Test RON2L-ABD035 Binding to Albumin

The ability of RON2L-ABD035 to bind to different mammalian species' albumins was analyzed. The albumin proteins tested were bovine, human, and mouse. This ELISA, done in a half-area 96-well plate, was optimized for the blocking buffer, the dilutions of ABD, and the dilutions of the primary and secondary antibodies. Since all three albumin variants were tested simultaneously, each species' albumin was applied to duplicate columns. Each albumin was coated at a concentration of 2µg/mL. The plate was stored at 4˚C overnight. The next day, the plate was incubated with ELISA Milk Blocking Buffer (1x PBS, 0.1% Tween 20, 1% skim milk) for 1 hour. The RON2L-ABD035 was diluted to 2µg/mL in ELISA Milk Blocking Buffer, with subsequent 3-fold dilutions down the columns of the plate. 1 hour later, the plate was washed 3 times with Wash Buffer (1x PBS, 0.1% Tween 20), then 1:1000 6x-His Tag Monoclonal Antibody (Invitrogen, Cat. #MA1-21315) in ELISA Milk Blocking Buffer was added to each well. After another hour, the plate was again washed 3 times, and 1:5000 HRP-Goat Anti-Mouse IgG (H+L) was added and let sit for one hour. Once the plate was washed another 3 times, room temperature BioFX TMB Super Sensitive One Component HRP Microwell Substrate was incubated in each well for 2 minutes. The reaction was stopped with an equal volume of TMB Stop Reagent, 450nm or BioFX 450nm Liquid Stop Solution for TMB Microwell Substrates; the plate was read at 450nm-650nm.

RON2L-ABD035 Sandwich ELISA

A sandwich ELISA for RON2L-ABD035, testing the ability of the protein to bind albumin and AMA1 simultaneously, was performed. Like with the *ELISA to Test ABD Binding to Albumin*, the half-area 96-well plate was coated with 2µg/mL of bovine, human, and mouse albumin. Each albumin occupied two columns in duplicate. After the coated plate was stored overnight at 4˚C, ELISA Milk Blocking Buffer (1x PBS, 0.1% Tween 20, 1% skim milk) was added to each well and allowed to sit for 1 hour. The RON2L-ABD035 underwent 3-fold dilutions down each column, beginning with a concentration of 2µg/mL. Then, AMA1 from *P. falciparum* 3D7 was diluted to 1µg/mL and added to every well. After 1 hour, a 1:1000 dilution (3µg/mL) of anti-AMA1 previously isolated from mice was prepared and added to each well. Next, 1:2500 HRP-Goat Anti-Mouse IgG (H+L) was added for an additional hour. The plate was washed 3 more times, and BioFX TMB Super Sensitive One Component HRP Microwell Substrate was added to each well. 2 minutes later, the reaction was quenched with an equal volume of TMB Stop Reagent, 450nm or BioFX 450nm Liquid Stop Solution for TMB Microwell Substrates. The plate was read at 450nm and 650nm, and those optical densities were subtracted.

Gel Shift Assay

The binding of the RON2L-ABD035 protein to its ligands, AMA1 and albumin, was visualized by gel shift assays. ABD was mixed with AMA1 at multiple different molar

ratios. In one experiment, the molar ratio of RON2L-ABD035 and AMA1 was 1:1. In another experiment, the number of moles of the ABD fusion varied, while the number of moles of the binding partners remained constant. Moles of RON2L-ABD035 was based off the expected molar mass of 12,102.69g/mol. After the proteins were incubated together for 30 minutes at room temperature, the mixtures were placed on ice. For a control for AMA1 binding, AMA1 was also mixed at a 1:1 molar ratio with the RON2L peptide. All of the mixtures were brought up to equal volumes.

The samples were then prepared for native gel electrophoresis using the NativePAGE™ Novex® Bis-Tris Gel System.[94] The 1x NativePAGE™ Anode Buffer was made by diluting the NativePAGE™ 20x Running Buffer (Invitrogen, Cat. #BN2001) in MiliQ water, and the 1x NativePAGE™ Dark Blue Cathode Buffer was made by diluting the NativePAGE™ 20x Running Buffer and the NativePAGE™ 20x Cathode Buffer Additive (Invitrogen, Cat. #BN2002) in MiliQ water. Each sample had enough NativePAGE™ 4x Sample Buffer (Invitrogen, Cat. #BN20032) added to reach 1x. 1µL of NativePAGE™ 5% G-250 Sample Additive (Invitrogen, Cat. #BN2004) was added for every 10µL of total volume. Each tube was brought up to the desired volume using MiliQ water. Each well of the NativePAGE™ 4-16% Bis-Tris Gel (Invitrogen, Cat. #BN2111BX10) was washed 3 times with 10µL of 1x NativePAGE™ Dark Blue Cathode Buffer. 10µL of that buffer was added to each well prior to the samples being loaded. The 1x NativePAGE™ Anode Buffer was added to the back of the gel tank, while the 1x NativePAGE™ Dark Blue Cathode Buffer was added to the front. The gel was run for 80 minutes at 120V and

400mA. The gel was then destained using a solution composed of 50% methanol, 40% water, and 10% glacial acetic acid. It was visualized on a Syngene G:Box imager.

In some cases, the gel was used for a western blot instead of being immediately destained. The gel was transferred to a 0.2µm PVDF membrane and incubated with a 1:500 dilution of anti-His primary antibody. 1:1000 HRP-Goat Anti-Mouse IgG (H+L) (Invitrogen, Cat. #62-6520) was used as the secondary antibody. The blot was incubated for 5 minutes with SuperSignal™ West Pico PLUS Chemiluminescent Substrate (Thermo, Cat. #34578). The blot was visualized on a Syngene G:Box imager.

GIA

In preparation for Growth Invasion Assays (GIAs), the proteins first needed to have their buffers exchanged into incomplete RPMI (KD Medical, Cat. #CUS-0645). Each sample was concentrated in an Amicon® Ultra-4 10kD Centrifugal Filter (Milipore, Cat. #UFC801096) that was pre-wet with 1x PBS. The incomplete RPMI was next mixed with the concentrated protein and spun down at 4000rpm and 4˚C; this step was performed a total of 3 times. The sample, now in iCM, was passed through an Ultrafree®-MC 0.22µm GV Durapore® Centrifugal Filter Unit (Millipore, Cat. #UFC30GV0S) and aliquoted into multiple tubes. The concentration of each Pep12-Fc sample was calculated by ELISA using the procedure detailed in *ELISA to Determine Pep12-Fc Sample Concentrations*. The concentration of each ABD sample was calculated using the Qubit™ Protein Assay Kit (Invitrogen, Cat. #Q33211) on a Qubit™ Fluorometer. The desired concentration for every sample was 10mg/mL.

For the GIA, infected RBCs at 0.5% parasitemia (schizonts) and 4% hematocrit were incubated with the proteins in a final volume of 40µL for 72 hours at 37˚C. Cells were collected at the end of the 72 hours and lysed in the presence of Thiazole Green (SYBR® Green I) (Biotium, Cat. #40086) for 30 minutes at room temperature to stain the parasite DNA. The plates were read with excitation and emission spectra around 480nm and 520nm, respectively. The results were blank subtracted and normalized with controls that did not receive the drug. The IC_{50} value was calculated in GraphPad Prism.

Results

Identification of Pep12, a Potent AMA1-RON2 Inhibitor

One peptide that will be used extensively is an enhanced version of RON2L known as Pep12. Pep12 was designed in collaboration with Dr. Gabriel Rocklin of Northwestern University and Dr. David Baker of the University of Washington. The schematic for the generation of Pep12 is shown in **Figure 7**. First, the crystal structure of the predicted interaction between RON2L and the hydrophobic pocket of AMA1 was analyzed, and the RON2L residues essential for interaction with AMA1 were identified. Those critical residues, which comprise a hairpin loop, became integral for the *de novo* generation of any protein designed to bind in the same location of AMA1. Fragments listed in PlasmoDB were assembled onto a backbone that also included the essential RON2L hairpin using "a Rosetta Monte Carlo-based fragment assembly protocol" (**Figure 7A**).[95] A library of potential AMA1 inhibitors were selected and tested for their ability to bind AMA1 using a yeast surface display approach.[96] Briefly, yeast cells displaying various designs on their surface were incubated with varying concentrations of fluorescently-labeled AMA1 proteins. Proteins binding to AMA1 Cells were then sorted by flow cytometry and identified for sequencing. Through iterative screening, peptides that had the strongest affinities were selected. The selected peptides were next evaluated for their ability to bind to a different allele of AMA1 to identify those that bind in a strain-transcendent manner. The designs were also tested for proteolytic and thermal stability using a similar method. The proteins were tagged with a c-Myc tag and labeled with a fluorescent antibody. Proteolytic cleavage resulted in the loss of the tag

and the attached fluorescent antibody, so exposure to increasing concentrations of proteases resulted in selection for the most stable peptides. This screening process is shown in **Figure 7B**.

Ultimately, Pep12 demonstrated the strongest affinity for AMA1 while still maintaining high proteolytic and thermal stability, so it was selected for further evaluation. Pep12 demonstrated inhibitory activity against parasite invasion, as demonstrated by GIA (**Figure 7C**). The Pep12 peptide exhibited an IC_{50} of 45nM, a 10-fold greater inhibition compared to RON2L.

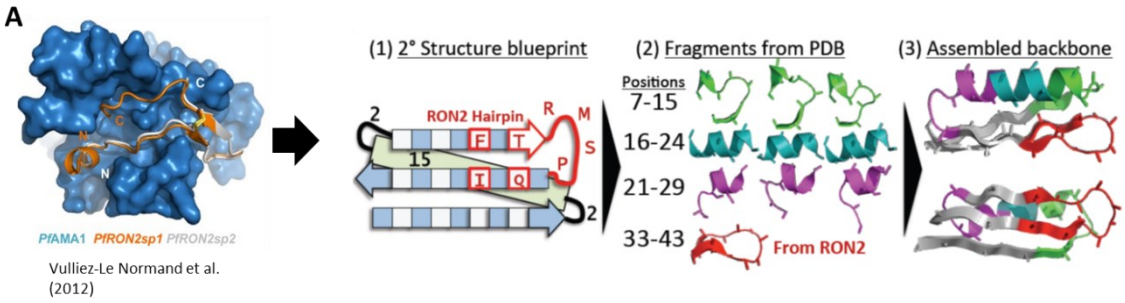

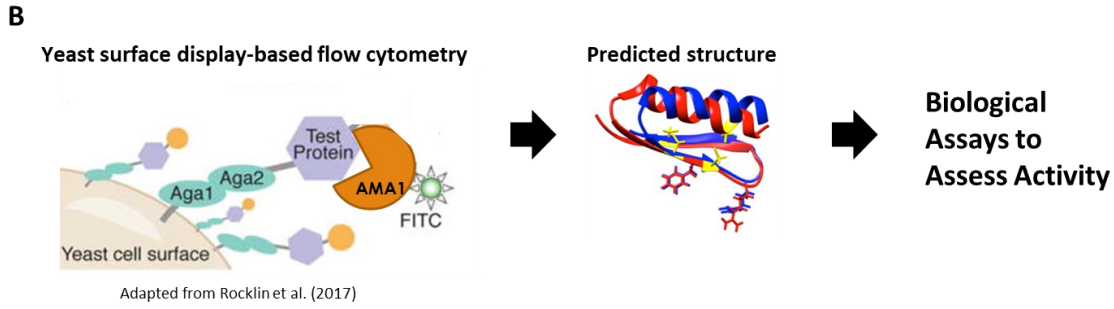

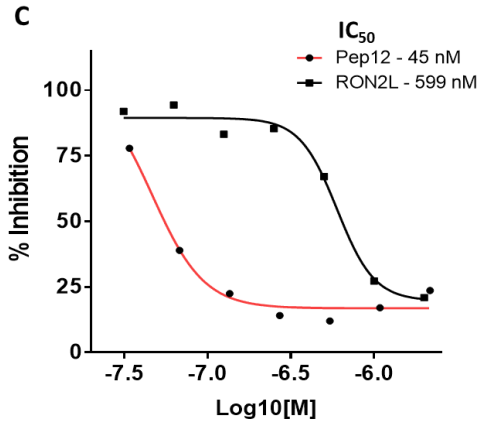

Figure 7. Process of Screening for Inhibitor Pep12. (**A**) *In silico* derivation of the peptide library. Based on the structure of the interaction between RON2L and AMA1, the critical RON2L residues were identified. Backbones using fragments from PDB and RON2L amino acids essential for binding AMA1 were assembled. (**B**) Chemical and biological screening of peptide library. The library of peptides was displayed on yeast and iteratively selected for the ability to bind AMA1 tightly. Similar yeast display experiments were used to test for proteolytic and thermal stability. The structures of the peptides were predicted. (**C**) GIA data of one peptide, Pep12, compared to RON2L. Based on this 10-fold greater inhibition, we have chosen to further test Pep12's function and ability to block AMA1 from binding Pep12. The crystallographic image of AMA1 and RON2L is from Vulliez-Le Normand et al. (2012).[48] The image of the yeast display experiment is adapted from Rocklin et al. (2017).[96]

HEK293T Expression of Pep12-Fc

Once the Pep12-Fc was successfully inserted into the pcDNA3.1 plasmid and sequence verified, the completed plasmid was transfected into HEK293T cells to produce protein. Pep12-Fc expression was monitored by ELISA and quantified using a human reference IgG standard curve (**Figure 8A**). RON2L-Fc was used as a positive control. Based on the calculated concentrations, we concluded that Pep12-Fc was being expressed in HEK293T cells (**Figure 8B**). Next, we evaluated the ability of Pep12-Fc to bind to AMA1, its intended target. RON2L-Fc was used as a positive control. This ELISA demonstrated that both RON2L-Fc and Pep12-Fc bound to AMA1 as expected (**Figure 8C**). Interestingly, while the amount of Pep12-Fc used was higher than RON2L-Fc (**Figure**

8B), its binding activity to AMA1 was lower than that of RON2L-Fc (**Figure 8C**), suggesting that not all Pep12-Fc expressed may be fully active.

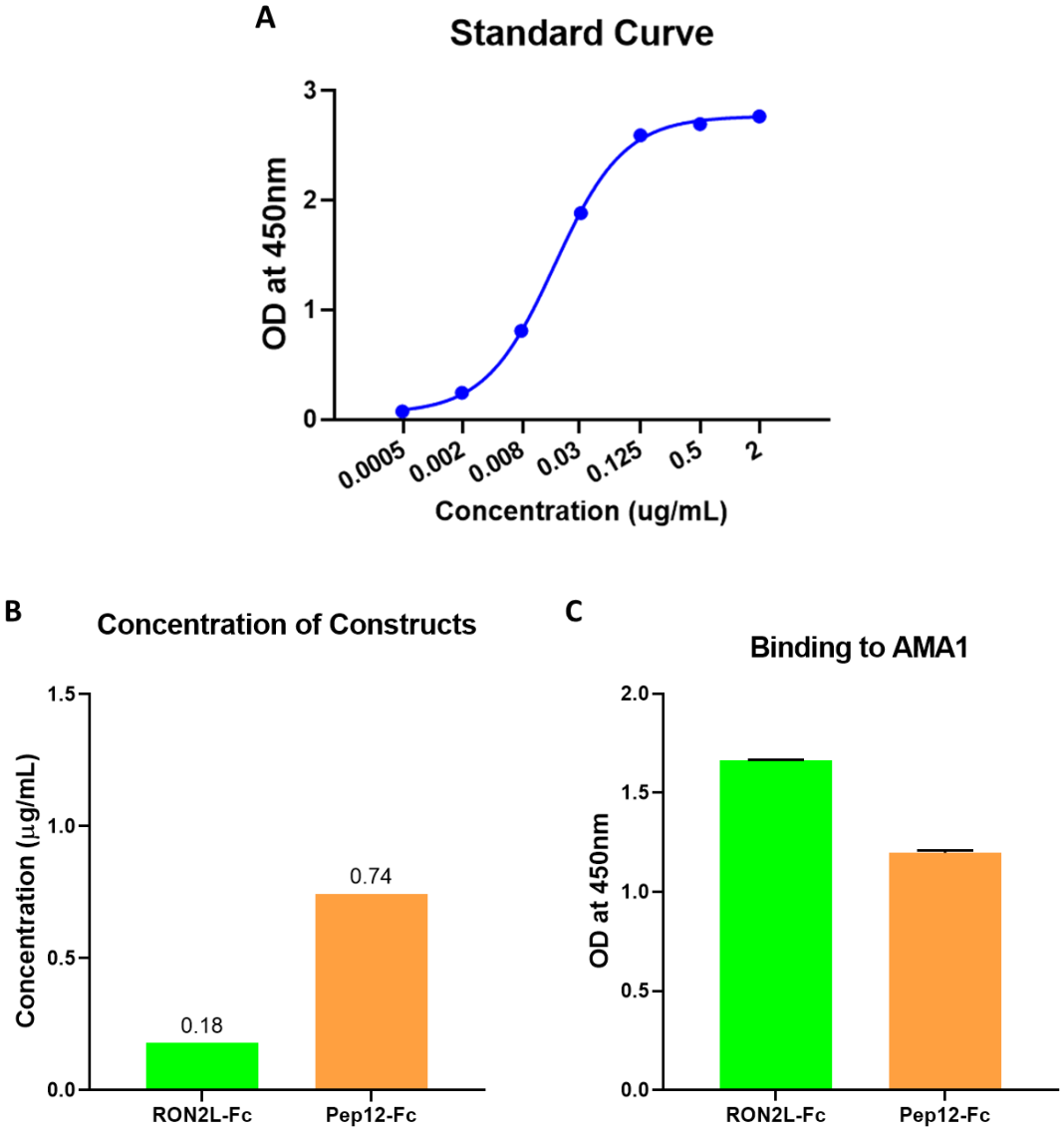

Figure 8. Expression of Pep12-Fc in HEK293T Cells. (**A**) Graph of a typical ELISA standard curve using Human Reference IgG. (**B**) The concentration Pep12-Fc expressed in HEK293T cells is shown in comparison to that of RON2L-Fc. (**C**) Qualitative comparison of RON2L-Fc and Pep12-Fc binding to AMA1 at the same dilutions used in **8B**.

Ammonium Sulfate Precipitation of Pep12-Fc

The ammonium sulfate (AS) precipitation method, based on the principle that different proteins precipitate at different percentages of AS saturation, was used to preferentially precipitate and purify Pep12-Fc from other proteins in the culture media. This approach is widely used to separate IgG in culture media.[89] Contaminants can be removed by first using a lower AS saturation, followed by a higher AS concentration that should yield most of the target protein.[89] To find the ideal AS concentrations, a test purification like the one diagrammed in **Figure 6** was set up. The starting AS percentages were 20%, 30%, 40%, 50%, and 60%. The resulting pellet was termed Precipitate 1. After that first round of purification, each sample had its AS saturation increased by 10%. The resulting pellet was called Precipitate 2. Based on the idea that 90% of a given protein can be precipitated with a 10% increase in AS saturation, the majority of the Pep12-Fc protein was expected to be located in Precipitate 2. The Supernatant is what remained after the second precipitation. **Figure 9A** shows the concentration of Pep12-Fc present in each precipitate and supernatant, as calculated by ELISA. A negligible amount of Pep12-Fc precipitated at below 30% AS, so 25% is an ideal percentage to remove contaminants without removing the target protein. 50% and 60% AS both contained very high concentrations of Pep12-Fc. Thus, 55% is sufficient to use for future purifications.

Precipitation may force proteins to misfold. We therefore performed an ELISA to confirm that Pep12-Fc could still bind its target. Even at the 50% and 60% AS, the most stressful of the environments, the precipitated Pep12-Fc could still bind AMA1 as effectively as the non-precipitated counterparts (**Figure 9B**). Ammonium sulfate

precipitation starting with 25% AS and followed with 55%, is a viable method for purifying functional Pep12-Fc protein.

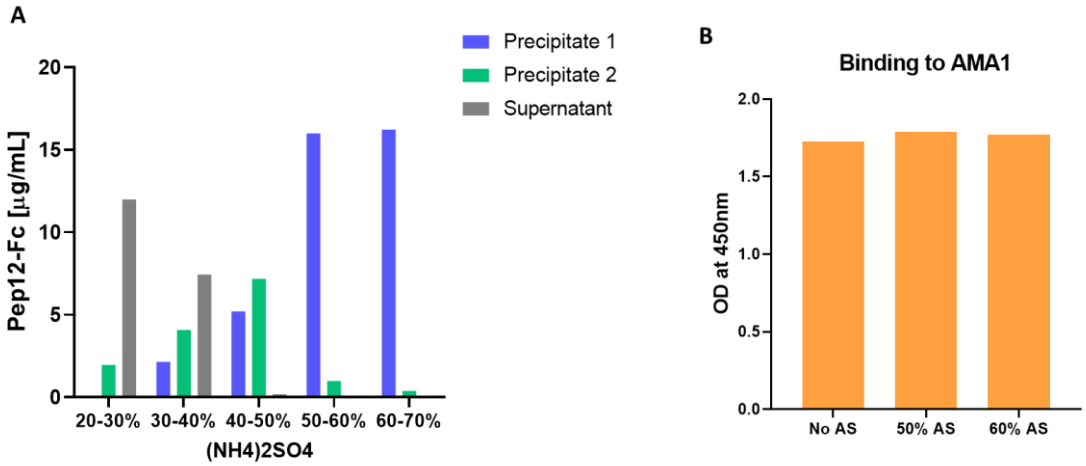

Figure 9. Ammonium Sulfate [$(NH_4)_2SO_4$] Precipitation of Pep12-Fc. (**A**) Concentration of Pep12-Fc in each pellet and supernatant from the AS precipitation test. (**B**) ELISA data showing the AMA1 binding of the 50% and 60% AS pellets, each at 1:10 dilutions, compared to the binding of undiluted, non-precipitated supernatant.

Expi293™ Expression of Pep12-Fc

The low yields of protein in HEK293T prompted us to evaluate the Expi™293 suspension cells that are optimized to produce high levels of recombinant antibodies. This system does not require any serum- or animal-origin proteins. [88] We wanted to see if the new cell line would yield more protein than the old line, and we also wanted to determine on which day post transfection to collect the Expi293™ supernatant to maximize protein expression. Supernatants from Expi cells were collected every day for 5 days and compared with supernatant collected on day 4 from HEK293T cells, and Pep12-Fc was quantified by ELISA (**Figure 10**). While the HEK293T cells, which were

collected on day 4 post-transfection, produced Pep12-Fc at a concentration of 1.86µg/mL, even Day 2 post-transfection in Expi293 cells produced 15 times more protein. When accounting for volume, Day 5 in Expi293 produced 3.75mg of protein compared to 18.6µg in HEK293T, a greater than 200-fold increase in total protein.

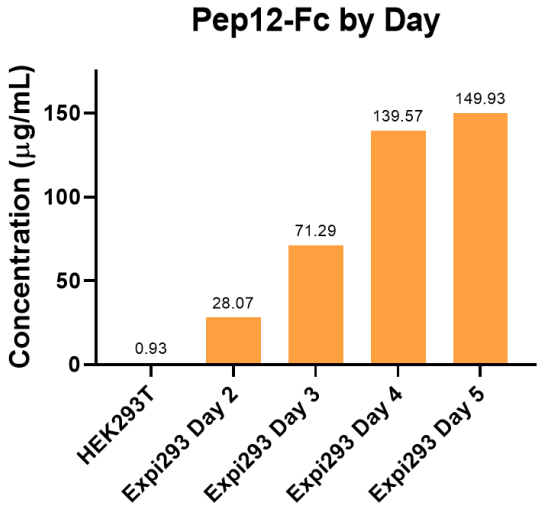

Figure 10. Pep12-Fc Protein Expression in Mammalian Cells. Concentrations of Pep12-Fc protein produced in either HEK293T on day 4 or Expi293™ cells on days 2 to 5.

Pep12-Fc Oligomerization

Once enough Pep12-Fc protein supernatant had been retrieved from Expi293™ cell cultures, individual batches of supernatant were purified on a Protein A column. Additionally, supernatant from HEK293T cells was precipitated by AS precipitation, then purified on the Protein A column. A typical chromatogram at 280nm resulting from a Protein A purification is shown in **Figure 11A**. For each purification, it was clear that the vast majority of the Pep12-Fc protein was located in Collections A/2 and A/3. The purified samples from Expi293 cells were run on SDS-PAGE under reducing and non-reducing conditions. The Pep12-Fc construct was expected to dimerize through the Fc

region. We compared the proteins expressed in both HEK293T and Expi293 cells (**Figure 11B**). The expected size of a Pep12-Fc monomer is around 32.5kD. In the reduced portion (left side) of the gel, the monomer is present in each sample. The dimer is expected to be around 65kD. Though the dimer is visible under non-reducing conditions (right side), higher molecular weight oligomers are seen in both. Based on the molecular weights of those other bands, we hypothesized that the Pep12-Fc protein was forming other oligomers in addition to the dimer and that oligomerization was not due to higher protein expression in Expi cells.

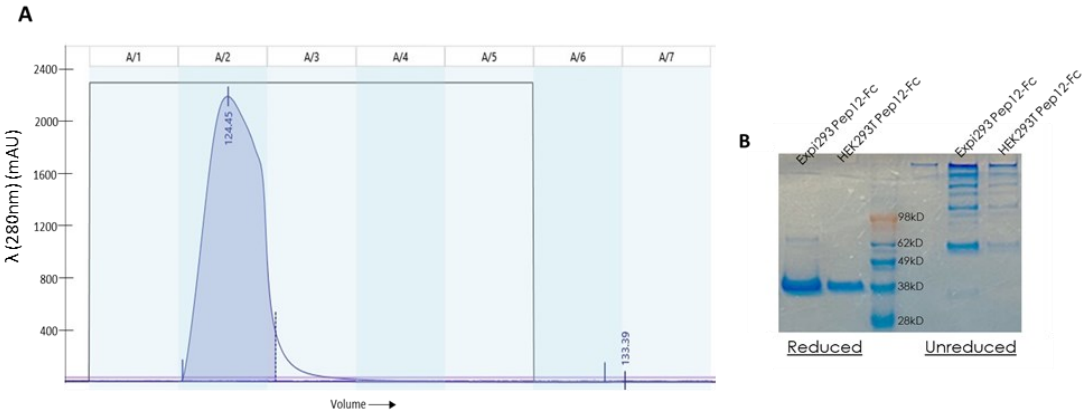

Figure 11. Pep12-Fc Oligomerization. (**A**) Typical 280nm chromatogram of Pep12-Fc Protein A purification. (**B**) Gel of Protein A-purified Pep12-Fc protein from Expi293 and HEK293T cells. The standard used was SeeBlue® Plus2 Prestained Standard (Invitrogen, Cat. #LC5925).

Pep12-Fc Oligomerization: A Function of Time?

We questioned if oligomerization was a result of the protein sitting in the supernatant for multiple days. If the oligomers form while the protein is sitting outside the cell, we could simply collect the supernatant sooner and avoid this issue. We took samples of supernatant from an Expi293™ transfection on each day leading up to

collection on Day 4. Each sample was tested by non-reducing SDS-PAGE. Days 2, 3, and 4 all show the same pattern of oligomers, suggesting that the oligomers likely form at the time of protein secretion in the supernatant (**Figure 12**). Even in Day 2, where there is comparatively little expression, the protein still oligomerizes. Based on this result, it appears that the Pep12-Fc monomers may aggregate inside the cell prior to exocytosis.

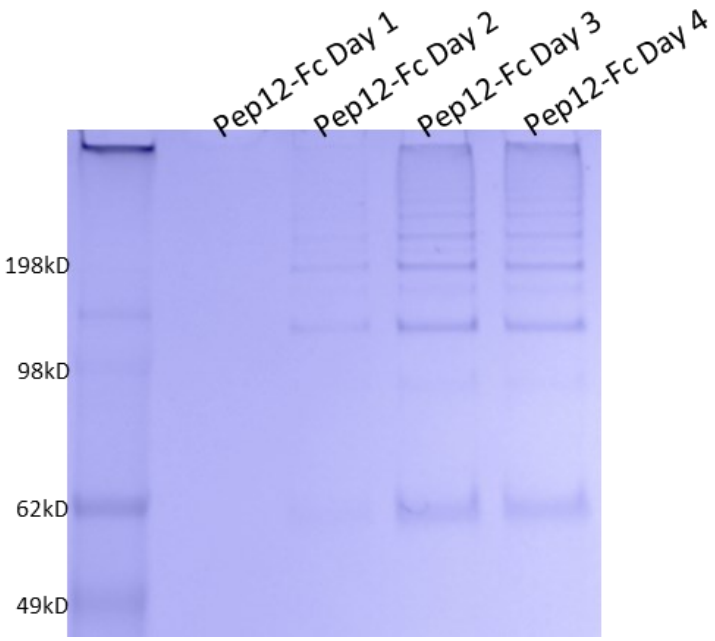

Figure 12. Pep12-Fc Over Time. Unreduced gel of supernatant samples from each day post-transfection in Expi293™ cells. The standard used was SeeBlue® Plus2 Prestained Standard.

Can Pep12-Fc Dimers be Separated from Oligomers?

We hypothesized that the form of Pep12-Fc may influence its ability to bind AMA1, thereby affecting its neutralizing activity. To test this hypothesis, it was necessary to separate the dimer from the oligomers. We tested this by size exclusion chromatography (SEC) to separate the protein forms based on size. The appearance of individual peaks, though they overlapped, indicated that the protein aggregates are

separating based on size (**Figure 13A**). The reduced SDS-PAGE gel illustrates that most of the protein coming out is Pep12-Fc, and the lower molecular weight bands may be fragments of the protein (**Figure 13B**). The non-reduced SDS-PAGE gel showed that fraction 14 and 15 contained higher proportions of the dimer compared to the oligomers (**Figure 13C**). However, SEC was not able to completely separate the dimers.

Next, we attempted to isolate the dimer using a Ceramic Hydroxyapatite (CHT) column. The CHT column separates protein based off differential binding affinity for the resin based on net charge.[92] However, analysis of the fractions by SDS-PAGE showed that this did not improve separation of the dimer and oligomers (**Figures 13D and 13E**). A western blot using anti-Fc antibodies confirmed that the higher molecular weight proteins are indeed Pep12-Fc oligomers (**Figure 13F**).

These results point to SEC as a better approach to enrich the Pep12-Fc dimers. Therefore, we optimized the purification conditions (flow rate, amount of protein loaded, and collection volumes) to further improve protein separation (**Figure 13G**). This optimized SEC resulted in much improved separation of the dimer, as seen by a well-separated peak in fraction A/8 (**Figures 13G and 13H**).

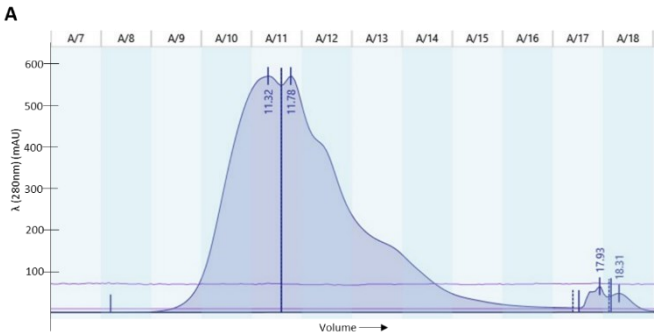
A
A/7
A/8
A/9
A/10
A/11
A/12
A/13
A/14
A/15
A/16
A/17
A/18
600
500
400
300
200
100
λ (280nm) (mAU)
11.32
11.78
17.93
18.31
Volume

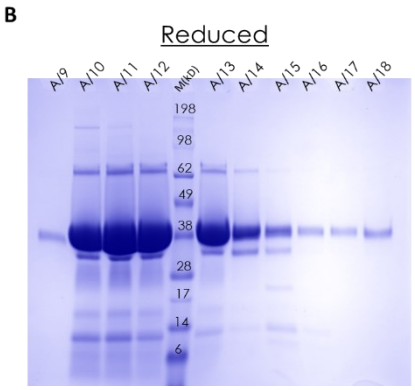
B
Reduced
A/9
A/10
A/11
A/12
M(kD)
A/13
A/14
A/15
A/16
A/17
A/18
198
98
62
49
38
28
17
14
6

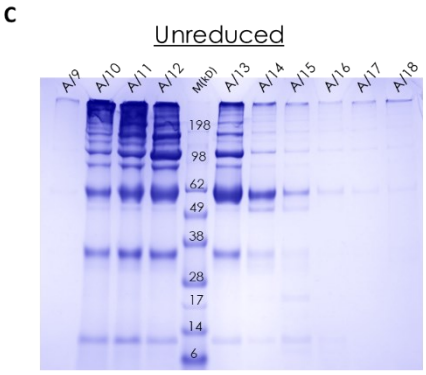
C
Unreduced
A/9
A/10
A/11
A/12
M(kD)
A/13
A/14
A/15
A/16
A/17
A/18
198
98
62
49
38
28
17
14
6

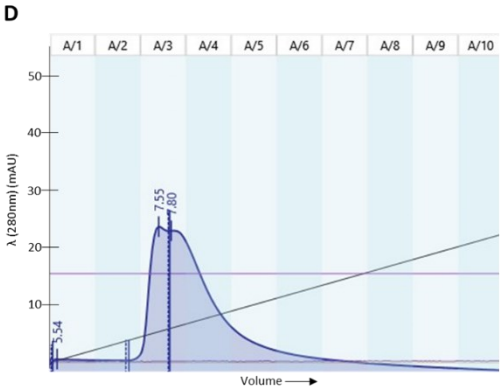
D
A/1
A/2
A/3
A/4
A/5
A/6
A/7
A/8
A/9
A/10
50
40
30
20
10
λ (280nm) (mAU)
7.55
7.80
5.54
Volume

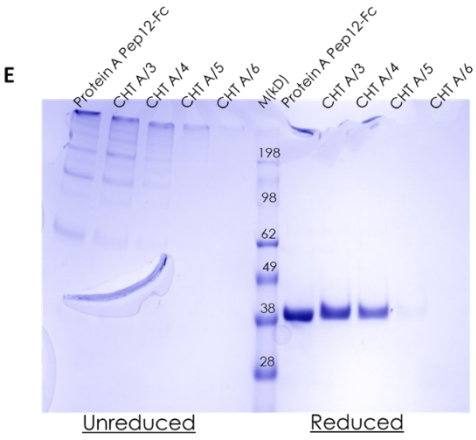
E
Protein A Pep12-Fc
CHT A/3
CHT A/4
CHT A/5
CHT A/6
M(kD)
Protein A Pep12-Fc
CHT A/3
CHT A/4
CHT A/5
CHT A/6
198
98
62
49
38
28
Unreduced
Reduced

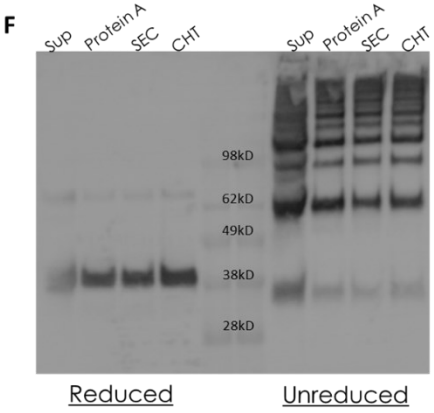
F
Sup
Protein A
SEC
CHT
Sup
Protein A
SEC
CHT
98kD
62kD
49kD
38kD
28kD
Reduced
Unreduced

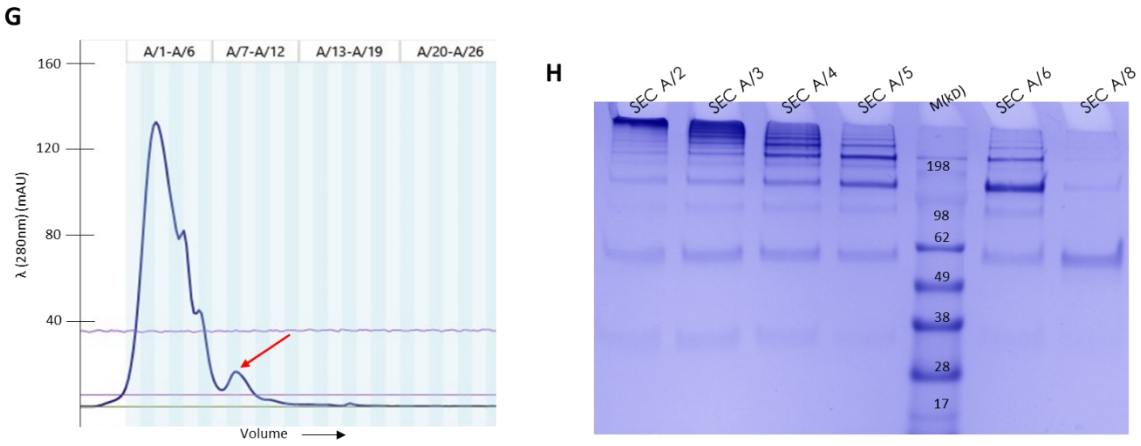

Figure 13. Separation of Pep12-Fc Dimers and Oligomers. (**A**) An A280 chromatogram from an SEC purification of Protein A-purified Pep12-Fc. Many collections from that purification were run on SDS-PAGE under reducing (**B**) and non-reducing (**C**) conditions. (**D**) Chromatogram resulting from a CHT purification of Protein A-purified Pep12-Fc. The dark diagonal line illustrates that the Elution step featured a linear increase in concentration of NaCl. (**E**) Samples from the CHT purification run on a gel under reducing and non-reducing conditions. (**F**) Western blot with reduced and unreduced sides demonstrating the presence of Pep12-Fc oligomers after multiple methods of protein purification. (**G**) Chromatogram at 280nm showing the successful separation of the dimer from the other oligomers by SEC. The red arrow points to A/8, the fraction that almost exclusively contains the dimer. (**H**) Unreduced gel of collections from the successful SEC purification. The standard used in each gel and blot was SeeBlue Plus2 Prestained Standard.

Pep12-Fc AMA1 Binding Activity—The Effect of Oligomerization

Next, we tested if the form of Pep12-Fc (dimer vs. oligomer) affected its ability to bind its target AMA1. An ELISA was performed to compare the Protein A-purified Pep12-Fc, which is comprised of a mixture of dimer and oligomers, and different fractions from SEC (fraction A/8, the Pep12-Fc dimer; and fractions A/5 and A/6, oligomers). Our

results indicate that the Pep12-Fc dimer binds AMA1 better than the oligomers (**Figure 14**).

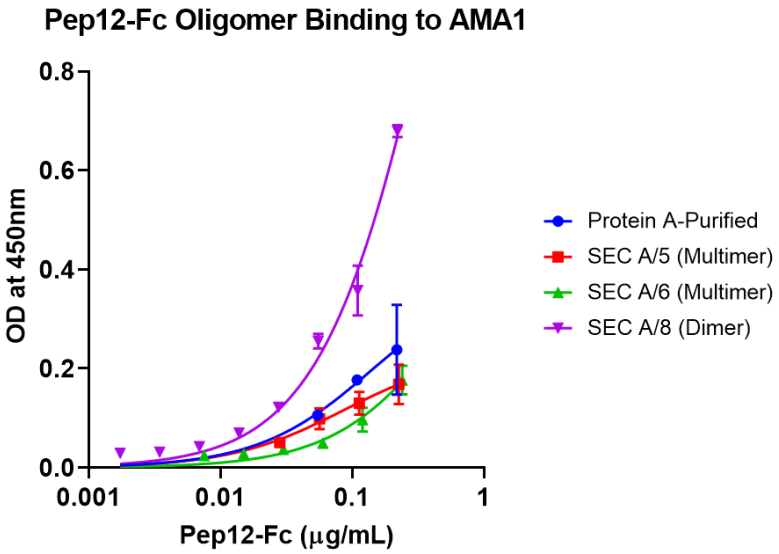

Figure 14. Pep12-Fc Binding to AMA1. Binding curves for AMA1 binding to various Pep12-Fc oligomeric fractions or a mix of all oligomers (Protein A-Purified).

Pep12-Fc Inhibition of P. falciparum *Parasite Invasion*

A growth invasion assay (GIA) was done with *P. falciparum* 3D7 to compare the neutralizing activities of Pep12-Fc and compare its activity to RON2L-Fc. Due to insufficient amount of purified dimer available for this assay, we used Protein-A purified Pep12-Fc that contains both dimer and oligomers. Our results show that the IC_{50} of Pep12-Fc was twice that of RON2L-Fc (**Figure 15**). Interestingly, when synthetic peptides corresponding to Pep12 or RON2L were used, a 10-fold higher potency for Pep12 was observed (**Figure 7C**). However, our ELISA results comparing activity of the different forms of Pep12-Fc indicated that the dimer is likely the active form (**Figure 14**). Since

only a small proportion of the Protein A-purified Pep12-Fc contains the dimeric form, this may be reflected in the neutralization assay. Future studies will evaluate methods to improve production and separation of the Pep12-Fc dimer and test its neutralizing activity against parasites.

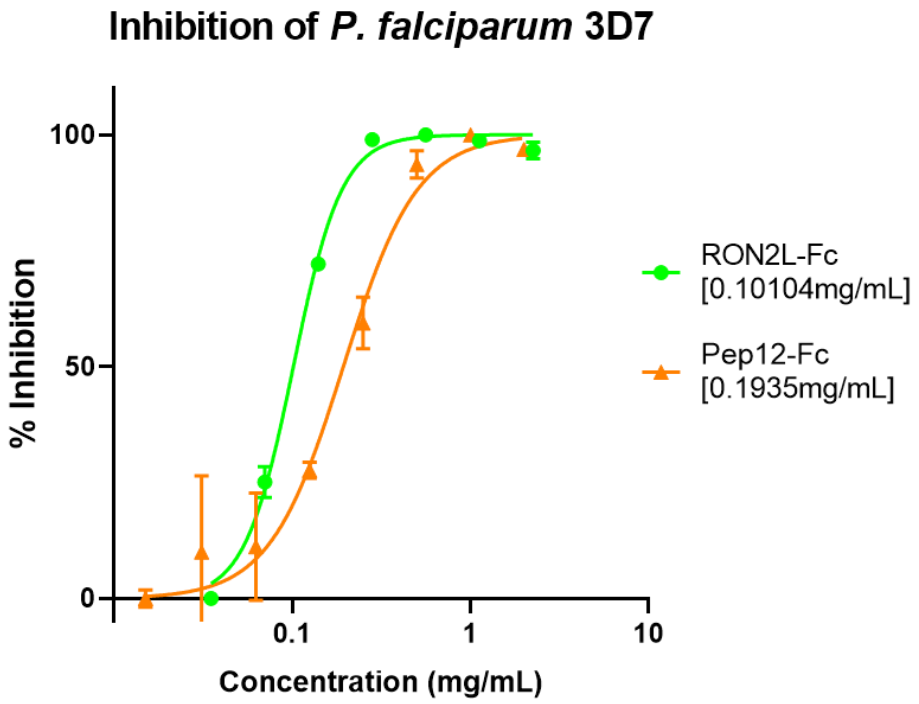

Figure 15. GIA data for Pep12-Fc Inhibition of *P. falciparum*. The corresponding IC_{50} value is shown in brackets.

Expi293™ Expression of SA21ABP-Nterm, SA21ABP-Cterm, and RON2L-ABD035

As described in *Section J* of the Introduction, researchers have developed and refined peptides that bind to albumin. The peptide SA21 was derived from phage display by Dennis et al. (2002); when used as a fusion peptide, it has extended the half-lives of pharmaceuticals without diminishing their functions.[65,66,69] Likewise, Jonsson et al. (2008) introduced ABD035, a peptide generated from Streptococcal protein G, which

has also demonstrated half-life extension as a fusion peptide.[68,69,71-74] We designed constructs that fuse the RON2L peptide to SA21 or ABD035 (plasmid maps in **Figure 5**).

As mentioned previously, the albumin-binding designs of the SA21ABP-Nterm, SA21ABP-Cterm, and RON2L-ABD035 constructs required expression in media that did not contain albumin. First, each plasmid was transfected in the Expi293™ Expression System. Unlike Pep12-Fc, these constructs only possessed a His tag. Since, the AMA1 protein we used also had a His tag, we devised another method for detecting expression, using HisPur™ Ni-NTA Resin to pull down the desired proteins. The boiled beads were then analyzed by SDS-PAGE under reducing conditions (**Figure 16A**). To confirm the gel results, a western blot was done from a second pull-down (**Figure 16B**). The expected sizes of ABP-Nterm, ABP-Cterm, and RON2L-ABD035 are around 8.9kD, 9.1kD, and 12.0kD, respectively. From **Figure 16**, it is clear that RON2L-ABD035 was pulled down and, therefore, is being produced. Conversely, ABP-Nterm and ABP-Cterm were not pulled down, so it is unknown whether they are being expressed. We narrowed our focus to isolating and testing RON2L-ABD035.

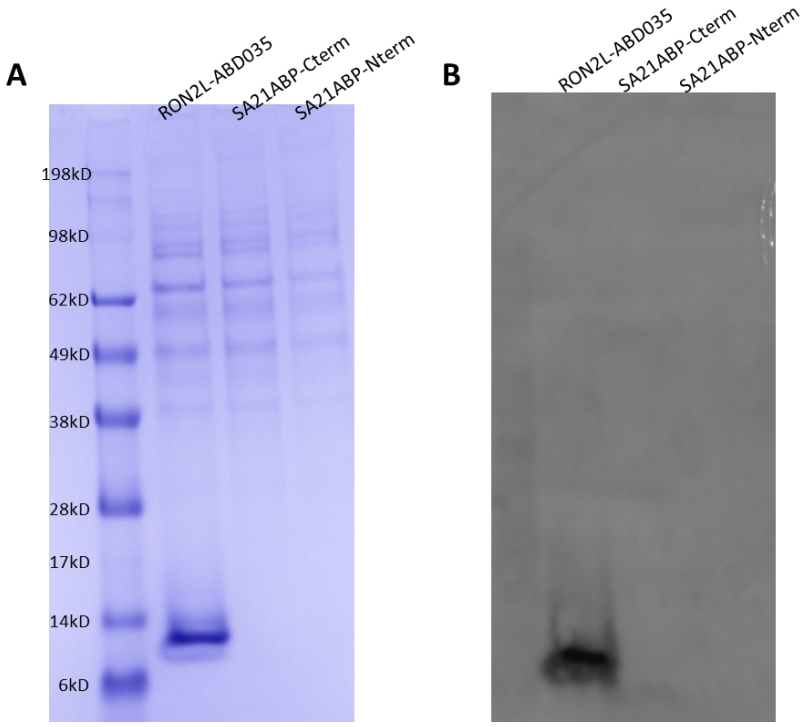

Figure 16. Expression of Albumin-Binding Constructs in Expi293™ Cells. Gel (**A**) and western blot (**B**) showing the presence of RON2L-ABD035 from the pull-downs but a lack of ABP-Cterm and ABP-Nterm. The expected sizes of ABP-Nterm, ABP-Cterm, and RON2L-ABD035 are around 8.9kD, 9.1kD, and 12.0kD, respectively. The standard used was SeeBlue® Plus2 Prestained Standard.

ABD Purification

Using the principle of metal ions binding to histidine tags, we tried to purify the ABD construct using HisPur™ Ni-NTA Resin.[91] Two separate elutions with 300mM imidazole were loaded onto a reducing gel alongside the flow-through, boiled beads, and original supernatant (**Figure 17**). Virtually all of the protein present in the supernatant bound to the beads, as evidenced by the lack of the 12kD protein in the Flow-through, and most of the protein eluted off the beads, shown by the boiled beads. Purification on an immobilized-metal affinity chromatography (IMAC) column yielded

very similar results. Both purification methods were effective in primarily isolating the ABD protein.

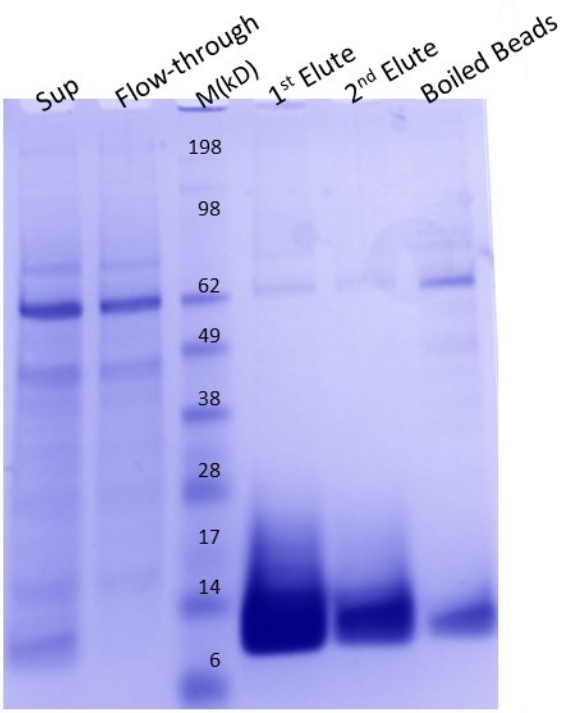

Figure 17. RON2L-ABD035 Purification. Reduced gel of a hand-purification of RON2L-ABD035 using Ni^{2+} beads. The beads were eluted twice, once with 100µL of 300mM imidazole and once with 200µL of 300mM imidazole. The remaining beads were boiled and loaded onto the gel.

RON2L-ABD035 Binding to Serum Albumin

The RON2L-ABD035 protein is composed of two components: a RON2L peptide designed to bind AMA1 and the ABD035 domain for binding albumin. We first assessed the ability of RON2L-ABD035 to bind to albumin. Previous research with albumin binding peptides has shown that the same peptide can exhibit differential binding strengths to different species of albumin.[97] Therefore, we assessed three types of albumin for our

tests by ELISA: bovine, human, and mouse. RON2L-ABD05 bound MSA and HSA but not to BSA (**Figure 18**).

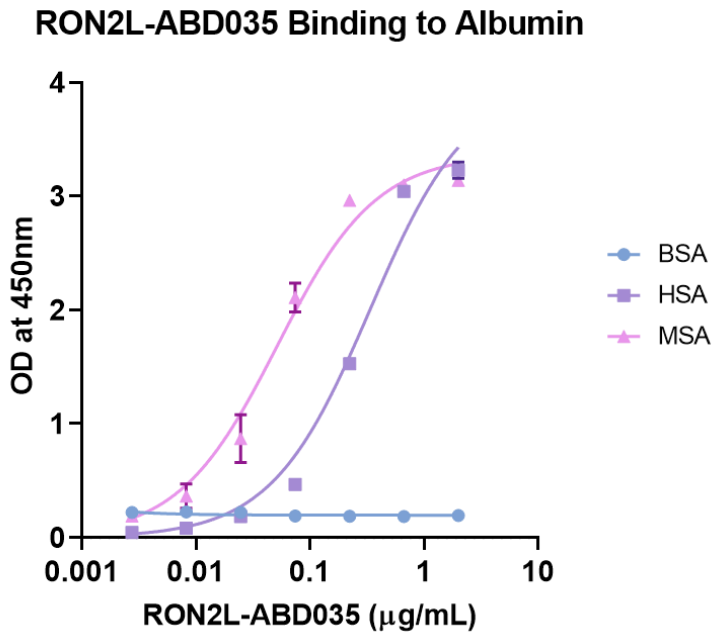

Figure 18. RON2L-ABD035 Binding to Albumin. ELISA showing binding of RON2L-ABD035 to albumin from different species.

RON2L-ABD035 Binding AMA1

Next, we assessed the binding of RON2L-ABD035 to AMA1 by ELISA. Our data demonstrates that RON2L-ABD035 binds to AMA1 in a dose-dependent manner (**Figure 19A**). Combined with the earlier results, our data indicates that the RON2L-ABD035 fusion protein associates with albumin through the ABD domain while successfully interacting with its parasite target AMA1.

We also assessed the RON2L-ABD035 binding to AMA1 by a native PAGE gel shift assay. When AMA1 was mixed with RON2L-ABD035 at a 1:1 molar ratio, a second, slightly higher molecular weight band is visible when compared to AMA1 run alone (**Figure 19B**).

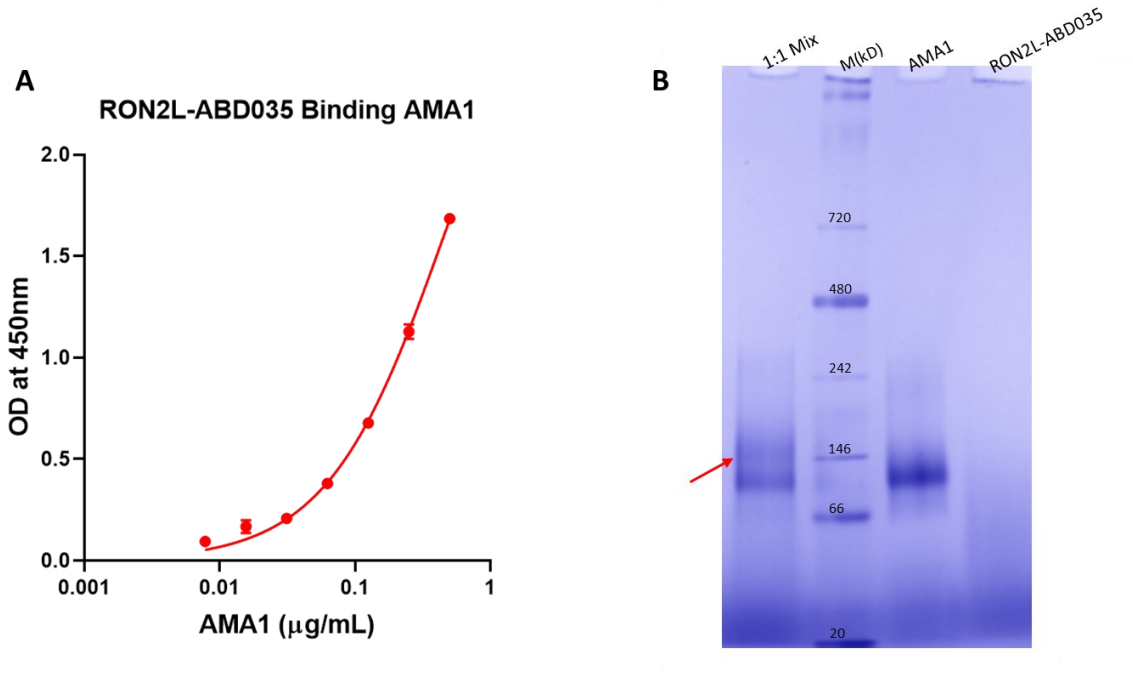

Figure 19. RON2L-ABD035 Binding to AMA1. (**A**) ELISA binding curve of the binding of *P. falciparum* 3D7 AMA1 to RON2L-ABD035. (**B**) Native gel following the gel shift assay of RON2L-ABD035 mixed with AMA1. 1:1 Mix is the mixture of 1mol RON2L-ABD035 and 1mol AMA1. The red arrow points to the higher molecular weight band, indicating the association of the construct with AMA1. The RON2L-ABD035 and AMA1 wells were each loaded with 1mol of the respective protein. The standard used was NativeMark™ Unstained Protein Standard (Thermo, Cat. #LC0725).

RON2L-ABD035 Binding AMA1 and Albumin Simultaneously

A crucial aspect of this protein's effectiveness is its ability to simultaneously bind albumin and AMA1. The protein must bind its parasite target, but albumin binding is critical for the half-life extension. To ensure that albumin binding does not severely diminish the ability to bind AMA1, we performed a sandwich ELISA. Briefly, this ELISA had a 2µg/mL coating of each albumin species. Once the plate was incubated with a spectrum of RON2L-ABD035 concentrations, the plate was exposed to 2µg/mL of AMA1. Protein was detected using 1:1000 of an anti-AMA1 antibody, followed by 1:2500 anti-mouse. The subsequent binding curves are shown in **Figure 20**. These curves show that RON2L-ABD035 is able to bind AMA1 while concurrently binding to MSA or HSA.

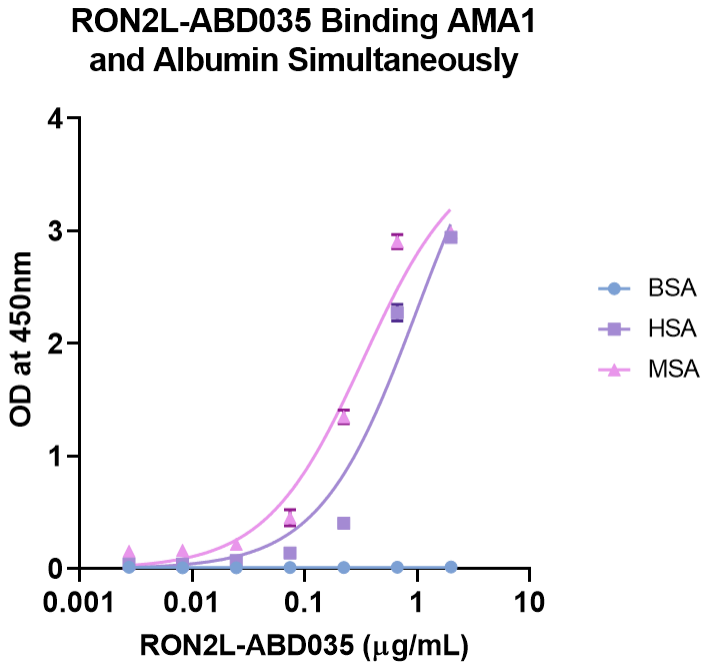

Figure 20. RON2L-ABD035 Binding AMA1 and Albumin Simultaneously. Binding curves of sandwich ELISA showing concurrent binding of RON2L-ABD035 to both AMA1 and albumin.

Discussion

Malaria is an ancient disease that has long been an incredible source of burden for people across the globe. The disease's historical burden is evident from the various mutations in the human genome that confer resistance to *P. falciparum* malaria, including abnormal hemoglobin traits (hemoglobinopathies) like Hemoglobin S—the mutation responsible for the sickle cell trait—and β-thalassemia.[98,99] Malaria has been so deadly that these mutations continue to persist, despite the numerous health defects they bring.[100] The global burden of malaria is not just an artefact of history, however. A comprehensive analysis of data from the Global Burden of Diseases, Injuries, and Risk Factors Study found that malaria was responsible for 45,000,000 disability adjusted life years (DALYs) in 2017.[101] In 2017, malaria comprised 6.5% of all DALYs resulting from all communicable diseases and 1.8% of all DALYs from all causes across 195 countries.[101] Malaria is particularly a problem in low-income countries, where it was the sixth leading cause of death in 2019.[102] The combination of this high public health burden, the lack of a long-term efficacious vaccine, and emerging drug resistance illustrates the need for better alternative therapeutics and vaccine candidates.

Here, we have devised two novel inhibitors of the parasite AMA1-RON2 interaction that is crucial for merozoite invasion into erythrocytes. The first, RON2L, is a small peptide derived from a region of the RON2 protein that binds to the hydrophobic pocket of AMA1.[37,48,49] The other is Pep12, a *de novo*-designed inhibitor based on creation derived from the RON2L structure. The Pep12 peptide was fused to the Fc region of human IgG1, while the RON2L was linked to ABD035, an albumin binding

domain first characterized by Jonsson et al. (2008).[68] We wanted to compare the inhibitory activities of RON2L and Pep12, which was selected for a stronger affinity to AMA1. We chose conjugation to Fc to encourage antibody-mediated complement-dependent inhibition, Ab-dependent cellular inhibition, and phagocytosis in addition to the Pep12 peptide inhibiting cellular entry by competitive binding to AMA1. Both Fc and ABD035 were also used as conjugates to extend the half-life of our construct in serum. We wanted to assess the effects of the two fusion partners on inhibitor activity.

We have demonstrated that our Pep12-Fc fusion can be expressed in HEK293T adherent cells and that those expressed proteins can bind to AMA1. We have also shown that the protein can be more expressed at a 75-fold higher concentration in the Expi293™ Expression System from Gibco. We showed that Pep12-Fc could be separated from other supernatant proteins by both ammonium sulfate and Protein A purifications. This protein is modeled after IgG antibodies, which form dimers *in vivo*. We found that the Pep12-Fc protein forms many different oligomers in addition to dimers, presumably through intermolecular interactions. The Pep12-Fc dimer was hypothesized to be the most active form of the protein, with the best ability to bind AMA1 and inhibit parasite invasion. The dimer proved incredibly difficult to separate from the other oligomers. Protein A purification only separated other proteins from the mix of Pep12-Fc oligomers, and the Ceramic Hydroxyapatite (CHT) column also proved unfit to separate the forms. Ultimately, Size Exclusion Chromatography (SEC) was able to separate the various oligomers. GIA showed that the mix of Pep12-Fc oligomers did not enhance neutralization compared to RON2L-Fc, compared to what was observed with the

corresponding synthetic peptides. Using an ELISA, we showed that the dimer is clearly able to bind AMA1 more effectively than the other oligomers individually and the mix of all the oligomers, possibly explaining the lack of enhancement in neutralizing activity when using a predominantly oligomeric form of Pep12-Fc.

Because the RON2L-ABD035035 protein binds albumin, HEK293T cells were not a viable option for expression of that protein. Instead, we demonstrated that the RON2L-ABD035 conjugate could be expressed in the Expi293™ Expression System. Additionally, the presence of a histidine tag allows the protein to bind to Ni^{2+}. We showed that the protein could be purified using either immobilized-metal affinity chromatography (IMAC) or Ni^{2+} beads. Through both a gel shift assay and an ELISA, we have shown that this RON2L fusion protein can bind to AMA1, its intended target. By ELISA, we found that RON2L-ABD035 can bind to the albumin proteins of mice, humans, and rats. Crucially, we found via sandwich ELISA that the RON2L-ABD035 protein can simultaneously bind albumin (from human, mouse, or rat) and AMA1, a critical aspect of the combination protein's effectiveness (conferred by the RON2L peptide) and longevity (resulting from the ABD035 binding to albumin).

Future Directions

The purification of the Pep12-Fc protein is critical for its viability as a potential drug or vaccine. Though the first stage of purification in this study was mostly done on a Protein A column, the slow flow rate necessary for the Protein A column renders it impractical to use for large-scale purifications. For those larger purifications, our

optimized ammonium sulfate purification is much more favorable. The most challenging aspect of the purification, however, is the effective separation of the dimer from the rest of the oligomers that form. While the RON2L contains 2 cysteines, which form a single disulfide bond, the Pep12 peptide has 4 cysteines. These cysteines may be linking various Pep12-Fc peptides together, or they may interfere with the disulfide bond in the hinge region that joins two IgG monomers together. Since such a small proportion of the secreted protein is in the dimeric form, it would also be prudent to find a way to convert the various oligomers into the dimer. Attempts to remove any remaining dimer using sequential purification with an Amicon® Ultra-15 100kD Centrifugal Filter Unit (Millipore, Cat. #UFC910024) followed by an Amicon® Ultra-15 30kD Centrifugal Filter Unit (Millipore, Cat. #UFC903024) were unsuccessful (data not shown). It will likely be necessary to separate the bonds holding the oligomers together and re-form them. However, before going through the rigorous process of resolving the oligomerization issue, the various Pep12-Fc fractions should be tested alongside the dimer by GIA to confirm that the dimer has superior inhibitory ability.

GIA data is needed to verify that Pep12-Fc, especially as a dimer, and RON2L-ABD035 effectively block parasite invasion. Moreover, other strains of *P. falciparum* aside from 3D7 should also be tested by GIA. An inhibitor with cross-strain activity is critical for any drug or vaccine candidate. The Pep12-Fc dimer should have lower IC_{50} values than Dr. Deepti Sarkar's RON2L-Fc conjugates, since the Pep12-Fc is supposed to be an enhanced version of Pep12-Fc. For RON2L-ABD035, it would also be useful to perform surface plasmon resonance with different species' albumin proteins to

generate dissociation constants. Once sufficient GIA data has been obtained, both constructs should have their inhibitors replaced with an analogous inhibitor of *P. yoelii*, a species of mouse malaria. From there, those mouse-adapted constructs will be dosed in mice to measure the longevity of the constructs in serum. For a control, other mice will be dosed with just the PyRON2L peptide. Once the constructs' time in serum has been determined, they will be assessed for their ability to prevent symptomatic disease in a mouse malaria challenge. While those studies are being conducted, the constructs should be tested for the ability to bind sporozoites and inhibit sporozoite invasion into hepatocytes. The ultimate goal for these constructs is for them to show promise as potential drugs or vaccines to prevent symptomatic and systematic malarial disease.

Part II: Evaluating a Surrogate Assay to Measure the Neutralizing Activity in Convalescent Plasma against SARS-CoV-2

Introduction

L. Global Burden of COVID-19

On December 30, 2019, ProMED reported the circulation of an "urgent notice on the treatment of pneumonia of unknown cause" coming out of the city of Wuhan in the Hubei province of the People's Republic of China.[103] The next day, the WHO's Country Office in China learned of these cases of "viral pneumonia."[104] Later analysis found that the earliest reported symptom onset occurred on December 1, 2019.[105] On January 9, 2020, the WHO reported that the outbreak was caused by a novel coronavirus that was termed 2019-nCoV shortly thereafter.[104] That January, researchers from the Wuhan Institute of Virology found that 2019-nCoV shared a 79.6% sequence homology with SARS-CoV BJ01, an isolate of the virus responsible for the severe acute respiratory syndrome (SARS) outbreak in 2003.[106,107] From this result, the authors concluded that 2019-nCoV was a part of the *SARSr-CoV* species of betacoronaviruses.[106] Furthermore, additional analysis found 96.2% sequence identity to BatCoV RaTG13, a coronavirus that infects bats.[106] Though the origins of the virus are unclear, it very likely entered the human population from an as yet unidentified animal reservoir.[108] Further molecular analysis has found that the virus is related to ones that circulate in bats and pangolins.[109] The Coronavirus Study Group of the International Committee on Taxonomy of Viruses named the novel coronavirus SARS-CoV-2 on February 11.[110]

The first death from SARS-CoV-2 was documented in China on January 11, 2020. According to the WHO's first Novel Coronavirus (2019-nCoV) Situation Report, published on January 21, a total of 6 deaths had been reported in Wuhan City.[111] The 282 total

confirmed cases were spread across four countries: China, Japan, Thailand, and the Republic of Korea. The first person in the United States diagnosed with the disease was formally diagnosed by the Centers for Disease Control and Prevention (CDC) on January 20.[112] Notably, a later analysis of serology samples found many samples collected prior to January 20 that were reactogenic to SARS-CoV-2, suggesting that the virus may have been introduced to the United States as early as December 13, 2019.[113] Per the WHO's eight Situation Report, published on January 28, the number of confirmed cases had ballooned to 4,593 across 15 countries, including Australia, France, and Germany along with the ones previously mentioned.[114] 106 deaths had occurred in China.[114] In a speech on February 11, Dr. Tedros Adhanom Ghebreyesus, the Director-General of the WHO, named the new disease COVID-19.[115] By that point, 393 cases and 1 death had been reported across 24 countries (excluding China); China had reported 42,708 cases and 1,017 deaths.[115] Exactly one month later, on March 11, Dr. Ghebreyesus declared COVID-19 as a pandemic.[116] At the time of that declaration, COVID-19 had accounted for a total of 118,000 cases and 4,291 deaths across 114 countries.[116] This pandemic still rages over one year later. According to the widget from the Johns Hopkins Coronavirus Resource Center, there have been 122,631,601 cumulative cases and 2,705,724 deaths across 192 countries as of March 20, 2021.[117] The United States leads the world in cases, with 29,780,301 in total, and deaths, with 541,738.[117]

M. Convalescent Plasma

Serum therapy, “the administration of immune serum for the treatment of infections,” was first discovered for the treatment of diphtheria in 1890.[118] Subsequently, serum therapy was used for a variety of infectious diseases, including tetanus, measles, and mumps, up until the 1940s.[118,119] Furthermore, convalescent plasma has also been used in several major public health events, like the 1918 influenza pandemic and the 2009-2010 H1N1 influenza pandemic.[120] Based on this precedent, Casadevall and Pirofski proposed the administration of COVID-19 convalescent sera for means of prophylaxis and treatment of disease in March 2020.[120] Its use, they argued, would be particularly beneficial in light of the lack of effective treatments or vaccines for COVID-19.[120]

In June 2020, Li et al. published the results of the first randomized clinical trial involving the use of COVID-19 convalescent plasma (CCP).[121,122] Within 28 days, the patients who received CCP did not improve any faster than those who did not, and there was also no significant difference in 28-day mortality or in “time from randomization to death” or randomization to discharge.[122,123] The study only used 103 participants, instead of the intended 200, so the statistical power of the results was reduced.[121,122] Based on the evidence provided by this and other clinical trials, the United States Food and Drug Administration (FDA) issued an Emergency Use Authorization (EUA) on August 23 for the use of CCP.[124] In its reasoning for granting the EUA, the FDA noted the possible benefits of this treatment appeared to outweigh the potential risks of its use.[125] However, the Infectious Diseases Society of America made the recommendation that CCP only be used in the context of a clinical trial.[126]

Randomized controlled trials since that point have yielded mixed results. A trial from the Randomised Evaluation of COVID-19 therapy (RECOVERY) series of trials was conducted with 11,558 participants.[127] This trial found no significant difference in survival or other clinical outcomes, and the results were consistent across all subgroups.[127] The authors of this study also performed a meta-analysis on nine other randomized trials and determined that, across all of those trials, CCP does not improve mortality.[127] Conversely, Libster et al. (2021) conducted a trial with 160 older adult patients with CCP administration within 72 hours of mild COVID-19 symptom onset.[128] They found that CCP administration reduced the risk of progression to severe disease by 48% as compared to the placebo group.[128] The treatment group also had a reduced risk of all secondary end points.[128] A retrospective analysis of 3082 patients from across the US found that transfusion of plasma with high antibody levels was associated with a lower risk of death in patients not receiving mechanical ventilation.[129] This study also found a lower risk of death in those who received plasma within 72 hours of diagnosis, reinforcing the results from Libster et al.[129] Therefore, the FDA modified the EUA for CCP on March 9, 2021, limiting the authorization to the use of high titer CCP for the treatment of hospitalized patients early in the disease course.[130] Low titer CCP use is not authorized.[130]

N. SARS-CoV-2 Structure and Entry

SARS-CoV-2, like other coronaviruses, is an enveloped virus with a Spike (S) glycoprotein on the surface of the particle.[131] The structure of the virion is shown in

Figure 21A. The S protein is a Class I fusion protein that exists in a trimeric conformation.[132,133] Like other Class I fusion proteins, this S protein binds to host cell receptors and can undergo a post-translational cleavage event to be able to fuse with the cell membrane.[133] In the case of SARS-CoV-2, the protein is cleaved by the protease furin and TMPRSS2.[133,134] Just like SARS-CoV (also known as SARS-CoV-1), the etiologic agent of SARS, the SARS-CoV-2 S protein uses the angiotensin-converting enzyme 2 (ACE2) on the surface of mammalian cells as an entry receptor.[106,135] The S1 subunit includes the receptor binding domain, which can be concealed ("down") or exposed ("up"), as shown in **Figure 21B**. During the entry process, the (RBD) will bind to ACE2 when it is exposed.[131-133] This binding event can trigger the other two RBDs in the trimer to also bind other ACE2 proteins, opening up the center of the S trimer (**Figure 21C**).[133] RBD binding to ACE2 causes a conformational change, triggering the fusion peptide of S2 to fuse with the host cell membrane.[133] Therefore, the interaction between ACE2 and the RBD of the S1 subunit of the S protein is the critical step in SARS-CoV-2 entry.

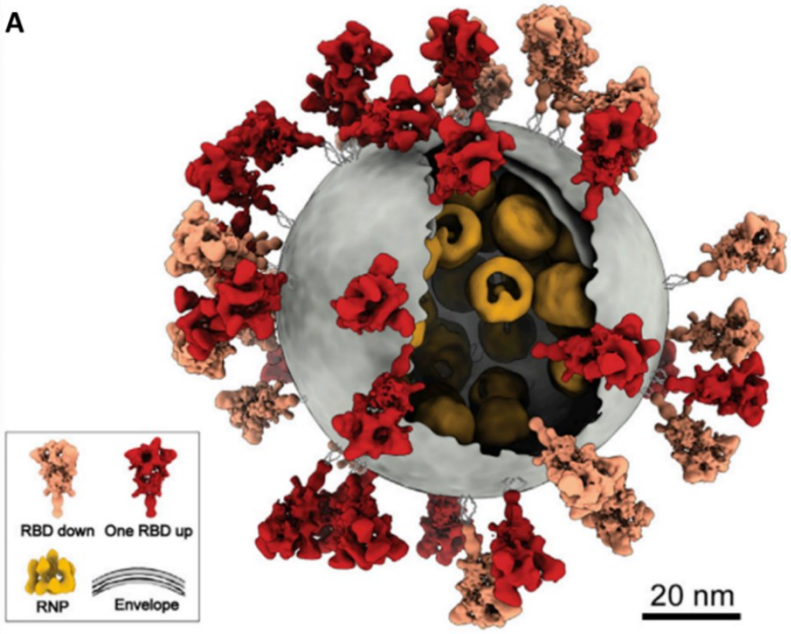

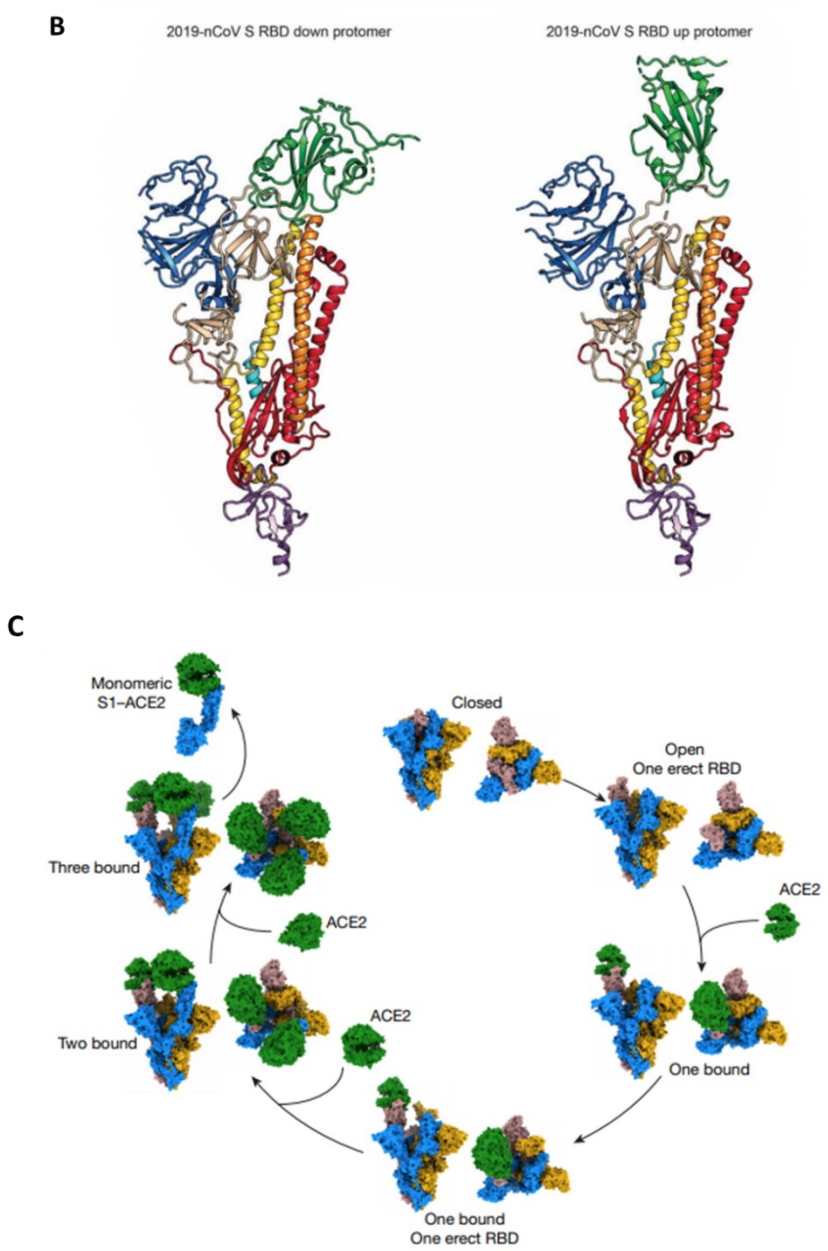

Figure 21. SARS-CoV-2 Structure and ACE2-Binding. (**A**) Structure of SARS-CoV-2 virion.[136] (**B**) Ribbon structure of S protein with RBD in down (left) and up (right) conformations.[132] The RBD is shown in green, the fusion peptide is in turquoise, the site of proteolytic cleavage is circled in black, and S2 is red. (**C**) Sequential binding of the S trimer to ACE2 on the surface of a cell.[133] The S monomers are shown in blue, rosy brown, and gold, and ACE2 is green. "Each step shows two views of the spike complexes: a trimer axis vertical view (left) and an orthogonal top-down view along the axis (right)."[133]

O. Antibody Neutralization of SARS-CoV-2

Antibodies, especially those with neutralizing abilities, are essential for immunity to any pathogen. The RBD is strongly immunodominant, and it is the target of 90% of the neutralizing antibodies to the virus.[137] Because of this strong immunodominance, many monoclonal antibody (mAb) therapies and drugs that target the RBD or the S protein more broadly are in development.[138] In another indication of the immunogenicity of the spike protein, the SARS-CoV-2 virus has been shown to mutate its RBD to evade neutralizing antibodies (nAbs).[139,140] On December 9, 2020, it was reported that a healthcare worker in Brazil presented with two separate clinical episodes of COVID-19.[141] Upon sequencing, it was determined that these two infections were caused by two different lineages of SARS-CoV-2: B.1.1.33 and B.1.1.28.[141] After further analysis, Resende et al. discovered that this sample of B.1.1.28 responsible for reinfection contained an E484K mutation in the S protein, a position known to be part of an epitope for neutralizing antibody binding.[141] They also determined that this variant was circulating in multiple states across Brazil.[141] The ability of the virus to mutate to evade memory-generated antibodies that target the spike protein may make CCP and vaccination efforts for COVID-19 much more challenging.

P. Summary

Because of the newest EUA for CCP, it is necessary to analyze donated serum samples to determine the level of neutralizing titers.[130] Klein et al. (2020) used virus neutralization assays and ELISAs to test the amounts of nAbs.[142] Their process of

collecting and analyzing donor plasma samples is shown in **Figure 22**. They showed that some subcategories of donors generated more nAbs than others, particularly in men, people who are older, and people who have previously been hospitalized for COVID-19.[142] Developing a viable ELISA test for neutralizing titers is important, however, because of the challenges associated with the other method used by Klein et al.[142] Specifically, that method requires the use of live, viable virus, which necessitates a BSL-3 clearance.[142]

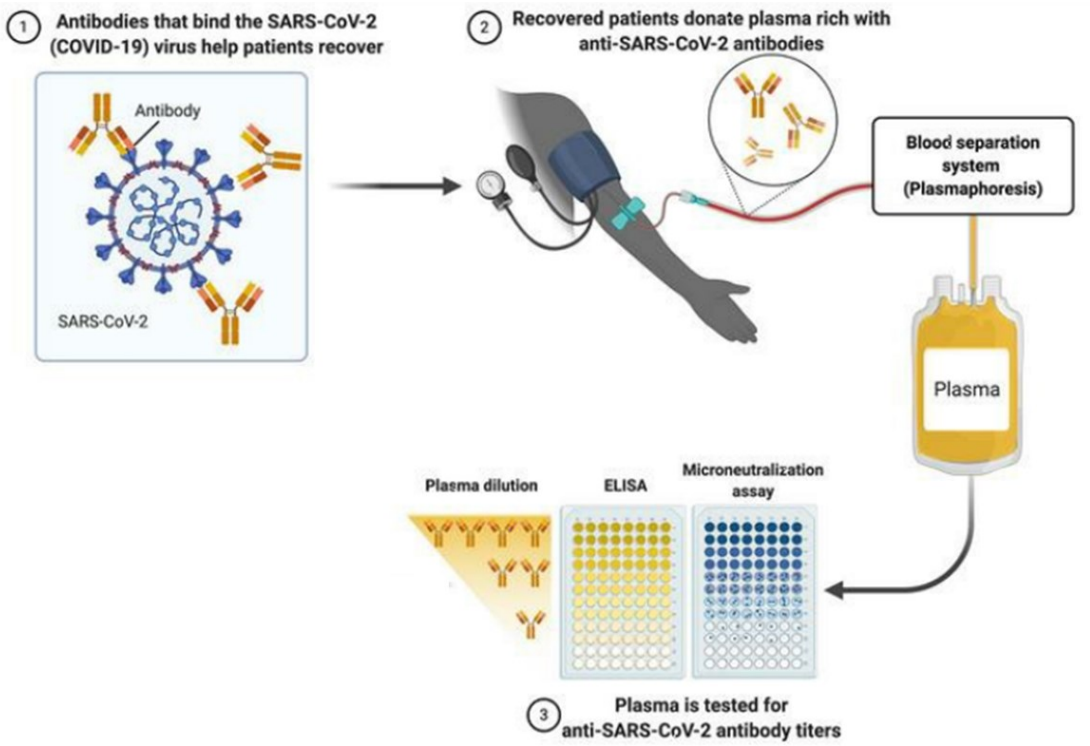

Figure 22. Process of Collecting and Screening Donor CCP Samples. Adapted from Klein et al. (2020).[142]

Here we expressed the RBD and the full-length S protein of SARS-CoV-2. We anticipate that our proteins will be able to functionally bind ACE2 and be bound by anti-SARS-CoV-2 antibodies. Additionally, we optimized a competition ELISA as a surrogate method to measure relative levels of nAbs in donor plasma samples. Finally, we

analyzed correlation between RBD-ACE2 blocking antibody levels, ELISA titer, and virus neutralizing titer.

Materials and Methods

Plasmid Design and Cloning

The plasmids for the receptor binding domain (RBD) and Spike protein from SARS-CoV-2 used were both described in Amanat et al.[143] In the Spike protein, one Ala replaced the polybasic/furin cleavage site (RRAR) (**Figure 23A**). Additionally, a thrombin cleavage site, T4 foldon tetramerization domain, and 6x histidine tag replaced the transmembrane and endodomain at the 3' end of the gene. The RBD also had a histidine tag inserted at the 3' end (**Figure 23B**).

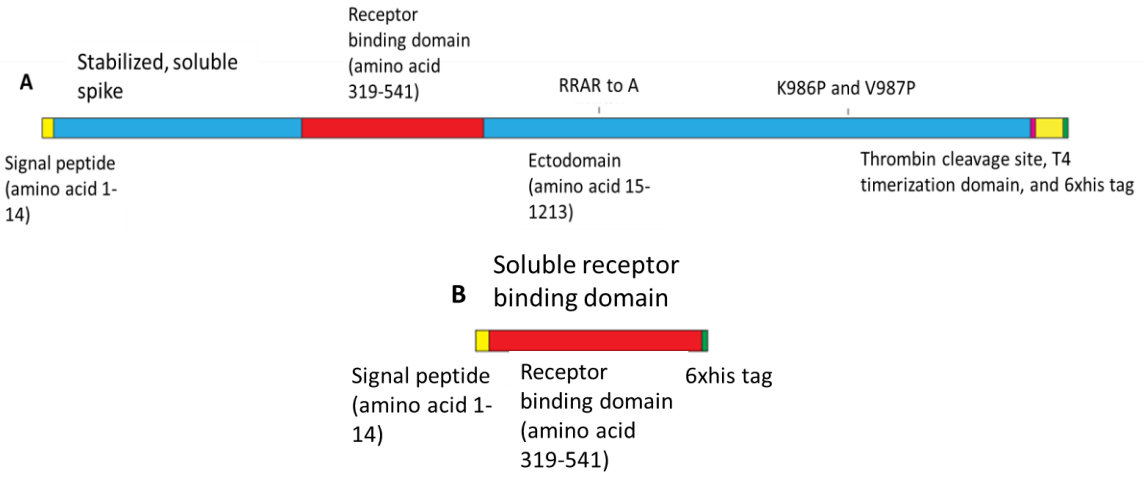

Figure 23. Plasmid Design of SARS-CoV-2 Proteins. Design for the Spike (**A**) and RBD (**B**) plasmids. The signal peptide is shown in yellow, the RBD is red, and the His tag is in green. The plasmids are described in Amanat et al.[143]

Transformation into E. coli *and Plasmid Preparation*

The SARS-CoV-2 RBD and SARS-CoV-2 SPIKE plasmids were generated in the lab of Dr. Andrew Pekosz. The plasmids were then transformed into XL-10 Gold® Ultracompetent Cells (Agilent Technologies, Cat. #200314). The transformation

procedure and plasmid preparation procedures are detailed in the Methods section in Part I.

Protein Production, Purification, and Analysis

HEK293T Cell Transfection

The plasmids were transfected into Human Embryonic Kidney 293T (HEK293T) cells using either jetPRIME Reagent (Polyplus, Cat. #114-15) or polyethylenimine (PEI) using the procedure outlined in *HEK293T Cell Transfection* in Part I (p. 23). Proteins were purified using nickel-NTA beads (or IMAC FPLC column) and analyzed by SDS-PAGE and western blotting, as described in the Part I Methods.

Size Exclusion Purification of RBD

To remove any proteins that were significantly larger or smaller, the RBD elute was further purified by size. For the RBD protein, the elute was first passed through an Amicon Ultra-2mL 50kD Centrifugal Filter (Millipore, Cat. #UFC205024) to remove larger proteins (the RBD construct was about 35kD). Next, the flow-through that contained the protein was passed through a Pierce™ 10kD Concentrator (Thermo, Cat. #88513) to remove any low molecular weight proteins. All fractions were run via SDS-PAGE or western blot to confirm the location of the desired protein.

Testing Activity of Recombinant RBD

An ELISA assay was performed to test the ability of recombinant RBD to bind to ACE2. A half-area 96-well ELISA plate was coated with serial dilutions of mFc tagged RBD (GenScript, Cat. #Z03491-100), His-tagged Spike S1 (GenScript, Cat. #Z03485-100), or in-house expressed recombinant RBD, each starting at concentrations of 4µg/mL, and the plate was stored overnight at 4˚C. All dilutions were done in 1x PBS. The next day, the plate was incubated with ELISA Blocking Buffer (1x PBS, 0.1% Tween 20, 1% BSA) for 1 hour. 2µg/mL of ACE-2 Fc Chimera, Human (GenScript, Cat. #Z03484-100) was added to each well and was allowed to incubate for 1 hour at room temperature. 1:5000 ACE2/Angiotensin-Converting Enzyme 2, Rabbit PAb (Sino Biological, Cat. #10108-T56) primary antibody, 1:2500 Anti-rabbit IgG (H+L) (Goat) Antibody Peroxidase Conjugated (Min x Human Serum Proteins) (Rockland, Cat. #611-1322-0100) secondary antibody, and HRP substrate were used to detect binding of ACE2 to RBD.

Plasma Sample Analysis

Convalescent Plasma Samples

Plasma A+ 6-23-2020; CP-COVID 18-6-2020; and CP-COVID A- 6-23-2020 were obtained from Dr. Arturo Casadevall's laboratory to optimize assays.

Ambulatory Plasma Samples

Ambulatory plasma samples (n=86) were collected by Dr. Yukari Manabe.[144] Dr. Andrew Pekosz provided aliquots of these samples for testing.

Optimization of ELISA using Convalescent Plasma

Convalescent samples Plasma A+ 6-23-2020; CP-COVID 18-6-2020; and CP-COVID A- 6-23-2020 were used to optimize ELISA conditions. Antibody titer was tested against both the RBD domain and the S1 subunit. The parameters optimized include the concentration and identity of the coating antigen, the length of incubation, the choice of secondary antibody, the substrate used, and the assay format (96-well, half-area 96-well, and 384-well plates). The assay after optimization was conducted as follows:

Wells of a half-area 96-well plate were coated with 0.5µg/mL of either RBD (GenScript, Cat. #Z03491-100) or S1 (GenScript, Cat. #Z03485-100) and stored overnight at 4˚C. The next day, ELISA Blocking Buffer (1x PBS, 0.1% Tween 20, 1% BSA) was added to each well and incubated for 1-2 hours. 2-fold serial dilutions of these plasma samples in ELISA Blocking Buffer were performed in triplicate, starting at a 1:40 dilution. The samples were added to the plate and incubated for 1 hour at room temperature. Plates were washed 3 times with Wash Buffer (1x PBS, 0.1% Tween 20), and incubated with 1:10000 diluted Goat Anti-Human IgG (H+L)-HRP (Southern Biotech, Cat. #2016-05). Then, BioFX TMB Super Sensitive One Component HRP Microwell Substrate (Surmodics, Cat. #TMBS-0100-01) was added to each well. After 2 minutes, an equal volume of TMB Stop Reagent, 450nm (Bioworld, Cat. #21530071-1) was added to each well. The plate was read at 450nm-650nm.

ELISA Using Ambulatory Plasma

Plasma samples were centrifuged for 15 minutes at 12,000rpm and 4˚C to remove debris. Each plasma sample was 3-fold serially diluted in duplicate, starting at 1:50. Normal hAB Plasma (Sigma) was used as a negative control. These dilutions were made on the same day the plate was coated, and the dilution plate was stored overnight at 4˚C. The ELISA was performed as described above, and bound anti-RBD antibodies were detected using anti-human IgG (H+L) (1:10000 dilution) and BioFX TMB HRP Substrate. A total of 57 plasma samples were tested by this assay.

Optimization of Competition ELISA to Measure RBD-ACE2 Blocking Activity using Convalescent Plasma

The three convalescent plasma samples (Plasma A+ 6-23-2020; CP-COVID 18-6-2020; and CP-COVID A- 6-23-2020) were tested in a competition ELISA to evaluate the levels of antibodies blocking binding of RBD to ACE2. 2-fold serial dilutions of the plasma samples in triplicate, starting at a 1:5 dilution, were used in these optimization assays. The parameters optimized include the concentration and identity of coating antigen, the duration of competition (i.e., incubation time of plasma with RBD), the choice of secondary antibody and substrate, and the assay format (96-well, half-area 96-well, and 384-well plates). The assay after optimization was conducted as follows:

Half-area 96-well ELISA plates were coated with 1µg/mL of mFc-tagged RBD and stored overnight at 4˚C. The following day, ACE-2 Fc Chimera, Human (GenScript, Cat. #Z03484-100) (2µg/mL final concentration per well) was added 2-fold serially diluted individual plasma samples in duplicate (starting at 1:2.5 dilution) and incubated for 5

minutes. This mixture was added to the RBD-coated plate and incubated for 1 hour at room temperature. Following 3 washes, ACE2/Antiotensin Converting Enzyme 2, Rabbit PAb (Sino Biological, Cat. #10108-T56) primary antibody and Anti-rabbit IgG (H+L) (Goat) Antibody Peroxidase Conjugated (Min x Human Serum Proteins) (Rockland, Cat. #611-1322-0100) secondary antibody were used and absorbance was measured at 450nm. Wells with no plasma were used as controls, and the absorbance OD from these wells were set as 100% ACE2 binding (max, no competition). The blocking activity (%) was calculated using the following formula: $\frac{OD_{Max(no\ competition)} - OD_{Sample}(competition)}{OD_{Max(no\ competition)}} * 100$, where OD_{Max} is the optical density of the wells that only included ACE2 (no plasma added). A total of 86 plasma samples were tested by this method.

Statistical Analysis

As described in Klein et al. (2020), the area under the curve (AUC) values were calculated by graphing the normalized OD values against the ELISA sample dilutions.[142] Correlations were calculated using Pearson's correlation coefficient.

Study Approval

Per Klein et al. (2020), "The Johns Hopkins University School of Medicine IRB reviewed and approved the sample collection protocols and overall study. All participating subjects provided written informed consent."[142]

Results

Expression of RBD and Spike in HEK293T Cells

The SARS-CoV-2 receptor binding domain (RBD) and full-length Spike protein plasmids were transfected into HEK293T cells to test for protein expression. Proteins in the culture supernatants were pulled down His-Tag Isolation and Pulldown using Dynabeads™. After washing, the beads were boiled, and samples were analyzed by SDS-PAGE under reducing conditions. The arrows in **Figure 24A** point to the bands corresponding to recombinant Spike (134kD) and RBD (35kD) proteins, respectively. Western blot using anti-His antibodies confirmed expression of the proteins (**Figure 24B**). The gel and the western blot indicated that both proteins were expressed.

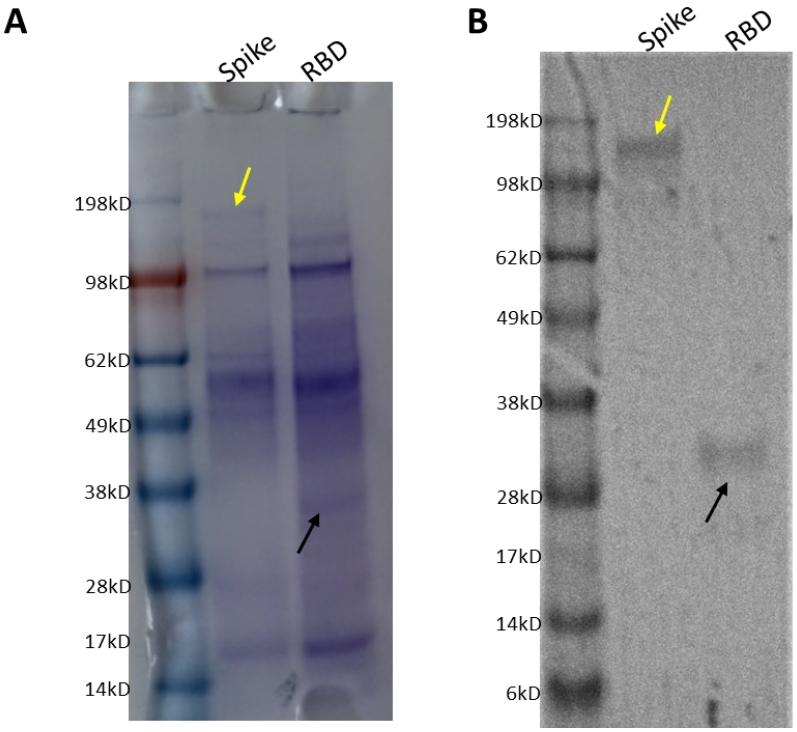

Figure 24. HEK293T Cell Expression of RBD and Spike Proteins. (**A**) Gel indicating expression of RBD and Spike in HEK293T cells. (**B**) Western blot showing Spike and RBD expression. The Spike protein (yellow arrow) is about 134kD, and the RBD protein (black arrow) is around 35kD.

Recombinant RBD Purification

Recombinant RBD protein was purified using a HisPur™ Ni-NTA Spin Column to isolate the RBD protein. Once the supernatant was passed through the column, the column was washed 7 times each with 25mM imidazole and 40mM imidazole in 20mM Sodium Phosphate Buffer pH 7.4, 300mM NaCl (25mM and 40mM IBB). Next, the protein was eluted stepwise with 100mM imidazole, 300mM imidazole, and 500mM imidazole. A typical purification is shown in **Figure 25A**. Higher molecular weight contaminating proteins were effectively removed by passing the elute through a 50kD filter, and the flow-through containing RBD was concentrated using a 10kD filter. The SDS-PAGE gel in **Figure 25B** shows the 50kD top concentrate, which contains the larger impurities, and the 10kD top concentrate showing the purified RBD sample. While some protein was lost in the 50kD filtration, the size exclusion was effective in providing highly pure RBD protein. An ELISA assay with a 4μg/mL RBD coating was performed to

test the ability of the recombinant RBD protein to bind ACE2. The RBD protein demonstrates a dose-dependent binding affinity for ACE2 (**Figure 25C**).

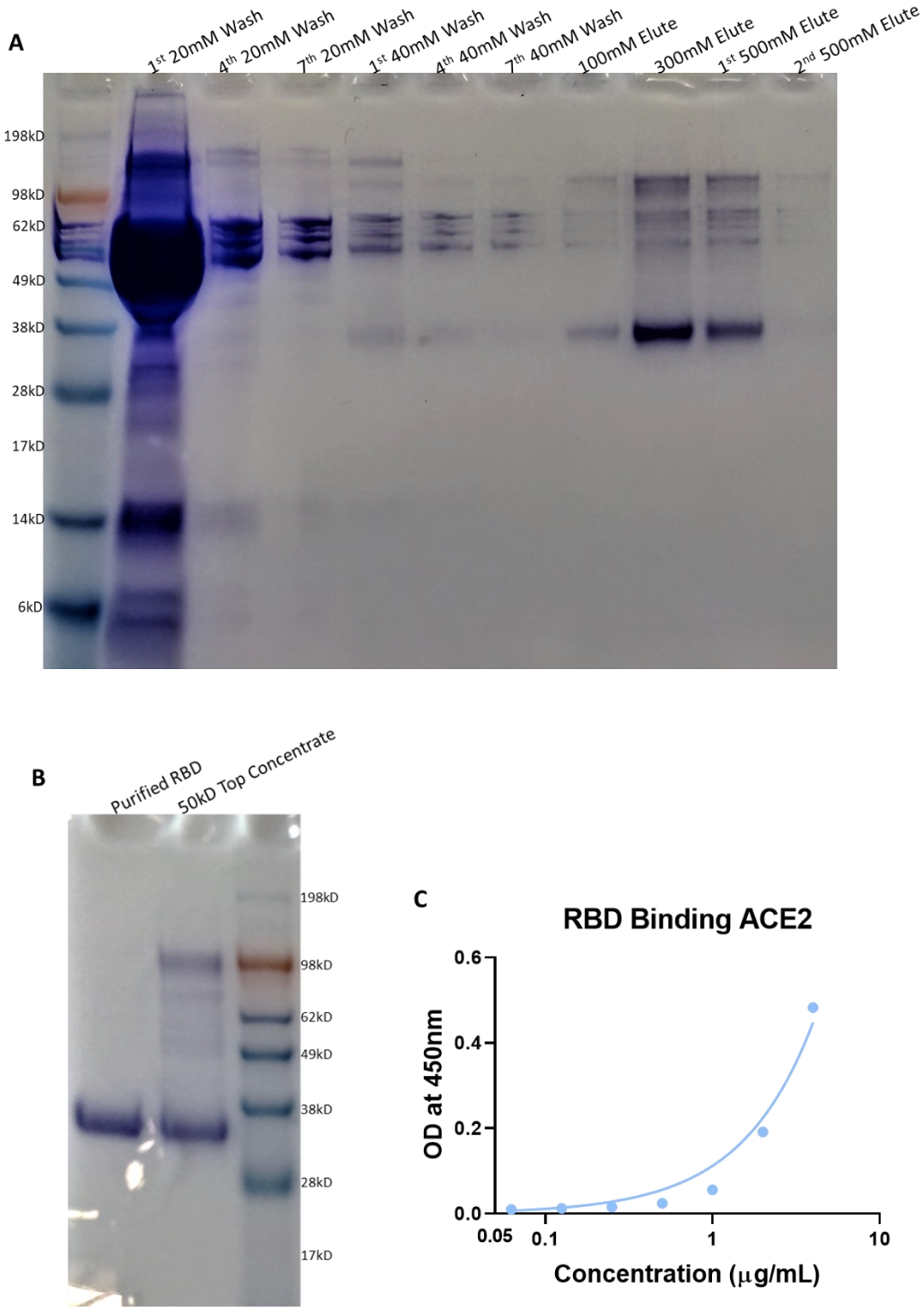

Figure 25. Purification of RBD Construct. (**A**) Typical purification of RBD in increasing concentrations of imidazole. The protein is primarily visible in the 100mM, 300mM, and 1st 500mM elutes. The RBD protein is about 35kD. (**B**) Size exclusion purification of RBD comparing the top concentrate from a 50kD filter to the protein purified through sequential passaging between 50kD and 10kD filters. (**C**) Results of ELISA testing the affinity of RBD for ACE2, its molecular target.

Spike Purification

Like with the RBD, we commenced with purifying the Spike protein once we established that it was being produced. Its purification procedure on the HisPur™ Ni-NTA Spin Column was identical to that done for RBD (**Figure 26A**).

Due to low expression levels of the full-length Spike protein, larger volumes of culture supernatants were purified. The protein was also purified on a 1mL Bio-Scale Mini Profinity IMAC Cartridge using an NGC Quest 10 Chromatography System (**Figure 26B**).

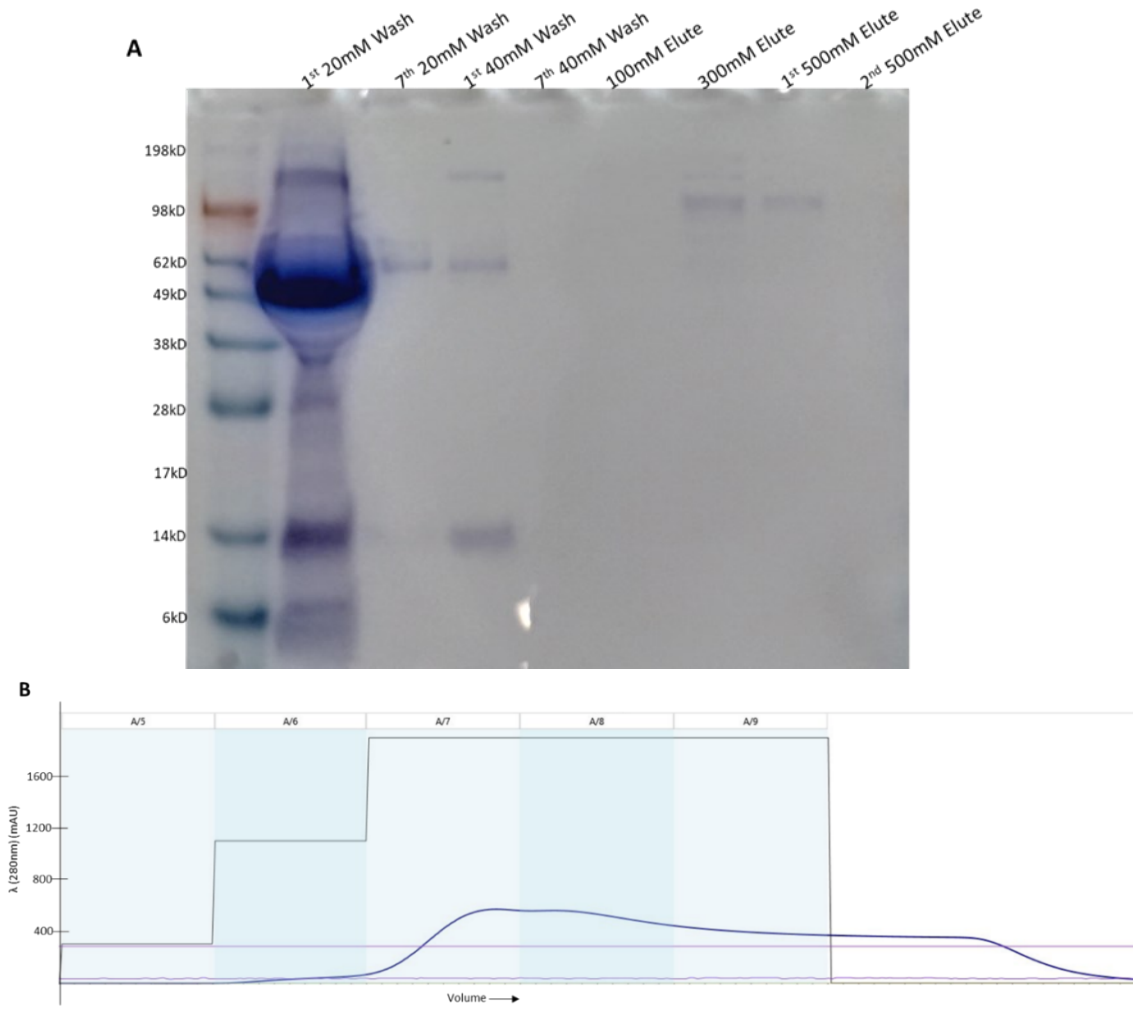

Figure 26. Purification of Spike Protein. (**A**) Typical purification of Spike in increasing concentrations of imidazole. The protein is primarily visible in the 300mM and 1st 500mM imidazole fractions. (**B**) A280 chromatogram of IMAC purification of Spike protein. The black lines represent the concentration of imidazole used in the gradient.

Evaluating Binding of Commercial RBD and S1 to ACE2

An ELISA assay was performed to test the ability of commercially available RBD (GenScript, Cat. #Z03491-100) and S1 (GenScript, Cat. #Z03485-100) proteins to bind

ACE2. The plate was coated with 4μg/mL of RBD or S1. Our results suggest that both of the purchased proteins functionally bind ACE2 in a dose-dependent manner (**Figure 27**). As a result, both proteins were used in our experiments with convalescent plasma samples, and this RBD was used for our tests with ambulatory plasma samples.

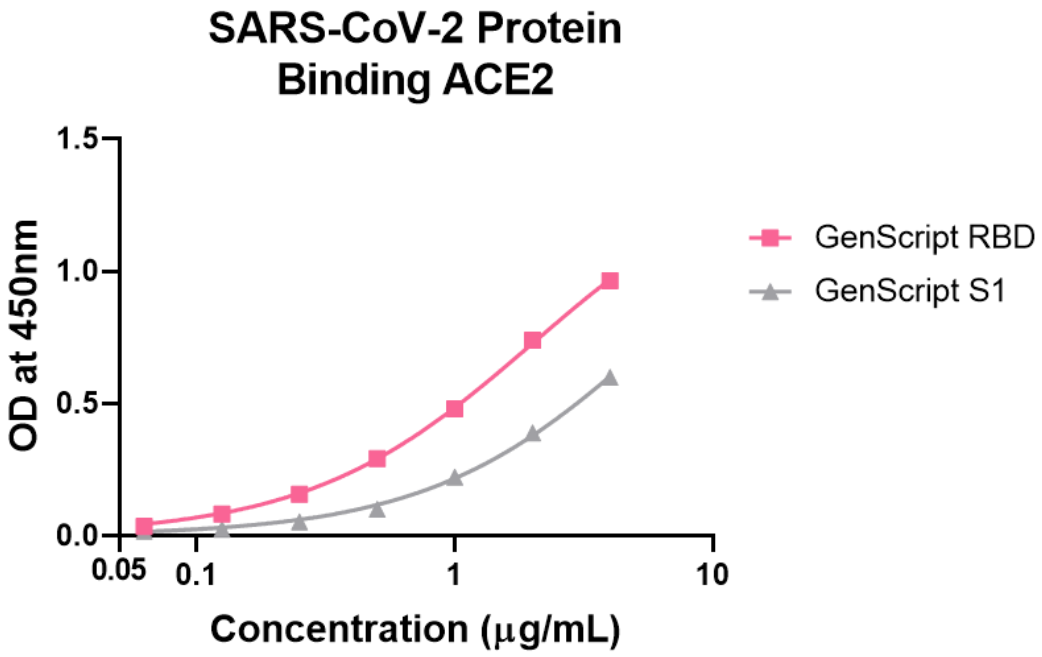

Figure 27. RBD and S1 Binding to ACE2. The commercial RBD is shown in pink, while the commercial S1 is in gray.

Analysis of Convalescent Plasma Samples by ELISA and Competition ELISA

First, the convalescent plasma samples (Plasma A+ 6-23-2020, CP-COVID 18-6-2020, and CP-COVID A- 6-23-2020) were evaluated for the level of anti-Spike antibodies by ELISA. Our results show that sample CP-COVID 18-6-2020 sample had the highest level of antibodies when tested against both RBD and the full-length S1 subunit a strong

affinity for either the RBD or the S1 (**Figure 28A**). This sample also demonstrated high levels of blocking activity in the competition assay (**Figure 28B**).

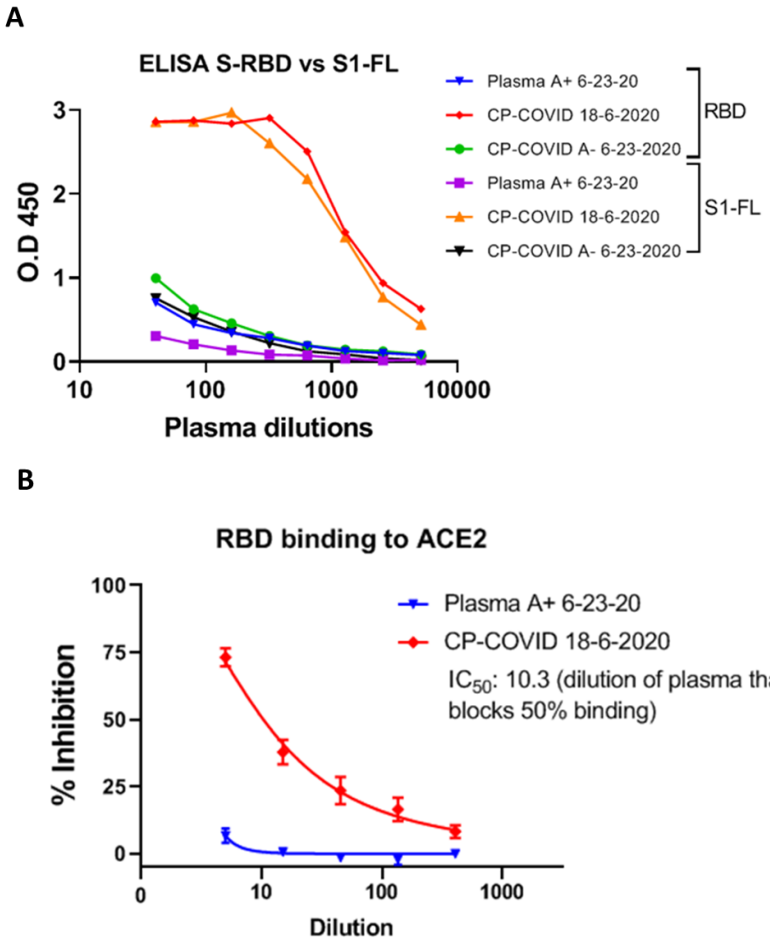

Figure 28. Analysis of Convalescent Plasma. (**A**) ELISA and (**B**) Competition ELISA. S-RBD refers to the RBD domain, and S1-FL refers to the full-length S1 subunit.

Analysis of Ambulatory Plasma Samples to Assess Levels of RBD-ACE2 Blocking Antibodies

Competition assays were performed using serially-diluted (starting at 1:5) ambulatory plasma samples (n=86). Dilutions of plasma samples were mixed with 2µg/mL ACE2, and this mixture was added to an ELISA plate coated with 1µg/mL RBD.

The amount of ACE2 that bound to RBD is proportional to the level of anti-RBD antibodies that can interfere with its binding to ACE2. Our experimental design of adding the receptor, ACE2, and the antibodies simultaneous allowed us to evaluate the competition for binding RBD in a more stringent manner. Blocking activity was calculated by comparing the amount of ACE2 binding to RBD at different dilutions of the individual samples compared to binding in the absence of antibody. **Figure 29A** shows a non-linear fit of the data. It is evident from our data that the level of RBD-ACE2 blocking antibody differed between samples.

Virus neutralization titer (NT) is currently considered the gold standard assay, as it strongly associates with protection from infection. Therefore, we assessed the association between NT and our ELISA. Since a majority of the samples did not show >50% inhibition in the competition assay, even at the lowest plasma dilution, we opted to use the activity observed at 1:5 dilution. Importantly, this was the dilution that demonstrated robust activity for most of the samples and also correlated well when tested pairwise against other, higher dilutions (**Figure 29B**). Interestingly, the level of RBD-ACE2 blocking activity strongly associated with virus neutralization titers (conducted by Dr. Pekosz) (**Figure 29C**).[142] A similar association was also observed between NT and anti-RBD titer (**Figure 29D**). As expected, our data also demonstrated a strong correlation between total anti-RBD titer and the level of RBD-ACE2 blocking activity in the corresponding plasma samples (**Figure 29E**). The high degree of correlation observed between RBD-ACE2 blocking activity and virus neutralization therefore offers a relatively simple biochemical assay to monitor/measure functional

antibodies. This assay may also be helpful in challenging environments as a surrogate to the gold standard NT assay.

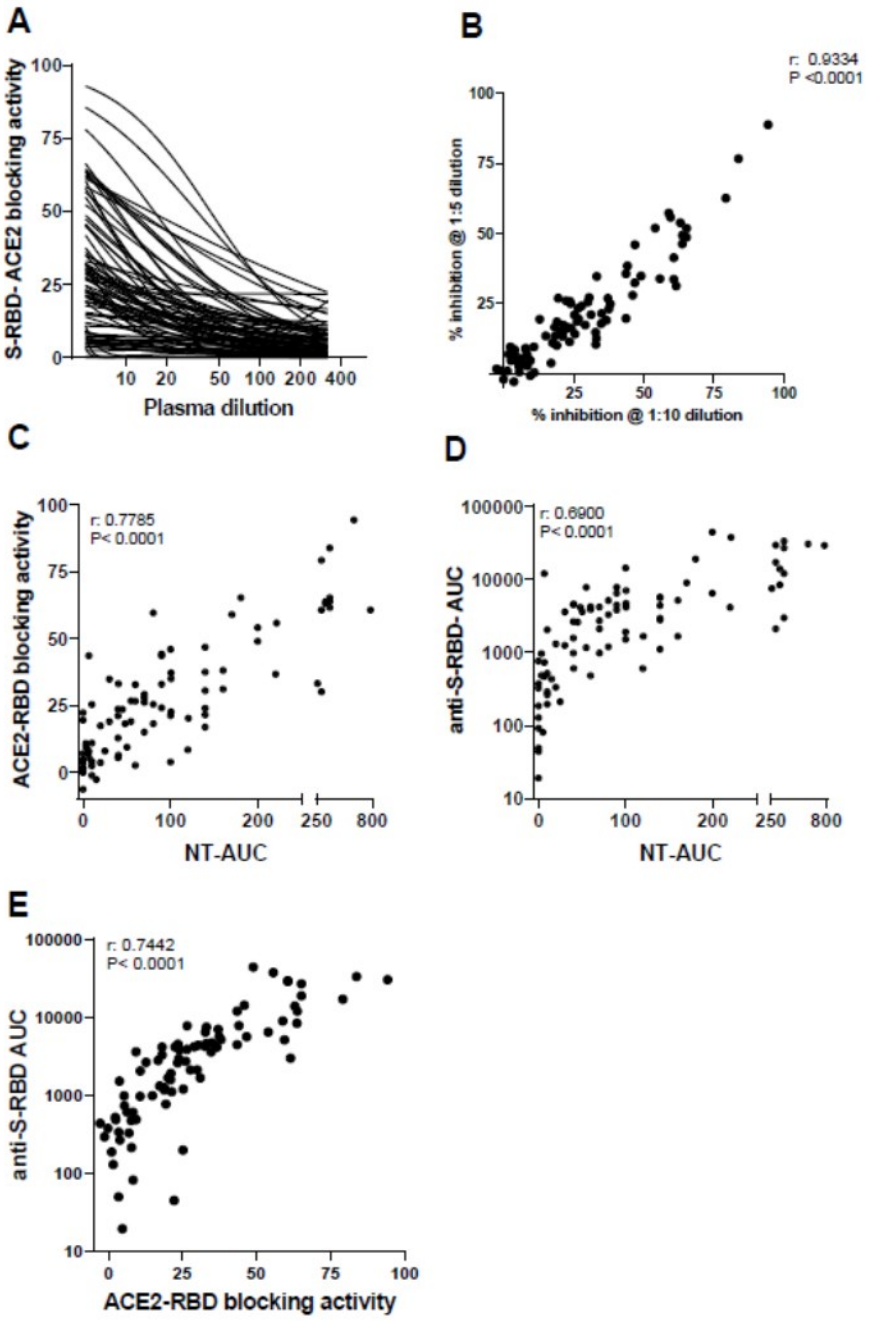

Figure 29. Analysis of Ambulatory Plasma for RBD-ACE2 Blocking Antibodies. (**A**) RBD-ACE2 blocking activity (%) measured in individual plasma. Data was fitted using a 4-parameter nonlinear sigmoidal curve. (**B**) Correlation between blocking activity measured at 1:5 vs. 1:10 plasma dilutions. (**C**) Correlation

between neutralizing antibody titer (NT) measured as area under the curve (AUC) vs. RBD-ACE2 blocking activity at 1:5 dilution. (**D**) Correlation between neutralizing antibody titer (NT-AUC) vs. anti-RBD titer AUC. (**E**) Correlation between RBD-ACE2 blocking activity at 1:5 dilution vs. anti-RBD titer AUC. Pearson's correlation coefficient (r) and p-value are indicated for each comparison. Data on neutralizing titers received from Dr. Pekosz.[142]

Discussion

The ongoing COVID-19 pandemic is the most impactful major public health event since the 1918 influenza pandemic. In addition to the millions who have succumbed to the disease so far, more will die as the pandemic continues.[117] It may also take years or decades to fully appreciate the latent health effects associated with the pandemic. For example, a 2009 study from Mazumber et al. found that prenatal exposure to the 1918 H1N1 influenza virus resulted in a significant increase in risk of heart disease above the age of 60.[145] Additionally, men between the ages of 19 and 27 who born in 1919 were significantly shorter than those born in surrounding years.[145] COVID-19 has also been found to be associated with an increased risk of stroke, possibly related to the presence of megakaryocytes in capillaries in the brain.[146,147] Additionally, the pandemic has also caused widespread socioeconomic changes that may take time to revert back to their pre-pandemic states.[148]

Definitive progress has been made in the process of COVID-19 vaccinations. On December 11, 2020, the FDA issued an EUA for a vaccine developed by Pfizer-BioNTech. This vaccine demonstrated an efficacy of 95% in preventing COVID-19 at least 7 days after receiving the booster.[149] On December 18, 2020, just a week after the EUA for the first COVID-19 vaccine, the FDA issued an EUA for a vaccine developed by Moderna.[150] This vaccine also demonstrated a high efficacy of 94.1% 7 days after the second dose. Both EUAs were reissued on February 25.[149,150] The FDA issued a third EUA on February 27 for one manufactured by Janssen.[151] The Janssen vaccine, which is a single dose, was 66.9% effective 14 days after vaccination and 66.1% effective after 28 days.[151]

Additionally, several other vaccines are still in development or have been dosed to patients in other countries.[152,153]

Here, we describe the expression of two recombinant proteins that comprise components of the SARS-CoV-2 Spike protein, the receptor binding domain (RBD) of the S1 subunit and the full-length protein. We demonstrated that we could express the RBD in HEK293T cells. We were successful in purifying the proteins, confirmed by SDS-PAGE and western blot. Using an ELISA, we demonstrated that our RBD was able to bind ACE2, its host cell receptor, albeit less so than RBD or full-length S1 bought commercially. We have demonstrated the design, expression, purification, and biological activity of the SARS-CoV-2 RBD.

We have also shown expression of the Spike protein, confirmed by SDS-PAGE and western blot. We purified Spike using nickel beads or by chromatography on an IMAC column. However, it was challenging to concentrate the protein; attempts to do so using a 100kD cut-off spin column were unsuccessful (data not shown). Because of the challenges in purification, we did not proceed with testing test the protein's ability to bind ACE2.

We have also developed multiple assays for testing COVID-19 convalescent plasma (CCP) samples. ELISAs testing plasma binding to RBD or the full-length S1 subunit showed agreement in binding titers to both proteins. The assay allowed us to differentiate between high-binding and low-binding plasma samples. We standardized an ELISA that measures the ability of plasma samples to bind RBD. This assay shows a high correlation ($r=0.6900$, $p<0.0001$) to neutralizing antibody (nAb) titers measured

using a neutralization assay in the lab of Dr. Andrew Pekosz, suggesting the reliability of our standardized assay.

Additionally, we have created an ELISA assay that tests the ability of a plasma sample to block the association between RBD and human ACE2. Our assay is able to distinguish between high-, medium-, and low-titer CCP samples. All blocking activity exhibits a similar dose-dependent effect, and the blocking activity is relatively consistent regardless of dilution. Our two ELISAs, the one which measures RBD binding and the competition ELISA, correlate with each other ($r=0.7442$, $p<0.0001$). Critically, the competition ELISA also correlates with the nAb titers calculated by neutralization assays ($r=0.7785$, $p<0.0001$).

The high correlations with data from neutralization assays show that the combination of our two ELISAs, the one measuring binding ACE2 and the one showing inhibition of RBD-ACE2 association, results in a viable alternative for measuring and assessing nAb titers. Given the updated EUA limiting the use of CCP to those with high nAb titers, it is critical to identify those with high blocking ability.[130] However, neutralization assays are dangerous and cumbersome, requiring live, viable virus and a BSL-3 clearance. Our assays allow labs to generate and evaluate neutralization data without the need for actual virus samples or a BSL-3 facility. Additionally, our ELISAs can quickly evaluate numerous plasma samples at a time.

Overall, we have successfully expressed, purified, and demonstrated biological activity of the RBD and full-length Spike protein from SARS-CoV-2. We have

demonstrated that our designed ELISAs can determine the level of nAb titer in a given plasma sample, saving time and avoiding the handling of live virus.

Future Directions

In our competition assay, most samples did not reach greater than 50% inhibition, and no samples reached 100% inhibition. However, it is possible that the samples would show a greater degree of blocking if we exposed the RBD to the plasma first, followed by incubation with ACE2 in a second step. It would be worthwhile to test this alternative competition. However, considering that our current assay correlates strongly with the data from the neutralization assay, we would expect that this modification would not drastically alter the value of the correlation coefficient.

It would be beneficial to optimize the expression and purification of SARS-CoV-2 Spike proteins and Spike components like the RBD. Additionally, once the Spike proteins of SARS-CoV-2 variants have been sequenced, we can quickly and effectively generate those Spike variants. We could then use the mutant RBD domains as coatings for our ELISAs to test how effectively CCP samples protect against the viral variants. We could also use these ELISAs to examine how effectively the various COVID-19 vaccines can generate antibodies that neutralize various viral strains. Additionally, CCP could still be an important prophylactic measure for those patients who are contraindicated for the vaccines, so our analysis of CCP would also be worthwhile.

References

1. Cunha CB, Cunha BA. Brief history of the clinical diagnosis of malaria: From hippocrates to osler. *J Vector Borne Dis*. 2008;45(3):194-199.

2. WHO. *Global technical strategy for malaria 2016-2030.* ; 2015:32. https://www.who.int/malaria/publications/atoz/9789241564991/en/.

3. WHO. *Eliminating malaria.* ; 2016. https://www.who.int/malaria/publications/atoz/eliminating-malaria/en/.

4. WHO. *World malaria report 2020.* ; 2020. https://www.who.int/publications/i/item/9789240015791.

5. Johns Hopkins University and Medicine. Johns hopkins coronavirus resource center. https://coronavirus.jhu.edu/. Updated 2021. Accessed January 26, 2021.

6. Phillips MA, Burrows JN, Manyando C, van Huijsduijnen RH, Van Voorhis WC, Wells TNC. Malaria. *Nat Rev Dis Primers*. 2017;3:17050. doi: 10.1038/nrdp.2017.50 [doi].

7. Cowman AF, Healer J, Marapana D, Marsh K. Malaria: Biology and disease. *Cell*. 2016;167(3):610-624. doi: S0092-8674(16)31008-X [pii].

8. Ajioka JW. Editorial. *Methods*. 1997;13(2):79-80. http://www.sciencedirect.com/science/article/pii/S1046202397905004. doi: https://doi.org/10.1006/meth.1997.0500.

9. Gubbels MJ, Duraisingh MT. Evolution of apicomplexan secretory organelles. *Int J Parasitol*. 2012;42(12):1071-1081. doi: S0020-7519(12)00232-9 [pii].

10. Yotoko K, Elisei C. Malaria parasites (apicomplexa, haematozoea) and their relationships with their hosts: Is there an evolutionary cost for the specialization? *J Zool Syst Evol Res*. 2006;44(4):265-273.

11. Milner DA,Jr. Malaria pathogenesis. *Cold Spring Harb Perspect Med*. 2018;8(1):a025569. doi: 10.1101/cshperspect.a025569. doi: 10.1101/cshperspect.a025569 [doi].

12. Su XZ, Lane KD, Xia L, Sá JM, Wellems TE. *Plasmodium* genomics and genetics: New insights into malaria pathogenesis, drug resistance, epidemiology, and evolution. *Clin Microbiol Rev*. 2019;32(4):e00019-19. Print 2019 Sep 18. doi: 10.1128/CMR.00019-19 [doi].

13. Gachelin G, Garner P, Ferroni E, Tröhler U, Chalmers I. Evaluating cinchona bark and quinine for treating and preventing malaria. *J R Soc Med*. 2017;110(1):31-40. doi: 10.1177/0141076816681421 [doi].

14. Barnett R. Malaria. *Lancet*. 2016;387(10037):2495-1. doi: S0140-6736(16)30799-1 [pii].

15. Slater AF. Chloroquine: Mechanism of drug action and resistance in *Plasmodium falciparum*. *Pharmacol Ther*. 1993;57(2-3):203-235. doi: 0163-7258(93)90056-J [pii].

16. Mita T, Kaneko A, Lum JK, et al. Recovery of chloroquine sensitivity and low prevalence of the *Plasmodium falciparum* chloroquine resistance transporter gene mutation K76T following the discontinuance of chloroquine use in malawi. *Am J Trop Med Hyg*. 2003;68(4):413-415.

17. Blasco B, Leroy D, Fidock DA. Antimalarial drug resistance: Linking *Plasmodium falciparum* parasite biology to the clinic. *Nat Med*. 2017;23(8):917-928. doi: 10.1038/nm.4381 [doi].

18. Kim J, Tan YZ, Wicht KJ, et al. Structure and drug resistance of the *Plasmodium falciparum* transporter PfCRT. *Nature*. 2019;576(7786):315-320. doi: 10.1038/s41586-019-1795-x [doi].

19. Laufer MK, Thesing PC, Eddington ND, et al. Return of chloroquine antimalarial efficacy in malawi. *N Engl J Med*. 2006;355(19):1959-1966. doi: 355/19/1959 [pii].

20. Walliker D, Hunt P, Babiker H. Fitness of drug-resistant malaria parasites. *Acta Trop*. 2005;94(3):251-259. http://www.sciencedirect.com/science/article/pii/S0001706X05000860. doi: https://doi.org/10.1016/j.actatropica.2005.04.005.

21. Dondorp AM, Nosten F, Yi P, et al. Artemisinin resistance in *Plasmodium falciparum* malaria. *N Engl J Med*. 2009;361(5):455-467. doi: 10.1056/NEJMoa0808859 [doi].

22. WHO. *Status report on artemisinin and ACT resistance.* ; 2015. https://www.who.int/malaria/publications/atoz/update-artemisinin-resistance-sep2015/en/.

23. Ménard D, Khim N, Beghain J, et al. A worldwide map of *Plasmodium falciparum* K13-propeller polymorphisms. *N Engl J Med*. 2016;374(25):2453-2464. doi: 10.1056/NEJMoa1513137 [doi].

24. WHO. Malaria vaccine technology roadmap. https://www.who.int/immunization/sage/meetings/2013/april/7_Malaria_Vaccine_TRM_Final.pdf?ua=1. Updated 2006. Accessed January 31, 2021.

25. Cohen J, Nussenzweig V, Nussenzweig R, Vekemans J, Leach A. From the circumsporozoite protein to the RTS, S/AS candidate vaccine. *Hum Vaccin*. 2010;6(1):90-96. doi: 9677 [pii].

26. Kaslow DC, Biernaux S. RTS,S: Toward a first landmark on the malaria vaccine technology roadmap. *Vaccine*. 2015;33(52):7425-7432. http://www.sciencedirect.com/science/article/pii/S0264410X15013377. doi: https://doi.org/10.1016/j.vaccine.2015.09.061.

27. RTS, S Clinical Trials Partnership. Efficacy and safety of RTS,S/AS01 malaria vaccine with or without a booster dose in infants and children in africa: Final results of a phase 3, individually randomised, controlled trial. *Lancet*. 2015;386(9988):31-45. doi: S0140-6736(15)60721-8 [pii].

28. White MT, Verity R, Griffin JT, et al. Immunogenicity of the RTS,S/AS01 malaria vaccine and implications for duration of vaccine efficacy: Secondary analysis of data from a phase 3 randomised controlled trial. *Lancet Infect Dis*. 2015;15(12):1450-1458. doi: S1473-3099(15)00239-X [pii].

29. Amanna IJ, Carlson NE, Slifka MK. Duration of humoral immunity to common viral and vaccine antigens. *N Engl J Med*. 2007;357(19):1903-1915. doi: 357/19/1903 [pii].

30. European Medicines Agency. Summary of opinion: Mosquirix--*Plasmodium falciparum* and hepatitis B vaccine (recombinant, adjuvanted). . 2015.

31. WHO. Malaria vaccine: WHO position paper--january 2016. *Weekly epidemiological record*. 2016;91(4):33-52. https://www.who.int/wer/2016/WER9104.pdf?ua=1.

32. Birkett AJ. Status of vaccine research and development of vaccines for malaria. *Vaccine*. 2016;34(26):2915-2920. doi: S0264-410X(16)00294-2 [pii].

33. Bannister LH, Hopkins JM, Fowler RE, Krishna S, Mitchell GH. A brief illustrated guide to the ultrastructure of *Plasmodium falciparum* asexual blood stages. *Parasitol Today*. 2000;16(10):427-433. doi: S0169-4758(00)01755-5 [pii].

34. Besteiro S, Dubremetz JF, Lebrun M. The moving junction of Apicomplexan parasites: A key structure for invasion. *Cell Microbiol*. 2011;13(6):797-805. doi: 10.1111/j.1462-5822.2011.01597.x [doi].

35. Cowman AF, Tonkin CJ, Tham W, Duraisingh MT. The molecular basis of erythrocyte invasion by malaria parasites. *Cell Host & Microbe*. 2017;22(2):232-245. http://www.sciencedirect.com.proxy1.library.jhu.edu/science/article/pii/S19313128170286X. doi: https://doi-org.proxy1.library.jhu.edu/10.1016/j.chom.2017.07.003.

36. Miller LH, Ackerman HC, Su XZ, Wellems TE. Malaria biology and disease pathogenesis: Insights for new treatments. *Nat Med*. 2013;19(2):156-167. doi: 10.1038/nm.3073 [doi].

37. Srinivasan P, Beatty WL, Diouf A, et al. Binding of *Plasmodium* merozoite proteins RON2 and AMA1 triggers commitment to invasion. *Proc Natl Acad Sci USA*. 2011;108(32):13275-13280. doi: 10.1073/pnas.1110303108 [doi].

38. Kato K. How does toxoplama gondii invade host cells? *J Vet Med Sci*. 2018;80(11):1702-1706. doi: 10.1292/jvms.18-0344 [doi].

39. Lamarque M, Besteiro S, Papoin J, et al. The RON2-AMA1 interaction is a critical step in moving junction-dependent invasion by apicomplexan parasites. *PLoS Pathog*. 2011;7(2):e1001276. doi: 10.1371/journal.ppat.1001276 [doi].

40. Silvie O, Franetich JF, Charrin S, et al. A role for apical membrane antigen 1 during invasion of hepatocytes by *Plasmodium falciparum* sporozoites. *J Biol Chem*. 2004;279(10):9490-9496. doi: M311331200 [pii].

41. Tufet-Bayona M, Janse CJ, Khan SM, Waters AP, Sinden RE, Franke-Fayard B. Localisation and timing of expression of putative *Plasmodium berghei* rhoptry proteins in merozoites and sporozoites. *Mol Biochem Parasitol*. 2009;166(1):22-31. doi: 10.1016/j.molbiopara.2009.02.009 [doi].

42. Yang ASP, Lopaticki S, O'Neill MT, et al. AMA1 and MAEBL are important for *Plasmodium falciparum* sporozoite infection of the liver. *Cell Microbiol*. 2017;19(9):10.1111/cmi.12745. Epub 2017 May 18. doi: 10.1111/cmi.12745 [doi].

43. Ishino T, Murata E, Tokunaga N, et al. Rhoptry neck protein 2 expressed in *Plasmodium* sporozoites plays a crucial role during invasion of mosquito salivary glands. *Cell Microbiol*. 2019;21(1):e12964. doi: 10.1111/cmi.12964 [doi].

44. Srinivasan P, Yasgar A, Luci DK, et al. Disrupting malaria parasite AMA1-RON2 interaction with a small molecule prevents erythrocyte invasion. *Nat Commun*. 2013;4:2261. doi: 10.1038/ncomms3261 [doi].

45. Harris KS, Casey JL, Coley AM, et al. Binding hot spot for invasion inhibitory molecules on *Plasmodium falciparum* apical membrane antigen 1. *Infect Immun*. 2005;73(10):6981-6989. http://iai.asm.org/content/73/10/6981.abstract. doi: 10.1128/IAI.73.10.6981-6989.2005.

46. Harris KS, Casey JL, Coley AM, et al. Rapid optimization of a peptide inhibitor of malaria parasite invasion by comprehensive N-methyl scanning. *J Biol Chem*. 2009;284(14):9361-9371. doi: 10.1074/jbc.M808762200 [doi].

47. Tyler JS, Boothroyd JC. The C-terminus of *Toxoplasma* RON2 provides the crucial link between AMA1 and the host-associated invasion complex. *PLoS Pathog*. 2011;7(2):e1001282. doi: 10.1371/journal.ppat.1001282 [doi].

48. Vulliez-Le Normand B, Tonkin ML, Lamarque MH, et al. Structural and functional insights into the malaria parasite moving junction complex. *PLoS Pathog*. 2012;8(6):e1002755. doi: 10.1371/journal.ppat.1002755 [doi].

49. Srinivasan P, Ekanem E, Diouf A, et al. Immunization with a functional protein complex required for erythrocyte invasion protects against lethal malaria. *Proc Natl Acad Sci USA*. 2014;111(28):10311-10316. doi: 10.1073/pnas.1409928111 [doi].

50. Srinivasan P, Baldeviano GC, Miura K, et al. A malaria vaccine protects aotus monkeys against virulent *Plasmodium falciparum* infection. *NPJ Vaccines*. 2017;2:10.1038/s41541-7. Epub 2017 May 22. doi: 14 [pii].

51. Xiao S. *Engineering a self-targeting entry inhibitor for malaria prophylaxis.* Johns Hopkins University Bloomberg School of Public Health; 2019.

52. Druilhe P, Pérignon JL. Mechanisms of defense against P. falciparum asexual blood stages in humans. *Immunol Lett*. 1994;41(2-3):115-120. doi: 0165-2478(94)90118-X [pii].

53. Boyle MJ, Reiling L, Feng G, et al. Human antibodies fix complement to inhibit *Plasmodium falciparum* invasion of erythrocytes and are associated with protection against malaria. *Immunity*. 2015;42(3):580-590. doi: S1074-7613(15)00087-4 [pii].

54. Bouharoun-Tayoun H, Oeuvray C, Lunel F, Druilhe P. Mechanisms underlying the monocyte-mediated antibody-dependent killing of *Plasmodium falciparum* asexual blood stages. *J Exp Med*. 1995;182(2):409-418. doi: 95355840 [pii].

55. Jafarshad A, Dziegiel MH, Lundquist R, Nielsen LK, Singh S, Druilhe PL. A novel antibody-dependent cellular cytotoxicity mechanism involved in defense against malaria requires costimulation of monocytes FcgammaRII and FcgammaRIII. *J Immunol*. 2007;178(5):3099-3106. doi: 178/5/3099 [pii].

56. Jafari R, Zolbanin NM, Rafatpanah H, Majidi J, Kazemi T. Fc-fusion proteins in therapy: An updated view. *Curr Med Chem*. 2017;24(12):1228-1237. doi: 10.2174/0929867324666170113112759 [doi].

57. Strohl WR. Fusion proteins for half-life extension of biologics as a strategy to make biobetters. *BioDrugs*. 2015;29(4):215-239. doi: 10.1007/s40259-015-0133-6 [doi].

58. Capon DJ, Chamow SM, Mordenti J, et al. Designing CD4 immunoadhesins for AIDS therapy. *Nature*. 1989;337(6207):525-531. doi: 10.1038/337525a0 [doi].

59. Sleep D. Albumin and its application in drug delivery. *Expert Opin Drug Deliv*. 2015;12(5):793-812. doi: 10.1517/17425247.2015.993313 [doi].

60. Zorzi A, Linciano S, Angelini A. Non-covalent albumin-binding ligands for extending the circulating half-life of small biotherapeutics. *Medchemcomm*. 2019;10(7):1068-1081. doi: 10.1039/c9md00018f [doi].

61. Yeh P, Landais D, Lemaître M, et al. Design of yeast-secreted albumin derivatives for human therapy: Biological and antiviral properties of a serum albumin-CD4 genetic conjugate. *Proc Natl Acad Sci USA*. 1992;89(5):1904-1908. doi: 10.1073/pnas.89.5.1904 [doi].

62. Smith BJ, Popplewell A, Athwal D, et al. Prolonged in vivo residence times of antibody fragments associated with albumin. *Bioconjug Chem*. 2001;12(5):750-756. doi: bc010003g [pii].

63. Subramanian GM, Fiscella M, Lamousé-Smith A, Zeuzem S, McHutchison JG. Albinterferon alpha-2b: A genetic fusion protein for the treatment of chronic hepatitis C. *Nat Biotechnol*. 2007;25(12):1411-1419. doi: nbt1364 [pii].

64. Miyakawa N, Nishikawa M, Takahashi Y, et al. Prolonged circulation half-life of interferon γ activity by gene delivery of interferon γ-serum albumin fusion protein in mice. *J Pharm Sci*. 2011;100(6):2350-2357. doi: 10.1002/jps.22473 [doi].

65. Dennis MS, Zhang M, Meng YG, et al. Albumin binding as a general strategy for improving the pharmacokinetics of proteins. *J Biol Chem*. 2002;277(38):35035-35043. doi: M205854200 [pii].

66. Miyakawa N, Nishikawa M, Takahashi Y, et al. Gene delivery of albumin binding peptide-interferon-gamma fusion protein with improved pharmacokinetic properties and sustained biological activity. *J Pharm Sci*. 2013;102(9):3110-3118. doi: 10.1002/jps.23493 [doi].

67. Nilvebrant J, Hober S. The albumin-binding domain as a scaffold for protein engineering. *Comput Struct Biotechnol J*. 2013;6:e201303009. doi: 10.5936/csbj.201303009 [doi].

68. Jonsson A, Dogan J, Herne N, Abrahmsén L, Nygren PA. Engineering of a femtomolar affinity binding protein to human serum albumin. *Protein Eng Des Sel*. 2008;21(8):515-527. doi: 10.1093/protein/gzn028 [doi].

69. Levy OE, Jodka CM, Ren SS, et al. Novel exenatide analogs with peptidic albumin binding domains: Potent anti-diabetic agents with extended duration of action. *PLoS One*. 2014;9(2):e87704. doi: 10.1371/journal.pone.0087704 [doi].

70. Bridges A, Bistas KG, Jacobs TF. Exenatide. In: *StatPearls.* Treasure Island (FL): StatPearls Publishing LLC; 2020. NBK518981 [bookaccession].

71. Orlova A, Jonsson A, Rosik D, et al. Site-specific radiometal labeling and improved biodistribution using ABY-027, a novel HER2-targeting affibody molecule-albumin-binding domain fusion protein. *J Nucl Med*. 2013;54(6):961-968. doi: 10.2967/jnumed.112.110700 [doi].

72. Altai M, Leitao CD, Rinne SS, et al. Influence of molecular design on the targeting properties of ABD-fused mono- and bi-valent anti-HER3 affibody therapeutic constructs. *Cells*. 2018;7(10):164. doi: 10.3390/cells7100164. doi: 10.3390/cells7100164 [doi].

73. Zhang Y, Guo Z, Cao Z, et al. Endogenous albumin-mediated delivery of redox-responsive paclitaxel-loaded micelles for targeted cancer therapy. *Biomaterials*. 2018;183:243-257. doi: S0142-9612(18)30417-4 [pii].

74. Tan H, Su W, Zhang W, Zhang J, Sattler M, Zou P. Albumin-binding domain extends half-life of glucagon-like peptide-1. *Eur J Pharmacol*. 2021;890:173650. doi: S0014-2999(20)30742-1 [pii].

75. Kober L, Zehe C, Bode J. Optimized signal peptides for the development of high expressing CHO cell lines. *Biotechnol Bioeng*. 2013;110(4):1164-1173. doi: 10.1002/bit.24776 [doi].

76. George RA, Heringa J. An analysis of protein domain linkers: Their classification and role in protein folding. *Protein Eng Des Sel*. 2002;15(11):871-879. doi: 10.1093/protein/15.11.871.

77. Argos P. An investigation of oligopeptides linking domains in protein tertiary structures and possible candidates for general gene fusion. *J Mol Biol*. 1990;211(4):943-958. doi: 0022-2836(90)90085-Z [pii].

78. Huston JS, Levinson D, Mudgett-Hunter M, et al. Protein engineering of antibody binding sites: Recovery of specific activity in an anti-digoxin single-chain fv analogue produced in *Escherichia coli*. *Proc Natl Acad Sci USA*. 1988;85(16):5879-5883. doi: 10.1073/pnas.85.16.5879 [doi].

79. Invitrogen. pcDNA 3.1 (+) mammalian expression vector. https://www.thermofisher.com/order/catalog/product/V79020#/V79020. Updated 2021. Accessed February 20, 2021.

80. Gibson DG, Young L, Chuang RY, Venter JC, Hutchison CA,3rd, Smith HO. Enzymatic assembly of DNA molecules up to several hundred kilobases. *Nat Methods*. 2009;6(5):343-345. doi: 10.1038/nmeth.1318 [doi].

81. New England BioLabs. Gibson assembly. https://www.neb.com/applications/cloning-and-synthetic-biology/dna-assembly-and-cloning/gibson-assembly. Updated 2021. Accessed February 22, 2021.

82. New England BioLabs. NEBuilder HiFi DNA assembly reaction protocol. https://www.neb.com/protocols/2014/11/26/nebuilder-hifi-dna-assembly-reaction-protocol. Updated 2021. Accessed February 22, 2021.

83. New England BioLabs. NEBio calculator: Ligation calculator. https://nebiocalculator.neb.com/#!/ligation. Updated 2021.

84. Zymo Research. ZymoPURE plasmid miniprep kit. https://files.zymoresearch.com/protocols/_d4208t_d4209_d4210_d4211_d4212_zymopure_plasmid_miniprep.pdf.

85. Zymo Research. ZymoPURE II plasmid midiprep kit. https://files.zymoresearch.com/protocols/_d4200_d4201_zymopure_ii_plasmid_midiprep.pdf.

86. Polyplus. jetPRIME transfection reagent short protocol-DNA transfection. https://www.polyplus-transfection.com/wp-content/uploads/2015/08/Short-Protocol-jetPRIME-DNA-vG.pdf. Accessed February 24, 2021.

87. Cold Spring Harbor Protocols. Polyethylenimine (PEI), linear (1mg/mL). http://cshprotocols.cshlp.org/content/2008/3/pdb.rec11323.full. Accessed March 4, 2020.

88. Gibco. Expi293 expression system: Structural biology and inducible expression modules user guide. https://assets.thermofisher.com/TFS-Assets/LSG/manuals/MAN0007814_Expi293_ExpressionSystem_UG.pdf. Updated 2020.

89. Burgess RR. Chapter 20 protein precipitation techniques. *Meth Enzymol*. 2009;463:331-342. https://www.sciencedirect.com/science/article/pii/S0076687909630202. doi: https://doi.org/10.1016/S0076-6879(09)63020-2.

90. Hober S, Nord K, Linhult M. Protein A chromatography for antibody purification. *Journal of Chromatography B*. 2007;848(1):40-47. https://www.sciencedirect.com/science/article/pii/S1570023206007999. doi: https://doi.org/10.1016/j.jchromb.2006.09.030.

91. Block H, Maertens B, Spriestersbach A, et al. Chapter 27 immobilized-metal affinity chromatography (IMAC): A review. *Meth Enzymol*. 2009;463:439-473. https://www.sciencedirect.com/science/article/pii/S0076687909630275. doi: https://doi.org/10.1016/S0076-6879(09)63027-5.

92. Bio-Rad. CHT ceramic hydroxyapatite type II media. https://www.bio-rad.com/en-us/product/cht-ceramic-hydroxyapatite-type-ii-media?ID=5ded4ec5-ff5a-47b7-bf10-07253005c83f. Updated 2021. Accessed February 28, 2021.

93. Bio-Rad. Ceramic hydroxyapatite application guide for process development and scale-up. .

94. Life Technologies. NativePAGE novex bis-tris gel system: A system for native gel electrophoresis. https://www.thermofisher.com/document-connect/document-connect.html?url=https%3A%2F%2Fassets.thermofisher.com%2FTFS-Assets%2FLSG%2Fmanuals%2Fnativepage_man.pdf&title=TmF0aXZlUEFHRSBOb3ZleCBCaXMtVHJpcyBHZWwgU3lzdGVt. Updated 2012. Accessed December 18, 2020.

95. Bhardwaj G, Mulligan VK, Bahl CD, et al. Accurate de novo design of hyperstable constrained peptides. *Nature*. 2016;538(7625):329-335. doi: 10.1038/nature19791 [doi].

96. Rocklin GJ, Chidyausiku TM, Goreshnik I, et al. Global analysis of protein folding using massively parallel design, synthesis, and testing. *Science*. 2017;357(6347):168-175. doi: 10.1126/science.aan0693 [doi].

97. Nguyen A, Reyes AE,2nd, Zhang M, et al. The pharmacokinetics of an albumin-binding fab (AB.fab) can be modulated as a function of affinity for albumin. *Protein Eng Des Sel*. 2006;19(7):291-297. doi: gzl011 [pii].

98. Harp KO, Botchway F, Dei-Adomakoh Y, et al. Hemoglobin genotypes modulate inflammatory response to *Plasmodium* infection. *Front Immunol*. 2020;11:593546. doi: 10.3389/fimmu.2020.593546 [doi].

99. Driss A, Hibbert JM, Wilson NO, Iqbal SA, Adamkiewicz TV, Stiles JK. Genetic polymorphisms linked to susceptibility to malaria. *Malar J*. 2011;10:271-271. doi: 10.1186/1475-2875-10-271 [doi].

100. Weatherall DJ. The inherited diseases of hemoglobin are an emerging global health burden. *Blood*. 2010;115(22):4331-4336. doi: 10.1182/blood-2010-01-251348 [doi].

101. GBD 2017 DALYs and HALE Collaborators. Global, regional, and national disability-adjusted life-years (DALYs) for 359 diseases and injuries and healthy life expectancy (HALE) for 195 countries and territories, 1990-2017: A systematic analysis for the global burden of disease study 2017. *Lancet*. 2018;392(10159):1859-1922. doi: S0140-6736(18)32335-3 [pii].

102. WHO. The top 10 causes of death. https://www.who.int/news-room/fact-sheets/detail/the-top-10-causes-of-death#:~:text=The%20top%20global%20causes%20of,birth%20asphyxia%20and%20birth%20trauma%2C. Updated 2020. Accessed March 11, 2021.

103. ProMED. Undiagnosed pneumonia - china (hubei): Request for information. https://promedmail.org/promed-post/?id=6864153%20#COVID19. Updated 2019. Accessed March 20, 2021.

104. WHO. Timeline: WHO's COVID-19 response. https://www.who.int/emergencies/diseases/novel-coronavirus-2019/interactive-timeline#!. Updated 2021. Accessed March 20, 2021.

105. Huang C, Wang Y, Li X, et al. Clinical features of patients infected with 2019 novel coronavirus in wuhan, china. *Lancet*. 2020;395(10223):497-506. doi: S0140-6736(20)30183-5 [pii].

106. Zhou P, Yang XL, Wang XG, et al. A pneumonia outbreak associated with a new coronavirus of probable bat origin. *Nature*. 2020;579(7798):270-273. doi: 10.1038/s41586-020-2012-7 [doi].

107. Bi S, Qin E, Xu Z, et al. Complete genome sequences of the SARS-CoV: The BJ group (isolates BJ01-BJ04). *Genomics Proteomics Bioinformatics*. 2003;1(3):180-192. doi: S1672-0229(03)01023-4 [pii].

108. Andersen KG, Rambaut A, Lipkin WI, Holmes EC, Garry RF. The proximal origin of SARS-CoV-2. *Nat Med*. 2020;26(4):450-452. doi: 10.1038/s41591-020-0820-9 [doi].

109. Wacharapluesadee S, Tan CW, Maneeorn P, et al. Evidence for SARS-CoV-2 related coronaviruses circulating in bats and pangolins in southeast asia. *Nat Commun*. 2021;12(1):972-1. doi: 10.1038/s41467-021-21240-1 [doi].

110. Gorbalenya AE, Baker SC, Baric RS, et al. *Severe acute respiratory syndrome-related coronavirus*: The species and its viruses – a statement of the coronavirus study group. *bioRxiv*. 2020:2020.02.07.937862. http://biorxiv.org/content/early/2020/02/11/2020.02.07.937862.abstract. doi: 10.1101/2020.02.07.937862.

111. WHO. Novel coronavirus (2019-nCoV) situation report-1. *WHO*. 2020.

112. Holshue ML, DeBolt C, Lindquist S, et al. First case of 2019 novel coronavirus in the united states. *N Engl J Med*. 2020;382(10):929-936. doi: 10.1056/NEJMoa2001191 [doi].

113. Basavaraju SV, Patton ME, Grimm K, et al. Serologic testing of U.S. blood donations to identify SARS-CoV-2-reactive antibodies: December 2019-january 2020. *Clin Infect Dis*. 2020. doi: 10.1093/cid/ciaa1785 [doi].

114. WHO. Novel coronavirus (2019-nCoV) situation report-8. *WHO*. 2020.

115. WHO. WHO director-general's remarks at the media briefing on 2019-nCoV on 11 february 2020. https://www.who.int/director-general/speeches/detail/who-director-general-s-remarks-at-the-media-briefing-on-2019-ncov-on-11-february-2020. Updated 2020. Accessed March 20, 2021.

116. WHO. WHO director-general's opening remarks at the media briefing on COVID-19 - 11 march 2020. https://www.who.int/director-general/speeches/detail/who-director-general-s-opening-remarks-at-the-media-briefing-on-covid-19---11-march-2020. Updated 2020. Accessed March 20, 2021.

117. Johns Hopkins University & Medicine. Johns hopkins coronavirus resource center. https://coronavirus.jhu.edu/. Updated 2021. Accessed March 20, 2021.

118. Casadevall A, Scharff MD. Return to the past: The case for antibody-based therapies in infectious diseases. *Clin Infect Dis*. 1995;21(1):150-161. doi: 10.1093/clinids/21.1.150 [doi].

119. Casadevall A, Dadachova E, Pirofski LA. Passive antibody therapy for infectious diseases. *Nat Rev Microbiol*. 2004;2(9):695-703. doi: nrmicro974 [pii].

120. Casadevall A, Pirofski LA. The convalescent sera option for containing COVID-19. *J Clin Invest*. 2020;130(4):1545-1548. doi: 138003 [pii].

121. Casadevall A, Joyner MJ, Pirofski LA. A randomized trial of convalescent plasma for COVID-19-potentially hopeful signals. *JAMA*. 2020;324(5):455-457. doi: 10.1001/jama.2020.10218 [doi].

122. Li L, Zhang W, Hu Y, et al. Effect of convalescent plasma therapy on time to clinical improvement in patients with severe and life-threatening COVID-19: A randomized clinical trial. *JAMA*. 2020;324(5):460-470. doi: 10.1001/jama.2020.10044 [doi].

123. Liu Z. Errors in trial of effect of convalescent plasma therapy on time to clinical improvement in patients with severe and life-threatening COVID-19. *JAMA*. 2020;324(5):518-519. doi: 10.1001/jama.2020.12607 [doi].

124. FDA. FDA issues emergency use authorization for convalescent plasma as potential promising COVID-19 treatment, another achievement in administration's fight against pandemic. https://www.fda.gov/news-events/press-announcements/fda-issues-emergency-use-authorization-convalescent-plasma-potential-promising-covid-19-treatment. Updated 2020. Accessed March 21, 2021.

125. FDA. COVID-19 convalescent plasma EUA decision memo 02052021. . 2021.

126. Infectious Diseases Society of America, AABB. Clarifying the emergency use authorization framework for COVID-19 convalescent plasma: Considerations for clinicians. . 2020.

127. Horby PW, Estcourt L, et al. Convalescent plasma in patients admitted to hospital with COVID-19 (RECOVERY): A randomised, controlled, open-label, platform trial. *medRxiv*. 2021:2021.03.09.21252736. http://medrxiv.org/content/early/2021/03/10/2021.03.09.21252736.abstract. doi: 10.1101/2021.03.09.21252736.

128. Libster R, Pérez Marc G, Wappner D, et al. Early high-titer plasma therapy to prevent severe covid-19 in older adults. *N Engl J Med*. 2021;384(7):610-618. doi: 10.1056/NEJMoa2033700 [doi].

129. Joyner MJ, Carter RE, Senefeld JW, et al. Convalescent plasma antibody levels and the risk of death from covid-19. *N Engl J Med*. 2021;384(11):1015-1027. doi: 10.1056/NEJMoa2031893 [doi].

130. FDA. Convalescent plasma EUA letter of authorization march 9, 2021. . 2021.

131. Lan J, Ge J, Yu J, et al. Structure of the SARS-CoV-2 spike receptor-binding domain bound to the ACE2 receptor. *Nature*. 2020;581(7807):215-220. doi: 10.1038/s41586-020-2180-5 [doi].

132. Wrapp D, Wang N, Corbett KS, et al. Cryo-EM structure of the 2019-nCoV spike in the prefusion conformation. *Science*. 2020;367(6483):1260-1263. doi: 10.1126/science.abb2507 [doi].

133. Benton DJ, Wrobel AG, Xu P, et al. Receptor binding and priming of the spike protein of SARS-CoV-2 for membrane fusion. *Nature*. 2020;588(7837):327-330. doi: 10.1038/s41586-020-2772-0 [doi].

134. Hoffmann M, Kleine-Weber H, Schroeder S, et al. SARS-CoV-2 cell entry depends on ACE2 and TMPRSS2 and is blocked by a clinically proven protease inhibitor. *Cell*. 2020;181(2):271-280.e8. doi: S0092-8674(20)30229-4 [pii].

135. Li W, Moore MJ, Vasilieva N, et al. Angiotensin-converting enzyme 2 is a functional receptor for the SARS coronavirus. *Nature*. 2003;426(6965):450-454. doi: nature02145 [pii].

136. Yao H, Song Y, Chen Y, et al. Molecular architecture of the SARS-CoV-2 virus. *Cell*. 2020;183(3):730-738.e13. doi: S0092-8674(20)31159-4 [pii].

137. Piccoli L, Park YJ, Tortorici MA, et al. Mapping neutralizing and immunodominant sites on the SARS-CoV-2 spike receptor-binding domain by structure-guided high-resolution serology. *Cell*. 2020;183(4):1024-1042.e21. doi: S0092-8674(20)31234-4 [pii].

138. Huang Y, Yang C, Xu XF, Xu W, Liu SW. Structural and functional properties of SARS-CoV-2 spike protein: Potential antivirus drug development for COVID-19. *Acta Pharmacol Sin*. 2020;41(9):1141-1149. doi: 10.1038/s41401-020-0485-4 [doi].

139. Weisblum Y, Schmidt F, Zhang F, et al. Escape from neutralizing antibodies by SARS-CoV-2 spike protein variants. *Elife*. 2020;9:10.7554/eLife.61312. doi: 10.7554/eLife.61312 [doi].

140. Kemp SA, Collier DA, Datir RP, et al. SARS-CoV-2 evolution during treatment of chronic infection. *Nature*. 2021. doi: 10.1038/s41586-021-03291-y [doi].

141. Resende PC, Bezerra JF, de Vasconcelos, Romero Henrique Teixeira, et al. Spike E484K mutation in the first SARS-CoV-2 reinfection case confirmed in brazil, 2020. *January*. 2021;10:2021.

142. Klein SL, Pekosz A, Park HS, et al. Sex, age, and hospitalization drive antibody responses in a COVID-19 convalescent plasma donor population. *J Clin Invest*. 2020;130(11):6141-6150. doi: 142004 [pii].

143. Amanat F, Stadlbauer D, Strohmeier S, et al. A serological assay to detect SARS-CoV-2 seroconversion in humans. *Nat Med*. 2020;26(7):1033-1036. doi: 10.1038/s41591-020-0913-5 [doi].

144. Blair PW, Brown DM, Jang M, et al. The clinical course of COVID-19 in the outpatient setting: A prospective cohort study. *Open Forum Infect Dis*. 2021;8(2):ofab007. doi: 10.1093/ofid/ofab007 [doi].

145. Mazumder B, Almond D, Park K, Crimmins EM, Finch CE. Lingering prenatal effects of the 1918 influenza pandemic on cardiovascular disease. *Journal of Developmental Origins of Health and Disease*. 2010;1(1):26-34. https://www.cambridge.org/core/article/lingering-prenatal-effects-of-the-1918-influenza-pandemic-on-cardiovascular-disease/26094395058187D6EFDCFCFAF2E584D6. Accessed 2021/03/26. doi: 10.1017/S2040174409990031.

146. Fridman S, Bres Bullrich M, Jimenez-Ruiz A, et al. Stroke risk, phenotypes, and death in COVID-19: Systematic review and newly reported cases. *Neurology*. 2020;95(24):e3373-e3385. doi: 10.1212/WNL.0000000000010851 [doi].

147. Nauen DW, Hooper JE, Stewart CM, Solomon IH. Assessing brain capillaries in coronavirus disease 2019. *JAMA Neurol*. 2021. https://doi.org/10.1001/jamaneurol.2021.0225. Accessed 3/26/2021. doi: 10.1001/jamaneurol.2021.0225.

148. Nicola M, Alsafi Z, Sohrabi C, et al. The socio-economic implications of the coronavirus pandemic (COVID-19): A review. *International Journal of Surgery*. 2020;78:185-193. https://www.sciencedirect.com/science/article/pii/S1743919120303162. doi: https://doi.org/10.1016/j.ijsu.2020.04.018.

149. FDA. Pfizer-BioNTech COVID-19 vaccine EUA letter of authorization. . 2021.

150. FDA. Moderna COVID-19 vaccine EUA letter of authorization. . 2021.

151. FDA. Janssen COVID-19 vaccine EUA letter of authorization. . 2021.

152. AJMC Staff. A timeline of COVID-19 developments in 2020. https://www.ajmc.com/view/a-timeline-of-covid19-developments-in-2020. Updated 2021. Accessed March 20, 2021.

153. AJMC Staff. A timeline of COVID-19 vaccine developments in 2021. https://www.ajmc.com/view/a-timeline-of-covid-19-vaccine-developments-in-2021. Updated 2021. Accessed March 20, 2021.

Appendix A: Table of Primers

Name	Sequence
pcDNA3.1 Seq. Fwd.	5’GCAGAGCTCTCTGGCTAACTAG3’
pcDNA3.1 Seq. Rvs.	5’ CAACTAGAAGGCACAGTCGAG3’

Appendix B: Sequences of Constructs

Pep12-Fc-pcDNA3.1 (Pep12-Fc):

MATGSRTSLLLAFGLLCLPWLQEGSAQIVNDVDQCINAAEELARRPGSPVHCFCTRMAPFQVICWV
ERKLGGGGSGGGGSGGGGSGTEPKSCDKTHTCPPCPAPELLGGPSVFLFPPKPKDTLMISRTPEVTC
VVVDVSHEDPEVKFNWYVDGVEVHNAKTKPREEQYNSTYRVVSVLTVLHQDWLNGKEYKCKVSN
KALPAPIEKTISKAKGQPREPQVYTLPPSRDELTKNQVSLTCLVKGFYPSDIAVEWESNGQPENNYKT
TPPVLDSDGSFFLYSKLTVDKSRWQQGNVFSCSVMHEALHNHYTQKSLSLSPGRK*

PfRON2L-ABD035-pcDNA3.1 (RON2L-ABD035):

MATGSRTSLLLAFGLLCLPWLQEGSAQIVNDITQQAKDIGAGPVASCFTTRMSPPQQICLNSVVNT
ALKLGGGGSGGGGSGGGGSGTLAEAKVLANRELDKYGVSDFYKRLINKAKTVEGVEALKLHILAALP
PRHHHHHH*

Key:

Signal Sequence. Pep12. PfRON2L. $(G_4S)_3$ Linker. Human IgG1 Fc. ABD035. 6x His Tag.

Zachary Berliner

907 Adana Rd., Pikesville, MD 21208
zachary.berliner@gmail.com (805) 796-9743

EDUCATION

Master of Science (ScM) *Expected May 2021*

Johns Hopkins Bloomberg School of Public Health, Baltimore, MD

Concentration: Molecular Microbiology and Immunology

Research: Thesis titled "Inhibition of Essential Protein-Protein Interactions in *Plasmodium* and SARS-CoV-2." Thesis research on a vaccine targeting a protein essential for the malaria parasite lifecycle in the lab of Dr. Prakash Srinivasan, sub-titled "Engineering an Inhibitor of an Essential *Plasmodium* Protein-Protein Interaction." Additional research, sub-titled "Evaluating a Surrogate Assay to Measure the Neutralizing Activity in Convalescent Plasma against SARS-CoV-2," on COVID-19 donor plasma immunity in collaboration with Drs. Andrew Pekosz, Sabra Klein, Arturo Casadevall, and Yukari Manabe.

Honors: Certificate in Tropical Medicine

GPA: 4.00

Bachelor of Science in Biology *May 2016*

Indiana University Hutton Honors College, Bloomington, IN

Minors: History, Psychology

Honors: Graduated Highest Distinction; Member of Phi Beta Kappa honor fraternity; 8-time College of Arts and Sciences Executive Dean's List; Burnett/Masters Junior Scholar Award Recipient; 4-time IU Founder's Scholar; IU Distinction Scholarship Recipient

GPA: 3.978

RESEARCH EXPERIENCE

Graduate Student Researcher *Oct. 2019—Present*

Srinivasan Lab, Johns Hopkins Bloomberg School of Public Health, Baltimore, MD

- Work under Dr. Prakash Srinivasan
- Conduct research targeting inhibition of a protein essential for the malaria parasite's life cycle
- Investigate immunity of donor plasma samples against COVID-19 to assist in convalescent plasma research
- Perform laboratory techniques including mammalian cell expression, ELISA, Western blotting, Gibson assembly, SDS-PAGE, and FPLC
- Interpret results from scientific experiments to inform decision-making
- Present research findings to professors and experts in microbiology and molecular biology
- Summarize research methods and results in a written thesis
- Maintain and organize laboratory supplies and equipment

Undergraduate Lab Assistant *May 2015—May 2016*

Innes Lab, Indiana University, Bloomington, IN

- Formulated solutions and materials necessary for scientific experimentation in a lab focused on understanding plant immunity
- Oversaw planting and care of subject plants
- Maintained laboratory organization and supplies

Biology Researcher *Jun. 2014—Aug. 2014*

Revie Lab, California Lutheran University, Thousand Oaks, CA

- Assisted senior researchers in conducting studies on Hepatitis C inhibition
- Isolated viral RNA from Hepatitis C Virus
- Performed laboratory techniques including PCR, rtPCR, and gel electrophoresis

WORK EXPERIENCE

Teaching Assistant, Clinical and Epidemiologic Aspects of Tropical Diseases *Mar. 2021—Present*

Johns Hopkins University Bloomberg School of Public Health, Baltimore, MD

- Assist Drs. David Sack and Kawsar Talaat in conducting class sections and evaluating quizzes and projects
- Monitor student participation and activity on course website
- Answer student questions

Substitute Teacher *Feb. 2019—May 2019*

Kelly Educational Services, Indianapolis, IN

- Taught at elementary, middle, and high schools across four public school districts and numerous public charter schools
- Developed and enhanced classroom management and communication skills
- Adapted to changing situations to meet the varying needs of the schools and students

Tutor *Oct. 2017—May 2019*

Club Z Tutoring, Fishers, IN

- Assisted middle and high school students with coursework and test preparation
- Tutored Algebra 1, Algebra 2, Chemistry, and English

Study Technician I *Jul. 2018—Nov. 2018*

Covance (Contractor: Aerotek), Greenfield, IN

- Assisted in preparing experimental pharmaceutical with the Dose Formulations department for drug development
- Formulated laboratory vehicles, control groups, and mixtures containing pharmaceutical test articles
- Complied with the FDA's Code of Federal Regulations Part 21, Title 58, for Good Laboratory Practices

Sample Handling Assistant *Nov. 2017—Apr. 2018*

Covance (Contractor: Apex Life Sciences), Indianapolis and Greenfield, IN

- Worked in the Biorepository at two company locations

- Responsible for retrieving, packing, discarding, and registering laboratory samples
- Authorized to formally close completed or cancelled studies

Math Teacher (Teach For America) *Jul. 2016—Jun. 2017*
Harshman Magnet Middle School, Indianapolis, IN

- Taught Pre-Algebra to 130 seventh graders in six classes
- Interpreted state education standards to devise curriculum calendar and create daily lesson plans
- Designed worksheets, quizzes, and tests
- Mentored students and led conversations on social justice issues in a special advisory class
- Assisted in educating staff on restorative classroom management
- Communicated with parents on students' progress and educational needs
- Completed 4 semesters toward a Master of Teaching (MAT) at Marian University in Indianapolis, IN, as part of the Teach For America program

Undergraduate Teaching Assistant, L211-Molecular Biology *Fall 2014*
Indiana University, Bloomington, IN

- Assisted Dr. David Kehoe in teaching Molecular Biology and evaluating examinations
- Taught a weekly discussion section and graded worksheets for fifteen undergraduate students
- Conducted review sessions for examinations

VOLUNTEER WORK AND ADDITIONAL EXPERIENCE

Diversity and Inclusion Committee Member *May 2020—Feb. 2021*
W. Harry Feinstone Department of Molecular Microbiology and Immunology, Johns Hopkins Bloomberg School of Public Health, Baltimore, MD

- Co-founder of the departmental Diversity and Inclusion Committee with ten other peers
- Communicated concerns regarding inclusion and diversity issues with professors and department administrators
- Conducted conversations about social justice issues in the department, university, and country with students and staff
- Organized student meetings to discuss potential improvements in equity and representation in the department

Script-Writer and Presenter *Feb. 2020—Mar. 2020*
COVideo-19, Johns Hopkins Bloomberg School of Public Health, Baltimore, MD

- Contributed to a student-led video series designed to inform the public on issues related to COVID-19 prevention and treatment
- Authored scripts and filmed short videos to answer public questions about COVID-19 on a dedicated URL, Facebook, and YouTube

Broadcaster, **Engineer, and Blogger** *Sep. 2012—May 2016*

WIUX, Indiana University, Bloomington, IN

- Broadcast and engineered live Indiana University sporting events for student-led radio station
- Produced and co-hosted weekly sports shows
- Wrote weekly statistics-based NFL blog for WIUX station website

PROFESSIONAL SKILLS

Computer Skills: Microsoft Office Suite, Benchling, Adobe Audition CC, NGC Chromatography System, GraphPad Prism, Countess II Automated Cell Counter

Languages: Mandarin Chinese (Conversational)

Lab Skills: HEK293T cell maintenance and expression, Expi293 cell maintenance and expression, ELISA, Western blotting, Gibson assembly, SDS-PAGE, FPLC, Restriction digestion, PCR, Plasmid design, Plasmid preparation, *E. coli* transformation, Ammonium sulfate precipitation, Gel shift assay, Solution preparation